LIGHT SCATTERING IN PLANETARY ATMOSPHERES

JAMES E. HANSEN and LARRY D. TRAVIS

Goddard Institute for Space Studies, New York, N.Y. 10025, U.S.A.

Abstract. This paper reviews scattering theory required for analysis of light reflected by planetary atmosphères. Section 1 defines the radiative quantities which are observed. Section 2 demonstrates the dependence of single-scattered radiation on the physical properties of the scatterers. Section 3 describes several methods to compute the effects of multiple scattering on the reflected light.

1. Description of Radiation

Sunlight incident on the Earth's atmosphere is scattered by molecules and particles, giving rise to our blue skys, white clouds and striking optical phenomena such as rainbows, halos and glories. The physical and mathematical descriptions of these scattering processes have been pursued for centuries, and this work has contributed greatly to our understanding of both light and the atmosphere.

Now, with the advent of instrumented space probes to the planets and meteorological satellites of the Earth, light scattering in planetary atmospheres has taken on a renewed interest. Reflected sunlight is remarkably rich in potential information on planetary atmospheres, and may prove to be the most valuable of our tools for *remote analysis* of clouds and aerosols.

Retrieval of the potential information in reflected sunlight requires a thorough understanding of the relationship between the radiation characteristics and the physical properties of the scattering particles. This task is made easier by an appropriate description of radiation. Although we employ a variety of ways to mathematically represent radiation, it is valuable to use a simple physical description in terms of the *intensity*, *linear polarization* (its degree and direction) and *circular polarization*.

1.1. BRIEF DESCRIPTION

The intensity of electromagnetic radiation is the rate of energy flow across a unit area perpendicular to the direction of propagation. If light were a scalar wave like sound, the intensity would provide a full description. However the transverse nature of light waves* allows the phenomenon of polarization which requires additional parameters for a complete description.

---

* The high intensity of sunlight allows us to restrict our description to the wave aspects of electromagnetic radiation. However, in Section 3 the concept of photons is employed as a convenient way of describing multiple scattering processes. The quantum side of the dual character of light must also be invoked to explain the nature of gaseous absorption and emission.
** By a simple wave we mean a plane-wave solution of Maxwell's equations; cf., van de Hulst (1957) and Born and Wolf (1959).

Light consists of many simple waves** with frequencies $\sim 10^{14}\ \text{s}^{-1}$ and with the duration of coherent wave trains $\lesssim 10^{-8}$ s. These simple waves are each monochromatic and completely (elliptically) polarized. Their geometric description is contained in many texts. In a plane perpendicular to the direction of light propagation the endpoint of a vector representing the electric field at a fixed point in space traces out an ellipse with time. Special cases of the ellipse are a straight line and a circle, corresponding to linear and circular polarization, respectively.

Light which is commonly measured is the net effect of many simple waves, and in general it is partially polarized. The light is completely polarized only if the orientation and ellipticity of the polarization ellipses are identical for each simple wave. Natural light, such as direct sunlight from the whole solar disk, represents the other extreme: it is a mixture of uncorrelated simple waves, and over a time period for usual measurements the electric vector exhibits no preferred direction of vibration.

An arbitrary beam of light of intensity I consists of an unpolarized part and a totally polarized part,

$$I = I_{\text{unpol}} + I_{\text{pol}}.$$ (1.1)

The degree of polarization is defined as the ratio I_{pol}/I. The polarized part of the beam is in general elliptically polarized, and it can be further separated into a linearly polarized part of 'intensity' I_{lp} and a circularly polarized part of 'intensity' I_{cp}, where

$$I_{\text{pol}} = (I_{lp}^2 + I_{cp}^2)^{1/2}.$$ (1.2)

Precise definitions of I_{lp} and I_{cp} are given below.

1.2. ANALYTIC REPRESENTATION

Consider a parallel beam of light of circular frequency ω traveling in a certain direction which we choose to call the positive z direction. The components of the electric field in any two mutually perpendicular directions (represented by unit vectors $\mathbf{r}$ and $\mathbf{l}$) may be written in terms of the amplitudes (a_l and a_r) and phases (ε_l and ε_r) as

$$E_l = a_l e^{i(\omega t - kz - \varepsilon_l)},$$
$$E_r = a_r e^{i(\omega t - kz - \varepsilon_r)}.$$ (1.3)

t represents time, $i = (-1)^{1/2}$, and k is the wave number, $2\pi/\lambda$. $\mathbf{r} \times \mathbf{l}$ is in the direction of propagation. In problems involving a single scattering event $\mathbf{r}$ is chosen perpendicular to the plane of scattering, which is defined as the plane containing the directions of incidence and scattering.

The Stokes parameters are the time averages

$$I = \langle E_l E_l^* + E_r E_r^* \rangle = \langle a_l^2 + a_r^2 \rangle$$
$$Q = \langle E_l E_l^* - E_r E_r^* \rangle = \langle a_l^2 - a_r^2 \rangle$$
$$U = \langle E_l E_r^* + E_r E_l^* \rangle = 2 \langle a_l a_r \cos \delta \rangle$$
$$V = i \langle E_l E_r^* - E_r E_l^* \rangle = 2 \langle a_l a_r \sin \delta \rangle$$ (1.4)

where $\delta = \varepsilon_l - \varepsilon_r$ and the asterisk represents the complex conjugate. I is the intensity* (say in erg s^{-1} cm^{-2}) and the other parameters have the same dimension. A constant factor common to all four parameters is omitted from (1.4) for convenience. The Stokes parameters of a mixture of independent waves are the sums of the respective Stokes parameters of the separate waves.
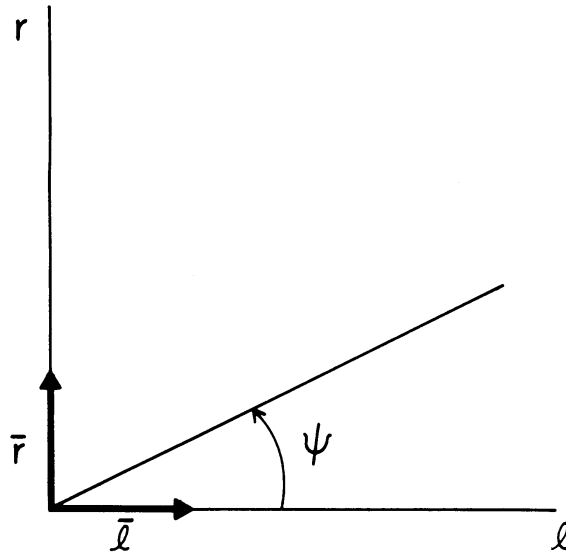

Fig. 1. Illustration of the angle ψ. The direction of propagation is into the page.

The significance of the individual Stokes parameters can be appreciated as follows. Suppose that E_r is subjected to a constant retardation ε with respect to E_l and let $I(\psi, \varepsilon)$ be the intensity of light due to vibrations in the direction making an angle ψ with the l direction (Figure 1). It can be shown that**

$$I(\psi, \varepsilon) = \tfrac{1}{2} \left[I + Q \cos 2\psi + (U \cos \varepsilon + V \sin \varepsilon) \sin 2\psi \right], \tag{1.5}$$

and thus we can obtain the Stokes parameters from the following 'measurements'

$$\begin{aligned}
I &= I(0°, 0) + I(90°, 0) = I_l + I_r, \\
Q &= I(0°, 0) - I(90°, 0) = I_l - I_r, \\
U &= I(45°, 0) - I(135°, 0), \\
V &= I(45°, \pi/2) - I(135°, \pi/2).
\end{aligned} \tag{1.6}$$

* In Sections 1 and 2 we use the definition of intensity usually employed in physics, which is the rate of energy flow across a unit area perpendicular to the direction of energy flow (say in erg s^{-1} cm^{-2}). In Section 3 we follow the common practice in multiple scattering theory of using the same term and symbol (intensity, I) to represent the photometric brightness (erg s^{-1} cm^{-2} sterad^{-1}); cf., Born and Wolf (1959, Section 4.8). Furthermore, in either case the intensity may refer to any specified spectral interval or to the monochromatic intensity; the units for monochromatic intensity include an additional factor, say μm^{-1}.

** Chandrasekhar (1950) has the opposite sign preceding $V \sin \varepsilon$. This arises from the definition of phase differences used in his Equation (154), p. 28, which is inconsistent with the definition of phase he employs for the Stokes parameters.

I is the total intensity. Q is the excess in intensity of light transmitted by a polarizer which passes linear polarization in the l direction ($\psi = 0°$), over the intensity of light transmitted by a polarizer which passes linear polarization in the r direction ($\psi = 90°$). U has an analogous interpretation with the intensity for $\psi = 45°$ compared to that for $\psi = 135°$. V is the excess in intensity of light transmitted by an instrument which passes right-handed circular polarization*, over that transmitted by an instrument which passes left-handed circular polarization.

For monochromatic light a_l, a_r and δ are independent of time and it follows from (1.4) that

$$I = (Q^2 + U^2 + V^2)^{1/2}, \tag{1.7}$$

corresponding to complete polarization. For polychromatic light (1.7) must in general be replaced by the inequality

$$I \geqslant (Q^2 + U^2 + V^2)^{1/2}. \tag{1.8}$$

It is clear that an arbitrary beam of radiation can be *mathematically* decomposed into two parts, one unpolarized with Stokes parameters $\{I - (Q^2 + U^2 + V^2)^{1/2}, 0, 0, 0\}$ and one elliptically polarized with Stokes parameters $\{(Q^2 + U^2 + V^2)^{1/2}, Q, U, V\}$. Thus the intensity of polarized light is

$$I_{pol} = (Q^2 + U^2 + V^2)^{1/2} \tag{1.9}$$

and the degree of (elliptical) polarization is

$$\frac{I_{pol}}{I} = \frac{(Q^2 + U^2 + V^2)^{1/2}}{I}. \tag{1.10}$$

We further define the intensity of linearly polarized light as

$$I_{lp} = (Q^2 + U^2)^{1/2}, \tag{1.11}$$

and the intensity of circularly polarized light as

$$I_{cp} = V, \tag{1.12}$$

from which (1.2) follows. The degree of linear polarization is I_{lp}/I and the degree of circular polarization I_{cp}/I.

It is valuable to also employ a geometric description for the polarization of a beam of radiation. The endpoint of the electric vector of the polarized part of the beam traces out an ellipse in time (Figure 2). If we let a and b be respectively the semi-major

---

* We say that the polarization is right-handed if, to an 'observer' looking in the direction of propagation, the endpoint of the electric vector moves in the clockwise sense. Thus for right-handed polarization the end of the electric vector, when it moves in the direction the light is moving, moves in the direction that a right-handed screw turns. This convention is adhered to in most modern physics books and by van de Hulst (1957), but note that the opposite convention is used by Born and Wolf (1959), Shurcliff (1962) and Deirmendjian (1969).

and semi-minor axes of the ellipse, then the ellipticity can be specified in terms of an angle β as

$$\tan \beta = \pm \, b/a \qquad (- \pi/4 \leqslant \beta \leqslant \pi/4). \tag{1.13}$$

The sign of β distinguishes the two senses in which the ellipse may be described, with positive β corresponding to right-handed polarization. As an example, the values 1, 0 and -1 for $\tan \beta$ correspond, respectively, to right-handed circular polarization, linear polarization and left-handed circular polarization. The angle which the major axis makes with the l direction is represented by the angle χ, $(0 \leqslant \chi < \pi)$.
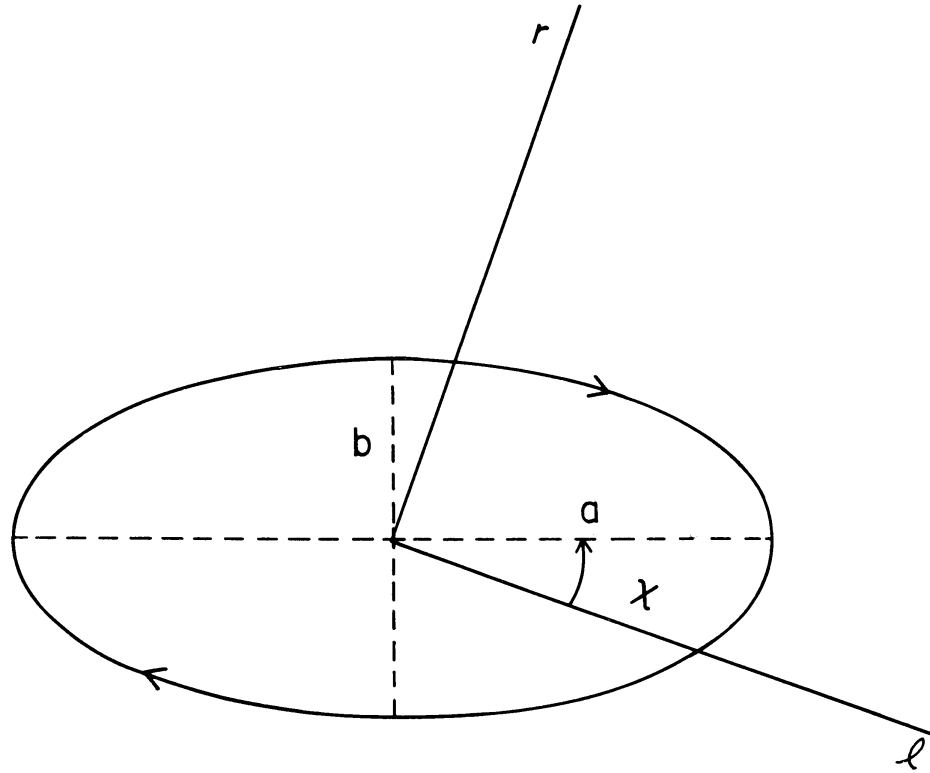

Fig. 2. Illustration of the polarization ellipse. The direction of propagation is into the page, and the indicated sense of rotation corresponds to right-handed polarization.

The shape and orientation of the polarization ellipse can be found from the Stokes parameters as follows

$$\sin 2\beta = V/(Q^2 + U^2 + V^2)^{1/2}, \tag{1.14}$$

$$\tan 2\chi = U/Q. \tag{1.15}$$

The convention is to choose the principal value of $\sin 2\beta$, $-\pi/4 \leqslant \beta \leqslant \pi/4$, as indicated in the paragraph above. Then from the two values of χ which are in the interval $0 \leqslant \chi < \pi$ and satisfy (1.15), the one must be chosen which makes $\cos 2\chi$ have the same sign as Q.

1.3. Observed quantities

It is apparent that *four* quantities are required to describe radiation. For numerical computations in multiple scattering problems it is convenient to employ the Stokes parameters. However, measurements and the results of computations are usually presented in the form of more intuitive quantities. Thus most textbooks employ the intensity, degree of polarization, direction of polarization and ellipticity. Alternatively, we can use the intensity, degree of linear polarization, direction of polarization and degree of circular polarization. This latter choice is advantageous in planetary studies, because it is common to measure either the linear polarization or the circular polarization rather than the complete (elliptical) polarization.

In remote investigations of planetary atmospheres scattered solar radiation can be measured as a function of wavelength and scattering geometry (with the directions of both the Sun and observer as variables), and of course as a function of time and location on the planet. The goal is to use the observed dependence of the radiation on these variables to extract information on the atmospheres by means of comparisons with theoretical computations and laboratory observations.

The *intensity* is the quantity most commonly measured, and it can be effectively used in a variety of ways. The visual brightness of a planet, including its variation with phase (Sun-planet-observer) angle and its variation across the planetary disk, provides an indication of the thickness of the atmosphere and can also reveal the presence of clouds. The spectral variation of the intensity at low resolution can be used to determine limits on the possible composition of planetary surfaces and cloud layers. Observations of absorption lines at high spectral resolution can provide the identification of *gaseous constituents*. Information on the vertical atmospheric structure is also attainable because of the dependence of absorption lines on the temperature and pressure distributions. However the reliability with which the atmospheric composition and structure can be obtained from the intensity of reflected sunlight depends in part on knowledge obtained in other ways on the nature and distribution of scatterers.

The *linear polarization* is less commonly measured than the intensity, perhaps in part because less work has been done in interpreting the polarization than in the case of the intensity. However the linear polarization can be obtained from a relative measurement with a high accuracy, and it has been demonstrated with laboratory and theoretical work that the errors of measurement can be kept much smaller than the characteristic features in the polarization of light scattered by small particles. For this reason the linear polarization can be effectively used for determining the nature of *cloud and aerosol particles*. The large difference between the polarization for gas molecules and that for typical cloud and aerosol particles makes the linear polarization also a potentially valuable tool for investigating the altitude and vertical distribution of atmospheric particles.

The *circular polarization* of sunlight reflected by planets has recently been measured and found to be very small (Kemp *et al.*, 1971a, b). However, with the very high

accuracies of measurement which have been demonstrated, the circular polarization has become an additional means for remote investigations of planets and a thorough investigation of its information content can be anticipated.

2. Single Scattering

The theoretical modeling of light scattering in planetary atmospheres is usually divided into two parts: single scattering by small volume elements in the atmosphere and multiple scattering by the entire atmosphere. This division requires that the scattering particles be sufficiently separated that they may be treated as independent scatterers, a condition which is met in planetary atmospheres.* An example is the reflection and transmission of sunlight by a water cloud: the Mie theory can be used to compute the single scattering by a small volume element containing a representative size distribution of cloud particles, and then the multiple scattering solution can be obtained from the equation of transfer or one of the other methods described in Section 3.

The aim in this section is to present definitions and illustrations which help to provide an understanding of single scattering by independent particles. Greater detail, including the rationale for some statements made here without proof, can be found in the books of van de Hulst (1957), Kerker (1969) and Deirmendjian (1969).

Let a small** volume (dv) containing particles be illuminated by parallel radiation (Figure 3). The intensity of the incident radiation, complete with polarization, may be represented by[†] $\mathbf{I}_0 = \{I_0, Q_0, U_0, V_0\}$. The scattered intensity at a distance R in the far-field (i.e., at $R \gg \lambda$) is

$$k_{\text{sca}} \mathbf{P} \mathbf{I}_0 \frac{dv}{4\pi R^2}, \tag{2.1}$$

where the two quantities describing the single scattering properties of the volume element are: $k_{\text{sca}} =$ scattering coefficient, dimension length^{-1}, and $\mathbf{P} =$ phase matrix, four rows and four columns of dimensionless numbers.

k_{sca} is the scattering cross-section per unit volume, i.e.,

$$k_{\text{sca}} = \sigma_{\text{sca}}/dv = \frac{1}{dv} \sum_i \sigma_{\text{sca}, i}, \tag{2.2}$$

where the sum is over all particles in dv and $\sigma_{\text{sca}, i}$ is the scattering cross-section of

* The assumption of independent scattering requires that interference of light scattered by different particles be undetectable. A rough rule of thumb is that the particles must be separated by a few times their radius (van de Hulst, 1957).
** The volume should be small enough that the fractional attenuation of the light beam passing through it is much less than unity.
† The Stokes parameters form a vector (column matrix) of four terms, but to conserve space we sometimes write them horizontally. The phrase 'intensity complete with polarization' refers to the full Stokes vector. Boldface letters are used to represent 4-vectors and 4-by-4 matrices.

the ith particle. $\sigma_{\mathrm{sca},i}$ is an area such that the total energy scattered by the ith particle is equal to the energy of incident radiation falling on $\sigma_{\mathrm{sca},i}$. It is useful to also introduce the efficiency factor for scattering, Q_{sca}, which is the dimensionless ratio of scattering cross-section to geometrical cross-section. For a single particle

$$Q_{\mathrm{sca},i} = \sigma_{\mathrm{sca},i}/G_i,$$ (2.3)

where G_i is the geometrical cross-section of the ith particle; for a unit volume

$$Q_{\mathrm{sca}} = \frac{\sigma_{\mathrm{sca}}}{G} = \frac{\sum_i \sigma_{\mathrm{sca},i}}{\sum_i G_i}.$$ (2.4)
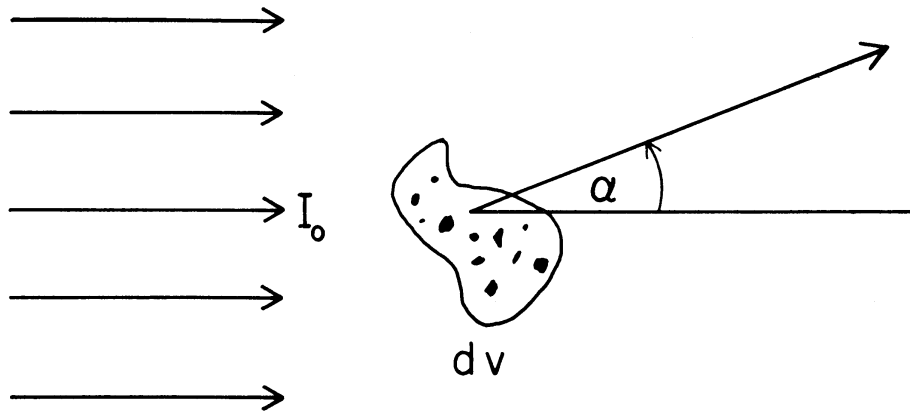

Fig. 3.   Illustration of small volume element, dv, and scattering angle, α.

P gives the angular distribution and polarization of the scattered light, for any polarization of incident radiation. The element in the first row and first column, P^{11}, is the phase function or scattering diagram; this represents the probability for scattering of unpolarized incident light in any given direction. **P** is normalized such that

$$\int_{4\pi} P^{11} \frac{d\Omega}{4\pi} = 1,$$ (2.5)

where $d\Omega$ is an element of solid angle. The shape of the phase function can be usefully characterized by a single number,

$$\langle\cos\alpha\rangle = \int_{4\pi} \cos\alpha \, P^{11} \frac{d\Omega}{4\pi},$$ (2.6)

where α is the scattering angle and $\langle\cos\alpha\rangle$ is called the anisotropy parameter. $\langle\cos\alpha\rangle$ varies between 1 and -1, and is 0 for isotropic scattering.

k_{sca} and **P** define the light scattered by a small volume element, but for the solution of multiple scattering problems it is essential to also know a third quantity:

$\tilde{\omega}$ = single scattering albedo, dimensionless.

$\tilde{\omega}$ is the fraction scattered, of the total energy removed from the incident beam. Since energy is removed by absorption as well as scattering, it is convenient to define k_{abs}, σ_{abs} and Q_{abs} in exact analogy to the above definitions for scattering. With the total removed energy defined as the extinction,

$$
\begin{aligned}
k_{ext} &= k_{sca} + k_{abs}, \\
\sigma_{ext} &= \sigma_{sca} + \sigma_{abs}, \\
Q_{ext} &= Q_{sca} + Q_{abs}.
\end{aligned}
\tag{2.7}
$$

In terms of these quantities

$$
\tilde{\omega} = \frac{k_{sca}}{k_{ext}} = \frac{\sigma_{sca}}{\sigma_{ext}} = \frac{Q_{sca}}{Q_{ext}}.
\tag{2.8}
$$

In general k_{sca}, $\mathbf{P}$ and $\tilde{\omega}$ depend upon the orientation of the volume dv to the direction of incidence. However in many practical applications k_{sca} and $\tilde{\omega}$ can be taken as constants and $\mathbf{P}$ as a function of only the scattering angle, with at most six independent parameters:

$$
\mathbf{P}(\alpha) = \left\{
\begin{matrix}
P^{11} & P^{21} & 0 & 0 \\
P^{21} & P^{22} & 0 & 0 \\
0 & 0 & P^{33} & -P^{43} \\
0 & 0 & P^{43} & P^{44}
\end{matrix}
\right\}.
\tag{2.9}
$$

This special case is valid for (1) randomly oriented particles, each of which has a plane of symmetry, (2) randomly oriented asymmetric particles, if half of the particles are mirror images of the others, and (3) an even more artificial case (No. 4, p. 50, van de Hulst, 1957). Also included in (2.9) are Rayleigh scattering (Section 2.2) and Mie scattering (Section 2.3).

The immediate aim of theoretical work on single scattering is to provide computations of k_{sca}, $\tilde{\omega}$ and $\mathbf{P}$ for different particles. The ultimate goal, however, is a systematic understanding of the manner in which scattered radiation depends on the nature (shape, size distribution and optical properties) of the particles. For spherical particles a complete quantitative understanding is possible. For non-spherical particles a partial understanding of the scattering behavior is available, based on (1) physical interpretations of features in the radiation scattered by spheres and the dependence of these features on particle shape, (2) theoretical computations for a few specific nonspherical particles, and (3) laboratory and field observations.

2.1. GEOMETRICAL OPTICS

Light scattering by large particles can be understood through the concepts of geometrical optics. The technique of ray-tracing can be used in particular cases to obtain accurate numerical results. However, the most useful function of such computations is the physical explanation they provide for many of the features in light scattered by particles of size $\gtrsim$ wavelength.

Light incident on a particle which is larger than the wavelength may be thought of as consisting of separate rays which pursue independent paths. If the particle size is at least several times the wavelength it is possible to distinguish between rays striking different local regions on the particle's surface. The qualitative basis for the localization of rays is contained in Huygen's notion that all points on a wavefront should be visualized as centers of secondary spherical waves; by adding the condition that the secondary waves interfere according to their phase differences Fresnel obtained a semi-quantitative description of ray localization (van de Hulst, 1957, Chapter 3).

Figure 4 illustrates the terminology for the different contributions to light scattered by a large particle. The division of rays into these components can be made for large particles of any shape, but the fraction of light going into the different components depends on the particle shape and orientation.
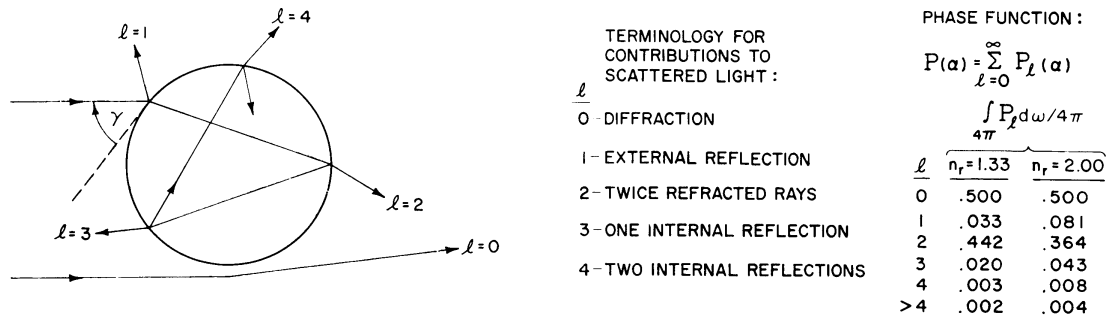

TERMINOLOGY FOR CONTRIBUTIONS TO SCATTERED LIGHT:	PHASE FUNCTION:

$$P(\alpha) = \sum_{\ell=0}^{\infty} P_\ell(\alpha)$$

ℓ		$\int P_\ell d\omega / 4\pi$
0 - DIFFRACTION		

		$n_r=1.33$	$n_r=2.00$
1 - EXTERNAL REFLECTION	ℓ		
2 - TWICE REFRACTED RAYS	0	.500	.500
3 - ONE INTERNAL REFLECTION	1	.033	.081
	2	.442	.364
4 - TWO INTERNAL REFLECTIONS	3	.020	.043
	4	.003	.008
	>4	.002	.004

Fig. 4.   Paths of light rays scattered by a sphere according to geometrical optics. $P \equiv P^{11}$ is the phase function, α the scattering angle, and γ the incident angle on the sphere for rays which strike the particle. The table on the right gives the fraction of the total scattered light contained in each value of l for non-absorbing spheres with refractive indices 1.33 and 2.0.

The light rays which miss the particle ($l=0$) are partially diffracted into its geometrical shadow. The amount of diffracted light is equal to the amount striking the particle, independently of the particle shape and refractive index. Thus for a large particle $Q_{ext}=2$, and if the particle is non-absorbing the diffraction constitutes exactly half of the scattered light. The diffraction is concentrated in the forward direction ($\alpha \sim 0°$), with its exact angular distribution a function only of the particle's geometrical shadow. The polarization of light diffracted by large particles is the same as that of the incident light.

The intensity and polarization of the light reflected and refracted by the particle surface may be computed from the Fresnel reflection coefficients (Born and Wolf, 1959, Section 13.4):

$$|R_r|^2 = \frac{(\sin\gamma - u)^2 + v^2}{(\sin\gamma + u)^2 + v^2},$$

$$|R_l|^2 = \frac{[(n_r^2 - n_i^2)\sin\gamma - u]^2 + (2n_r n_i \sin\gamma - v)^2}{[(n_r^2 - n_i^2)\sin\gamma + u]^2 + (2n_r n_i \sin\gamma + v)^2}, \tag{2.10}$$

where

$$u = \left\{ \frac{n_r^2 - n_i^2 - \cos^2\gamma + [(n_r^2 - n_i^2 - \cos^2\gamma)^2 + 4n_r^2 n_i^2]^{1/2}}{2} \right\}^{1/2},$$

$$v = \left\{ \frac{-(n_r^2 - n_i^2 - \cos^2\gamma) + [(n_r^2 - n_i^2 - \cos^2\gamma)^2 + 4n_r^2 n_i^2]^{1/2}}{2} \right\}^{1/2}.$$

$$(2.10)$$

$|R_r|^2$ and $|R_l|^2$ are the reflection coefficients for the components of the intensity perpendicular and parallel, respectively, to the plane of scattering.

The intensity and polarization for reflection from the outside of the particle ($l=1$) follow immediately from (2.10). For a nonabsorbing sphere with $n_r \lesssim 1.5$ the externally reflected light makes up only a few percent of the total scattered light, but the fraction increases as n_r or n_i increases. For randomly oriented convex nonspherical particles the angular distribution and polarization of the externally reflected light are the same as for spheres.

The rays which are refracted twice without any internal reflections ($l=2$) make up a large fraction of the scattered light for transparent or partially transparent spheres. This is generally true for nonspherical particles, but the exact fraction does depend on the particle shape even if the particles are randomly oriented.

The light which is internally reflected in particles ($l \geqslant 3$) represents no more than a few percent of the scattered light. However, for spheres the energy in the $l=3$ and $l=4$ terms is sufficiently concentrated to give rise to the primary and secondary rainbows.

Numerical results for single scattering can be obtained in the approximation of geometrical optics by considering a number of uniformly spaced rays striking a particle, computing the reflection and transmission coefficients from Fresnel's equations, using Snell's law for the directions of the refracted parts of the rays and summing the results over all incident rays and all significant components ($l=0$, 1, 2, etc.). In the results for spheres illustrated in this section, obtained by Liou and Hansen (1971), the contributions from the different rays and components were added without regard to phase. This is acceptable because in nature there is usually a size distribution of particles present which tends to wash out phase effects.

A comparison of geometrical optics and Mie theory* is illustrated in Figure 5, where the results of computations for single scattering by spheres are shown for two values of the refractive index, $n_r = 1.33$ and 1.50. These computations are for the particular size distribution*

$$n(x) = x^6 \exp(-9x/x_{\text{eff}}), \tag{2.11}$$

where $n(x)\,dx$ is the number of particles with size parameter $(2\pi r/\lambda)$ between x and $x+dx$. For the purpose of comparing geometrical optics and Mie theory the size

---

* Both Mie scattering and the influence of the size distribution on the scattered light are treated in detail in Section 3.3.
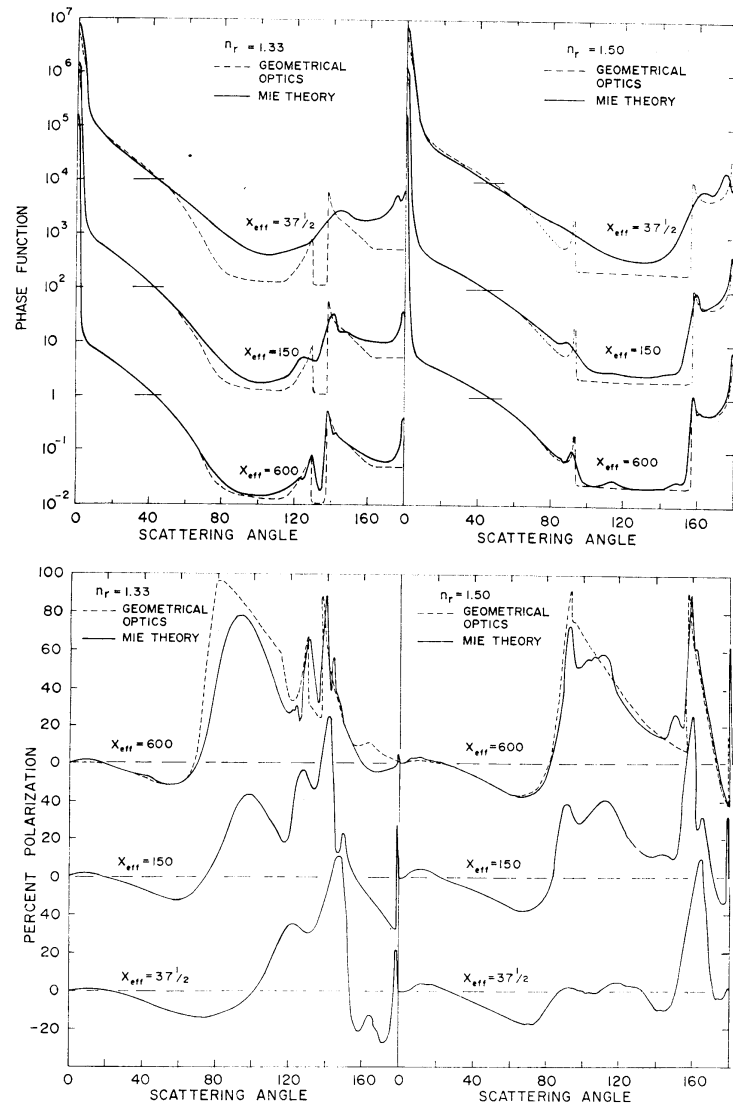
Fig. 5. Comparison of geometrical optics and Mie theory. The phase function (upper figure) and percent polarization (lower figure) are for single scattering of unpolarized light by spheres. Results are shown for two real refractive indices and three values of x_{eff}, which is the effective size parameter for the size distribution (2.11). For the phase function the scale applies to the curves for $x_{\text{eff}} = 600$, the other curves being successively displaced upward by a factor of 100.

distribution is adequately characterized by the effective size parameter, x_{eff}, which is a certain average size parameter for the distribution. The width of the size distribution does have a noticeable influence on Mie results, for which phase effects are exactly computed. However, the width of the distribution (2.11), is sufficient to wash out interference effects except for one mentioned below.

The concentration of light near $\alpha = 0°$ is the diffraction ($l = 0$), which is unpolarized for the assumed case of unpolarized incident light. The external reflection ($l = 1$) does not leave any apparent feature in the intensity, but it is strongly polarized and causes the broad positive polarization for $\alpha \sim 80-120°$. The energy contained in the twice

refracted rays $(l=2)$ is concentrated in the forward-scattering hemisphere and is negatively polarized.

The features at $\alpha \sim 137°$ and $130°$ for $n_r = 1.33$ ($157°$ and $93°$ for $n_r = 1.5$) are the primary and secondary 'rainbows'. Rainbows occur for $l \geqslant 3$ when the scattering angle has an extremum as a function of the incident angle on the sphere, γ (Figure 4). For example, for $n_r = 1.33$ as γ varies from $90°$ (central incidence) to $0°$ (grazing incidence) the scattering angle for rays internally reflected once, computed with Snell's law, decreases from $180°$ until it reaches $\sim 137°$ (the angle of 'minimum deviation') from which it then increases. The resulting concentration of energy at $137°$ and just greater angles is the primary rainbow. Similarly the second rainbow arises from $l = 4$ rays at an angle of maximum deviation.*

The minor feature on the large scattering angle side of the primary rainbow is the first 'supernumerary bow'. This is not rendered by the geometrical optics computations of Figure 5 because it is an interference feature. At these scattering angles there are $l = 3$ rays with two different incident angles emerging with the same scattering angle; these rays optically interfere causing the supernumerary bows. The number and strength of the supernumerary bows depends on the shape of the size distribution, as discussed in Section 2.3.

The enhanced intensity in the backscattering direction, $\alpha \sim 180°$, is the so-called 'glory'. This is caused specifically by the spherical shape** of the scatterers which serves to focus certain rays at $\alpha \sim 180°$.[†] There are essentially two origins for these rays: edge rays $(\gamma \sim 0°)$ which set up surface waves on the sphere and noncentral rays $(0° < \gamma < 90°)$ which emerge at $\alpha = 180°$ after internal reflection. The surface waves are not included in the formulation of geometrical optics, and their contribution decreases as the particle size increases. For refractive indices in the range $\sqrt{2} \leqslant n_r \leqslant 2$ a noncentral ray can emerge at $\alpha = 180°$ after just one internal reflection; this gives rise to the intense glory shown in Figure 5 for $n_r = 1.5$. Bryant and Jarmie (1974) give a good detailed discussion of the glory.

With these interpretations of the features in the light scattered by spheres, geometrical optics and Mie theory can be compared to determine the extent to which different rays can be localized. Figure 5 illustrates that there is a close quantitative agreement between geometrical optics and Mie theory only if the value of the size parameter is at least several hundred. However, most of the features of geometrical optics remain visible to a much smaller particle size. With decreasing particle size the light in the individual features is blurred over a wider range of angles than predicted by geometrical optics, and the higher values of l are affected first because they have a more detailed path within the sphere. Thus the second rainbow $(l=4)$ is quite smooth in the intensity for $x_{\mathrm{eff}} = 150$, and is lost for $x_{\mathrm{eff}} = 37\frac{1}{2}$ while the primary rainbow $(l=3)$ is still easily visible in both cases.

---

* Thus by 'rainbow' we refer to a concentration of rays from an internally reflected component $(l \geqslant 3)$ at an angle of minimum or maximum deviation other than $0°$ or $180°$.

** Unlike the rainbow, which requires only that the particle have a circular cross-section.

† The same type of focusing occurs at $\alpha \sim 0°$, but the effect is lost in the much stronger diffracted light.

Figure 5 also illustrates that the polarization for single scattering, as compared to the intensity, contains stronger imprints of most of the features occurring in the scattered light. In addition, for the polarization these features remain visible to smaller size parameters. These conclusions hold for the rainbows, the supernumerary bows, the glory and the external reflection, but not for the light which is diffracted or twice refracted.

2.2. RAYLEIGH SCATTERING

The simplest scattering behavior is that of small particles. This is called Rayleigh scattering because its basic characteristics were deduced by Lord Rayleigh (1871) in a successful explanation of the color and polarization of skylight.

Two conditions are required for Rayleigh scattering. The particle size must be much less than the wavelength of the incident radiation and much less than the wavelength of the radiation after it penetrates into the particle:

$$\text{size} \ll \lambda,$$

and

$$\text{size} \ll \lambda/|n_c|,$$

where $n_c = n_r - in_i$ is the complex refractive index of the particle. The first condition means that the particle can be considered as being in a homogeneous external electric field. The second condition means that the incident radiation penetrates the particle so quickly that the particle's own field is set up in a time which is short compared to the period of the incident radiation.

The incident radiation induces a dipole moment in the particle proportional to the

$$E_r^s \propto E_r^i$$

$$E_\ell^s \propto E_\ell^i \cos\alpha$$

$$\text{Polarization} = \frac{I_r - I_\ell}{I_r + I_\ell}$$
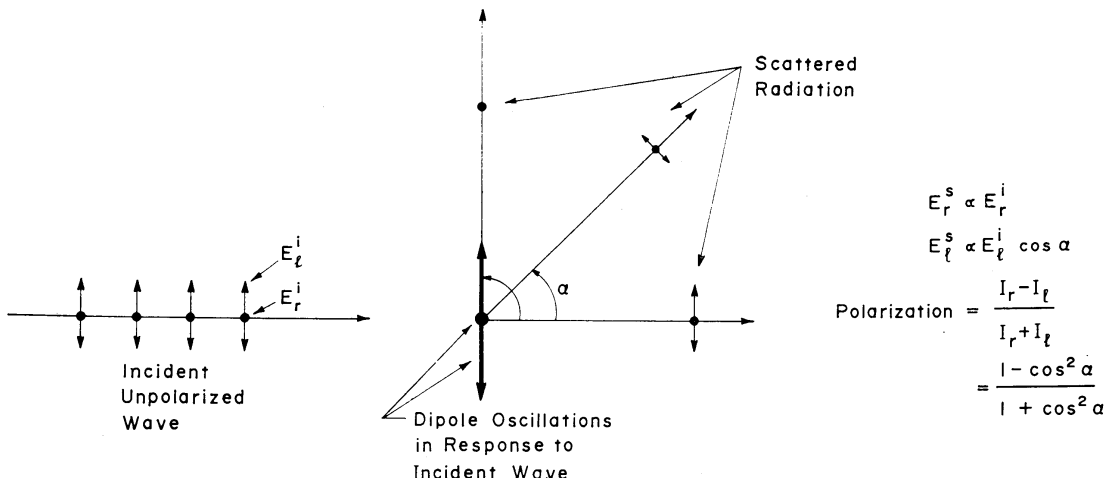
$$= \frac{1 - \cos^2\alpha}{1 + \cos^2\alpha}$$

Fig. 6. Schematic representation of isotropic Rayleigh scattering. The unpolarized wave incident from the left can be represented by two linearly polarized waves vibrating at right angles to each other with equal electrical field strengths ($E_\ell^i = E_r^i$) and a random phase relationship. The electrons in a small particle oscillate in response to the electric components of the incident wave, giving rise to the dipoles represented by the heavy arrow and dot. The dipole radiation is proportional to $\sin\beta$ (2.13), where $\beta = \pi/2$ for the perpendicular component and $\beta = \pi/2 - \alpha$ for the parallel component.

incident electric field,

$$p = \alpha_p E^i,\tag{2.12}$$

where the proportionality constant, α_p, is called the polarizability. For a particle with isotropic polarizability the induced dipole moment is in the same direction as the applied field, for any particle orientation. In the far-field, i.e., at a distance $R \gg \lambda$, the electric field of the scattered wave is (Born and Wolf, 1959, Section 2.2.3).

$$E^s = \frac{k^2 p \sin \beta}{R} \exp(-ikR),\tag{2.13}$$

where β is the angle between the direction of the dipole moment and the direction of scatter. Thus the dipole does not radiate in its direction of vibration, and for incident unpolarized light the angular distribution of the intensity of scattered light is proportional to $(1+\cos^2 \alpha)$, cf. Figure 6.

Phase matrix. For isotropic* Rayleigh scattering the phase matrix follows from (2.13), (cf. Chandrasekhar, 1950):

$$\mathbf{P}(\alpha) = \begin{cases} \frac{3}{4}(1 + \cos^2 \alpha) & -\frac{3}{4}\sin^2 \alpha & 0 & 0 \\ -\frac{3}{4}\sin^2 \alpha & \frac{3}{4}(1 + \cos^2 \alpha) & 0 & 0 \\ 0 & 0 & \frac{3}{2}\cos \alpha & 0 \\ 0 & 0 & 0 & \frac{3}{2}\cos \alpha \end{cases}.\tag{2.14}$$

The major application of Rayleigh scattering is to gaseous molecular scattering. Although most real molecules exhibit some anisotropy, this can be accounted for without any fundamental difficulty. The phase matrix for anisotropic Rayleigh particles in random orientation is**

$$\mathbf{P}(\alpha) = \Delta \begin{cases} \frac{3}{4}(1 + \cos^2 \alpha) & -\frac{3}{4}\sin^2 \alpha & 0 & 0 \\ -\frac{3}{4}\sin^2 \alpha & \frac{3}{4}(1 + \cos^2 \alpha) & 0 & 0 \\ 0 & 0 & \frac{3}{2}\cos \alpha & 0 \\ 0 & 0 & 0 & \Delta'\frac{3}{2}\cos \alpha \end{cases}$$

$$+ (1 - \Delta) \begin{cases} 1 & 0 & 0 & 0 \\ 0 & 0 & 0 & 0 \\ 0 & 0 & 0 & 0 \\ 0 & 0 & 0 & 0 \end{cases},\tag{2.15}$$

where

$$\Delta = \frac{1 - \delta}{1 + \delta/2},$$

$$\Delta' = \frac{1 - 2\delta}{1 - \delta},\tag{2.16}$$

---

* Isotropic of course refers here to a property of the particle, and not to the directional distribution of the scattered light.

** The problem of scattering by anisotropic Rayleigh particles in random orientation was solved by Rayleigh (1918). The results were put in a form close to that of (2.15) by Chandrasekhar (1950).

and δ, the so-called depolarization factor, is the ratio of intensities parallel and perpendicular to the plane of scattering, I_l/I_r, for light scattered at $\alpha = 90°$ with the incident light unpolarized. For isotropic Rayleigh scattering $\delta = 0$, and in general $0 \leqslant \delta \leqslant 1/2$. A table of measured values of δ for a number of gases is given by Penndorf (1957); some values are: $H_2 \sim 0.02$, $N_2 \sim 0.03$, air ~ 0.03, $O_2 \sim 0.06$ and $CO_2 \sim 0.09$.

For unpolarized incident light the degree of linear polarization for anisotropic Rayleigh scattering is

$$\frac{I_{pol}}{I} = \frac{\sin^2 \alpha}{1 + \cos^2 \alpha + 2\delta/(1 - \delta)}. \tag{2.17}$$

Thus it is clear that the anisotropy reduces the degree of polarization at all scattering angles.

Hansen (1971b) has shown that the fourth row and fourth column of the phase matrix may, for all practical purposes, be omitted in many problems involving Mie scattering or a combination of Mie and Rayleigh scattering. Equation (2.15) illustrates that the required three-by-three phase matrix for anisotropic Rayleigh scattering has a very simple form, as has also been shown by Chandrasekhar (1950). It is the sum of two terms, one proportional to isotropic Rayleigh scattering and one proportional to isotropic scattering,

$$P(\alpha) = A P_r(\alpha) + (1 - A) P_I(\alpha). \tag{2.18}$$

Scattering coefficient. The scattering and absorption cross-sections for small particles of several different shapes are given by van de Hulst (1957). The most important results are those for isotropic Rayleigh spheres, for which the efficiency factors are

$$Q_{sca} = \tfrac{8}{3} x^4 \left| \frac{n_c^2 - 1}{n_c^2 + 2} \right|, \tag{2.19}$$

and

$$Q_{abs} = -4x \operatorname{Im} \left\{ \frac{n_c^2 - 1}{n_c^2 + 2} \right\}. \tag{2.20}$$

Thus, if the refractive index is complex, the absorption dominates over the scattering as $x \to 0$. The dependence of Q_{sca} on the fourth power of x contrasts to the result $Q_{sca} = $ constant for geometrical optics. The reason for this fundamental difference is that all parts of the Rayleigh particle scatter in phase; thus the electric field of the scattered radiation is proportional to r^3, the intensity is proportional to r^6 and Q_{sca} is proportional to r^4.

The scattering coefficient per unit length for anisotropic gaseous molecules in random orientation, due to Rayleigh (1918) and Cabannes (1929), is

$$k_{sca} = \frac{8\pi^3}{3} \frac{(n_g^2 - 1)^2}{\lambda^4 N} \frac{6 + 3\delta}{6 - 7\delta}, \tag{2.21}$$

where N is the number of molecules per unit volume, n_g is the refractive index of the

gas, and the last factor arises from the anisotropy. Thus the average scattering cross-section per particle is

$$\bar{\sigma}_{\text{sca}} = \frac{k_{\text{sca}}}{N} = \frac{8\pi^3}{3} \frac{(n_g^2 - 1)^2}{\lambda^4 N^2} \frac{6 + 3\delta}{6 - 7\delta}. \tag{2.22}$$

The basis for (2.21) and (2.22) is Rayleigh's relation for the intensity of light scattered by a small particle:

$$I(\alpha) = I_0 \left(\frac{2\pi}{\lambda}\right)^4 \alpha_p^2 \tfrac{1}{2} (1 + \cos^2 \alpha) \tag{2.23}$$

(2.22) can be obtained by averaging (2.23) over all scattering angles, using the relation between the polarizability and the experimentally measurable index of refraction,

$$\alpha_p = \frac{n_g^2 - 1}{4\pi N}, \tag{2.24}$$

and including the factor arising from anisotropy.

For a mixture of gases

$$k_{\text{sca}} = \frac{8\pi^3}{3\lambda^4 N} \sum_i v_i (n_{g,i}^2 - 1)^2 \frac{6 + 3\delta_i}{6 - 7\delta_i}, \tag{2.25}$$

where v_i is the fraction by volume of gas i.

P-τ relation. A relation between atmospheric pressure and the optical thickness due to Rayleigh scattering can be simply derived. Outside of absorption bands the Rayleigh optical thickness due to the gaseous atmosphere above height h is

$$\tau_R(h) = \int_h^\infty \kappa_{\text{sca}} \, \varrho \, dh', \tag{2.26}$$

where ϱ is the density of gas and κ_{sca} is the scattering coefficient per unit mass. Assuming hydrostatic equilibrium the pressure is

$$P(h) = \int_h^\infty g \, \varrho \, dh', \tag{2.27}$$

where g is the acceleration of gravity. In the common case in which the dependence of κ_{sca} and g on height can be neglected, we obtain immediately

$$P = \frac{g \tau_R}{\kappa_{\text{sca}}}. \tag{2.28}$$

Since $k_{\text{sca}} = \kappa_{\text{sca}} \varrho$ and $\varrho = \bar{\mu} N$, where $\bar{\mu}$ is the mean molecular mass,

$$P = g \bar{\mu} \tau_R \left[\frac{8\pi^3}{3\lambda^4 N^2} \sum_i v_i (n_{g,i}^2 - 1)^2 \frac{6 + 3\delta_i}{6 - 7\delta_i} \right]^{-1}. \tag{2.29}$$

Values for the temperature and pressure dependent quantities in the square brackets can be taken for any single set of conditions, e.g., for STP; in the latter case N is equal to Loschmidt's number. A relation between P and τ analogous to (2.29) was obtained by Pollack (1967). The path followed by Pollack is longer, however, and includes a detour through the properties of air.

The optical thickness of the Earth's atmosphere, obtained by treating air as a single gas with $\delta = 0.031$ (de Vaucouleurs, 1951) and taking the other numerical quantities from Allen (1963, p. 114), is

$$\tau_0 = 0.008569\,\lambda^{-4}(1 + 0.0113\,\lambda^{-2} + 0.00013\,\lambda^{-4}) \qquad [\lambda \text{ in } \mu] \qquad (2.30)$$

for the standard surface pressure $P_0 = 1013.25$ mb. For $\lambda = 0.55\mu$ (2.30) yields $\tau_0 \sim$ ~ 0.0973. This equation differs slightly from a λ^{-4} law, due to the wavelength dependence of the index of refraction. The optical depth above any pressure level, P, can be found from

$$\tau = \tau_0\,\frac{P}{P_0}. \qquad (2.31)$$

The optical thickness of a pure CO_2 atmosphere provides another useful example for application of (2.29). For $\delta = 0.09$, $\bar{\mu} = 44 \times 1.66 \times 10^{-24}$ gm, surface pressure and gravity appropriate for Venus ($P = 93\,P_0$, $g = 870$ cm s^{-2}) and other constants from Allen (pp. 87, 114) we obtain

$$\tau_0 = 1.527\,\lambda^{-4}(1 + 0.013\,\lambda^{-2}). \qquad [\lambda \text{ in } \mu] \qquad (2.32)$$

For $\lambda = 0.55\mu$ this yields $\tau_0 \sim 17.4$. For the surface pressure and gravity of Earth the result is $\tau_0(\lambda = 0.55\mu) \sim 0.166$ for a pure CO_2 atmosphere; this is about 70% greater than the optical thickness for air.

2.3. Mie scattering

For particles of an arbitrary shape and composition the electric field of the scattered radiation at a distance R from the particle (in the far-field) may be represented by

$$\begin{Bmatrix} E_r^s \\ E_l^s \end{Bmatrix} = \frac{\exp(-ikR + ikz)}{ikR} \begin{Bmatrix} S_1(\alpha, \varphi) & S_4(\alpha, \varphi) \\ S_3(\alpha, \varphi) & S_2(\alpha, \varphi) \end{Bmatrix} \begin{Bmatrix} E_r^i \\ E_l^i \end{Bmatrix}, \qquad (2.33)$$

where the incident radiation propagates in the positive z direction. Computation of the two-by-two scattering matrix $\mathbf{S}$ is the primary task in single scattering theory, since the quantities k_{sca}, $\mathbf{P}$ and $\tilde{\omega}$ can be obtained from $\mathbf{S}$. The four elements of this matrix are in general complex numbers which are functions of the scattering angle, α, and an azimuth angle, φ, measured about the direction of scatter.

For the special case of isotropic homogeneous spheres* the scattering matrix in

---

* For simplicity the adjectives 'isotropic homogeneous' are omitted in the remainder of this paper. The scattering of electromagnetic radiation by such spheres is referred to as Mie scattering, after G. Mie (1908) who presented a complete mathematical solution along with computations and illustrations. A solution for nonabsorbing spheres had been given by Lorenz (1898) and contributions were also made by many others (cf. Kerker, 1969, Section 3.4).

(2.33) has the simple form

$$\mathbf{S} = \begin{Bmatrix} S_1(\alpha) & 0 \\ 0 & S_2(\alpha) \end{Bmatrix}.$$ (2.34)

It follows that the Stokes parameters, Equation (1.4), of the incident and scattered radiation are related by

$$\mathbf{I} = \frac{1}{k^2 R^2} \mathbf{F} \mathbf{I}_0,$$ (2.35)

where, following van de Hulst (1957), we use the symbol **F** for the four-by-four transformation matrix:

$$\mathbf{F} = \begin{Bmatrix} \frac{1}{2}(S_1 S_1^* + S_2 S_2^*) & \frac{1}{2}(S_1 S_1^* - S_2 S_2^*) & 0 & 0 \\ \frac{1}{2}(S_1 S_1^* - S_2 S_2^*) & \frac{1}{2}(S_1 S_1^* + S_2 S_2^*) & 0 & 0 \\ 0 & 0 & \frac{1}{2}(S_1 S_2^* + S_2 S_1^*) & \frac{i}{2}(S_1 S_2^* - S_2 S_1^*) \\ 0 & 0 & -\frac{i}{2}(S_1 S_2^* - S_2 S_1^*) & \frac{1}{2}(S_1 S_2^* + S_2 S_1^*) \end{Bmatrix}.$$ (2.36)

The transformation matrix is proportional to the phase matrix,

$$\mathbf{F} = c\mathbf{P}.$$ (2.37)

The proportionality constant follows from the normalization condition on **P**, Equation (2.5), which yields

$$c = \int_{4\pi} F^{11} \frac{d\Omega}{4\pi}$$ (2.38)

and the definition of the scattering cross-section,

$$\sigma_{sca} = \int_{4\pi} I R^2 \, d\Omega / I_0 = \frac{1}{k^2} \int_{4\pi} F^{11} \, d\Omega.$$ (2.39)

Thus

$$c = \frac{k^2 \sigma_{sca}}{4\pi}$$ (2.40)

and the specific relations between the matrix elements are

$$F^{11} = \frac{k^2 \sigma_{sca}}{4\pi} P^{11} = \frac{1}{2}(S_1 S_1^* + S_2 S_2^*),$$

$$F^{21} = \frac{k^2 \sigma_{sca}}{4\pi} P^{21} = \frac{1}{2}(S_1 S_1^* - S_2 S_2^*),$$ (2.41)

$$F^{33} = \frac{k^2 \sigma_{\text{sca}}}{4\pi} P^{33} = \tfrac{1}{2}(S_1 S_2^* + S_2 S_1^*),$$

$$F^{43} = \frac{k^2 \sigma_{\text{sca}}}{4\pi} P^{43} = -\frac{i}{2}(S_1 S_2^* - S_2 S_1^*). \tag{2.41}$$

Single sphere. The Mie theory provides the solution for the scattering matrix of a single sphere in the form of two infinite series:

$$S_1 = \sum_{n=1}^{\infty} \frac{2n+1}{n(n+1)} [a_n \pi_n + b_n \tau_n],$$

$$S_2 = \sum_{n=1}^{\infty} \frac{2n+1}{n(n+1)} [b_n \pi_n + a_n \tau_n]. \tag{2.42}$$

S_1, S_2, a_n and b_n are in general complex.

π_n and τ_n are functions of only the scattering angle α. They are simply related to the Legendre polynomials and are easily computed from recursion relations. The first two are:

$$\begin{aligned} \pi_1(\alpha) &= 1 & \tau_1 &= \cos\alpha \\ \pi_2(\alpha) &= 3\cos\alpha & \tau_2 &= 3\cos 2\alpha. \end{aligned} \tag{2.43}$$

The heart of the Mie scattering problem is the computation of the coefficients a_n and b_n. These are functions of only the complex refractive index, $n_c = n_r - i n_i$, and the size parameter, $x = 2\pi r/\lambda$. The expressions for a_n and b_n (van de Hulst, 1957), which involve spherical Bessel functions, can also be computed with recursion relations. Appropriate methods of numerical computation have been discussed by Kattawar and Plass (1967) and Dave (1969).

The scattering and extinction efficiency factors also follow from the coefficients a_n and b_n (van de Hulst, 1957),

$$Q_{\text{sca}} = \frac{2}{x^2} \sum_{n=1}^{\infty} (2n+1)(a_n a_n^* + b_n b_n^*), \tag{2.44}$$

$$Q_{\text{ext}} = \frac{2}{x^2} \sum_{n=1}^{\infty} (2n+1) \operatorname{Re}(a_n + b_n), \tag{2.45}$$

as does the asymmetry factor,

$$\langle \cos\alpha \rangle = \frac{4}{x^2 Q_{\text{sca}}} \sum_{n=1}^{\infty} \left[\frac{n(n+2)}{n+1} \operatorname{Re}(a_n a_{n+1}^* + b_n b_{n+1}^*) + \frac{2n+1}{n(n+1)} \operatorname{Re}(a_n b_n^*) \right]. \tag{2.46}$$

As noted by Irvine (1963), the asterisks in (2.46) were inadvertently omitted by van de Hulst (1957).

The total number of terms which must be used in these series is slightly larger than the size parameter x, since the values of a_n and b_n rapidly approach zero as n becomes larger than x. The physical explanation for this is important and is related to the concept of ray localization. According to the localization principle the nth term in each of the above series roughly corresponds to the contribution from the light ray passing the center of the sphere at a distance $n\lambda/2\pi$, provided $x \gg 1$. (This is analogous to partial wave analysis in quantum theory, in which the nth term is associated with an orbital angular momentum h/λ at an impact parameter $n\lambda/2\pi$.) Thus the series converges shortly after n exceeds x, because higher terms correspond to light rays missing the sphere.

The infinite series in (2.42) can be physically interpreted as a multipole expansion of the scattered light (Mie, 1908). The coefficients a_1, a_2 and a_3, for example, specify the amount of electric dipole, quadrupole and octupole radiation, while the b_n are the coefficients for magnetic multipole radiation. For particles which are small and do not have a large refractive index only the electric dipole radiation is significant, and the well-known Rayleigh scattering results. In the case of small x and large $|n_c|$ there are sharply defined values of x for which a single a_n or b_n becomes very large; these are resonance phenomena (cf., van de Hulst, 1957, Section 10.5). However for large particles all multipoles with $n \lesssim x$ contribute, and the physical concept of multipole radiation does not prove to be of much practical value.

Size distribution. In nature a distribution of particle sizes is usually encountered. Under the assumption of independent scattering the transformation matrix for a unit volume is given by

$$F^{ij}(\alpha) = \int\limits_{r_1}^{r_2} F^{ij}(\alpha, r)\, n(r)\, dr,$$ (2.47)

where $n(r)\, dr$ is the number of particles per unit volume with radius between r and $r + dr$, r_1 and r_2 are the smallest and largest particles in the size distribution, and $F^{ij}(\alpha, r)$ is one of the elements of the transformation matrix for a particle of radius r. The scattering and extinction coefficients are

$$k_{\text{sca}} = \int\limits_{r_1}^{r_2} \sigma_{\text{sca}}(r)\, n(r)\, dr = \int\limits_{r_1}^{r_2} \pi r^2 Q_{\text{sca}}(r)\, n(r)\, dr,$$

$$k_{\text{ext}} = \int\limits_{r_1}^{r_2} \sigma_{\text{ext}}(r)\, n(r)\, dr = \int\limits_{r_1}^{r_2} \pi r^2 Q_{\text{ext}}(r)\, n(r)\, dr.$$ (2.48)

The normalized (dimensionless) phase matrix follows from

$$P^{ij}(\alpha) = \frac{4\pi}{k^2 k_{\text{sca}}}\, F^{ij}(\alpha),$$ (2.49)

and the single scattering albedo from

$$\tilde{\omega} = \frac{k_{\text{sca}}}{k_{\text{ext}}}.$$ (2.50)

It is straightforward to make computations for any size distribution of spheres. However it is important to have systematic computations which allow an understanding of the effect of the size distribution. This is required if measurements are to be inverted to yield properties of scattering particles.

To facilitate inversion of radiation measurements the size distribution must be described with the minimum number of parameters. Clearly the first parameter should be some measure of the mean particle size. The arithmetic mean is

$$\bar{r} = \frac{\displaystyle\int_{r_1}^{r_2} r n(r)\, dr}{\displaystyle\int_{r_1}^{r_2} n(r)\, dr} = \frac{1}{N}\int_{r_1}^{r_2} r n(r)\, dr,$$ (2.51)

where N is the total number of particles per unit volume. But since each particle scatters an amount of light proportional to $\sigma_{\text{sca}} = \pi r^2 Q_{\text{sca}}$, the 'best' single parameter describing the scattered light is the *mean radius for scattering*,

$$r_{\text{sca}} = \frac{\displaystyle\int_{r_1}^{r_2} r\pi r^2 Q_{\text{sca}}(x, n_r, n_i)\, n(r)\, dr}{\displaystyle\int_{r_1}^{r_2} \pi r^2 Q_{\text{sca}}(x, n_r, n_i)\, n(r)\, dr}.$$ (2.52)

The appearance of $Q_{\text{sca}}(x, n_r, n_i)$ in (2.52) makes r_{sca} an inconvenient parameter. However, if r_{sca} is larger than the wavelength a parameter which is almost as 'good' can be obtained by omitting Q_{sca} in (2.52).

Thus we define the *effective radius* as

$$r_{\text{eff}} = \frac{\displaystyle\int_{r_1}^{r_2} r\pi r^2 n(r)\, dr}{\displaystyle\int_{r_1}^{r_2} \pi r^2 n(r)\, dr} = \frac{1}{G}\int_{r_1}^{r_2} r\pi r^2 n(r)\, dr,$$ (2.53)

where G is the geometric cross-sectional area of particles per unit volume. Similarly, as a measure of the width of the size distribution, we define the *effective variance*,

$$v_{\text{eff}} = \frac{1}{G r_{\text{eff}}^2}\int_{r_1}^{r_2} (r - r_{\text{eff}})^2\, \pi r^2 n(r)\, dr,$$ (2.54)

where r_{eff}^2 in the denominator makes v_{eff} dimensionless. As a measure of the departure

ture of the distribution from symmetry we define the *effective skewness*,

$$S_{\text{eff}} = \frac{1}{Gr_{\text{eff}}^3 v_{\text{eff}}^{3/2}} \int_{r_1}^{r_2} (r - r_{\text{eff}})^3 \, \pi r^2 n(r) \, dr.$$ (2.55)

These definitions are analogous to characteristics used in statistics to describe frequency distribution (e.g., Kendall and Stuart, 1963), with $\pi r^2 n(r)$ corresponding to the frequency distribution.

It is useful to have a standard analytic size distribution for theoretical computations. We employ the distribution used by Hansen (1971b),

$$n(r) = \text{constant } r^{(1-3b)/b} e^{-r/ab}$$ (2.56)

as a standard distribution*, because it has the simple properties

$$\begin{aligned} a &= r_{\text{eff}} \\ b &= v_{\text{eff}} \end{aligned} \quad \text{for the size distribution (2.56)},$$ (2.57)

as may be verified by substitution into (2.53) and (2.54) with $r_1 = 0$ and $r_2 = \infty$. The standard distribution (2.56) is a variation of the gamma distribution; other forms of the gamma distribution have been used extensively for cloud particles, e.g., by Khrgian (1961) and Deirmendjian (1964). Figure 7 illustrates the standard distribution for several values of a and b. This distribution, including the normalization constant, is defined for $0 \leqslant b = v_{\text{eff}} < 0.5$ and has an effective skewness $S_{\text{eff}} = 2\sqrt{b}$. Larger values of v_{eff} can be obtained by adding a third parameter to (2.56) or by using the log-normal or power-law distribution described in the following subsection.

Numerical examples. Mie scattering computations** are a simple task for modern computers and there now exist several books and reports containing extensive tables of numerical results. Nevertheless it is useful to have graphical examples which clearly illustrate the effect of the size distribution and refractive index on the scattered light.

The first graphs which we show are for quantities independent of the scattering angle, Q_{sca}, $\tilde{\omega}$ and $\langle \cos \alpha \rangle$. Q_{sca}, the efficiency factor for scattering, is defined for a size distribution as

$$Q_{\text{sca}} = \frac{k_{\text{sca}}}{G} = \frac{\int_{r_1}^{r_2} \pi r^2 Q_{\text{sca}}(r) \, n(r) \, dr}{\int_{r_1}^{r_2} \pi r^2 n(r) \, dr}.$$ (2.58)

Q_{sca} is shown in Figure 8 for the refractive index $n_r = 1.33$, $n_i = 0$ and the standard size distribution (2.56). The computations were made for many values of a (0(0.1) 30(0.5) 100) and the results graphed as a function of $2\pi a/\lambda$, which is the effective size paramater for the standard distribution.

---

* If N is the total number of particles per unit volume, then $\text{constant} = N(ab)^{(2b-1)/b}/\Gamma[(1-2b)/b]$, where Γ is the gamma function. However, if only the normalized phase matrix is needed, the value of constant is not required.

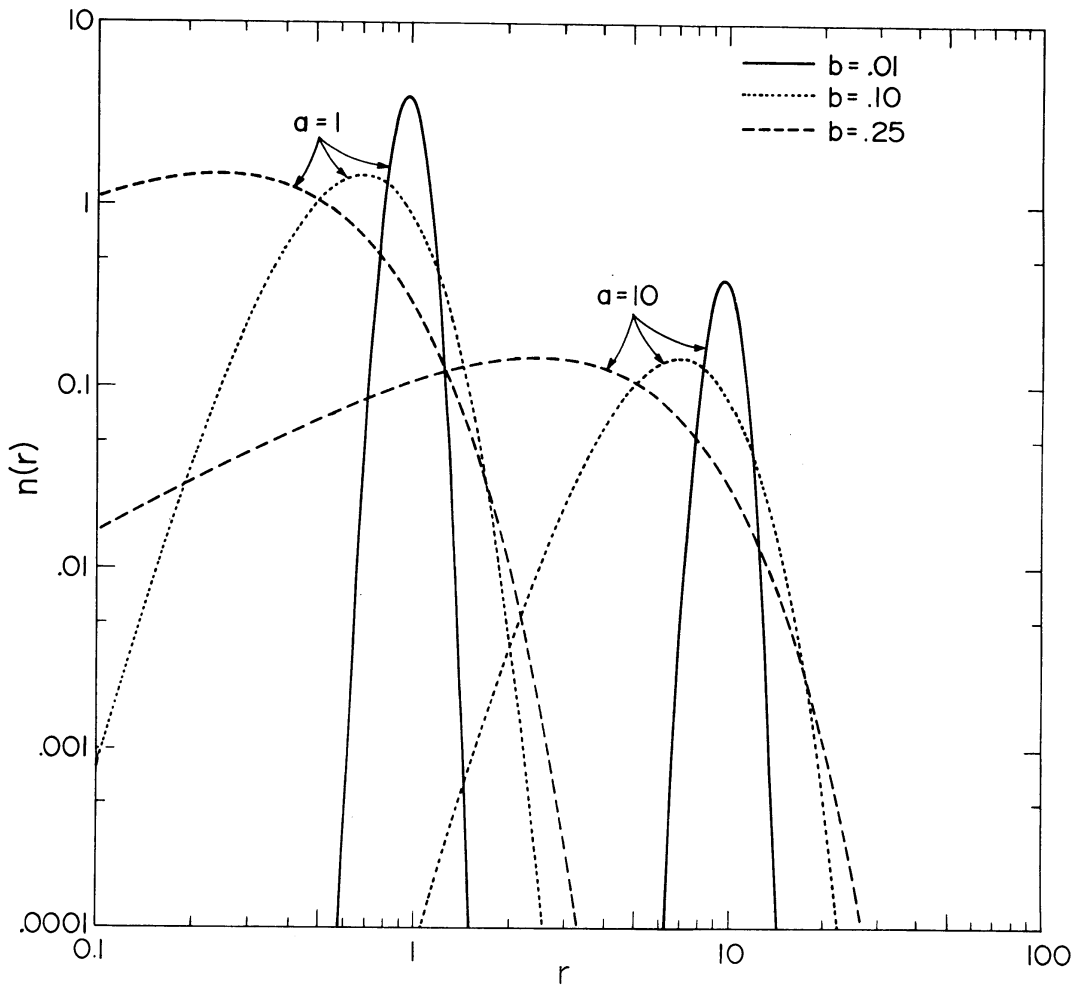** An efficient computer program is available from the author.

Fig. 7.   Standard size distribution (2.56) for 2 values of a and three values of b. The size distribution is normalized so that the integral over all sizes is $N = 1$.

The curve $b = 0$ in Figure 8 gives Q_{sca} for a single particle, as a function of $x = 2\pi r/\lambda$. This curve is characterized by a series of major maxima and minima of wavelength ~ 10 in x and superimposed 'ripples' of wavelength ~ 0.8 in x. The major maxima and minima are due to interference of light diffracted ($l = 0$) and transmitted ($l = 2$) by the particle, these two components making up $\sim 95\%$ of the scattered light (Figure 4). The phase shift for a light ray passing through the sphere along a diameter is $\varrho = 2x(n_r - 1)$. Thus constructive (or destructive) interference occurs successively at intervals $\sim 2\pi$ in ϱ, or ~ 9.5 in x for $n_r = 1.33$. The curves of Q_{sca} for other values of n_r are qualitatively similar if graphed as a function of ϱ, as shown in Figure 32 of van de Hulst (1957).

The ripple on the Q_{sca} curve for a single particle arises from the last few significant terms in the Mie series, (2.42), as demonstrated by Bryant and Cox (1966). According to the localization principle these terms arise from edge rays, i.e., from the light rays grazing the sphere. These rays set up surface electromagnetic waves which travel around the sphere spewing off energy in all directions. Since there are focal points at

$\alpha = 0°$ and $\alpha = 180°$ the main effect of the surface waves is noticed in these directions. At $\alpha = 180°$ the surface waves give rise to an enhanced intensity which contributes to the glory, and is the main cause of the glory for cases in which there is no contribution from geometrical optics. At $\alpha = 0°$ the intensity due to surface waves is small compared to the intensity of diffracted light. However the diffracted radiation and the radiation arising from the surface waves optically interfere, causing the ripples in the extinction curve. van de Hulst (1957) and Bryant and Cox (1966) suggest different phenomenological models to explain the wavelength of the ripple. In the model of van de Hulst the surface waves are assumed to take short cuts by jumping through the sphere; in the model of Bryant and Cox it is assumed that the surface waves are only slightly damped, i.e., that they involve hundreds of circumvolutions. Numerical results presented below for absorbing spheres suggest that the model of van de Hulst may be the closer to reality.
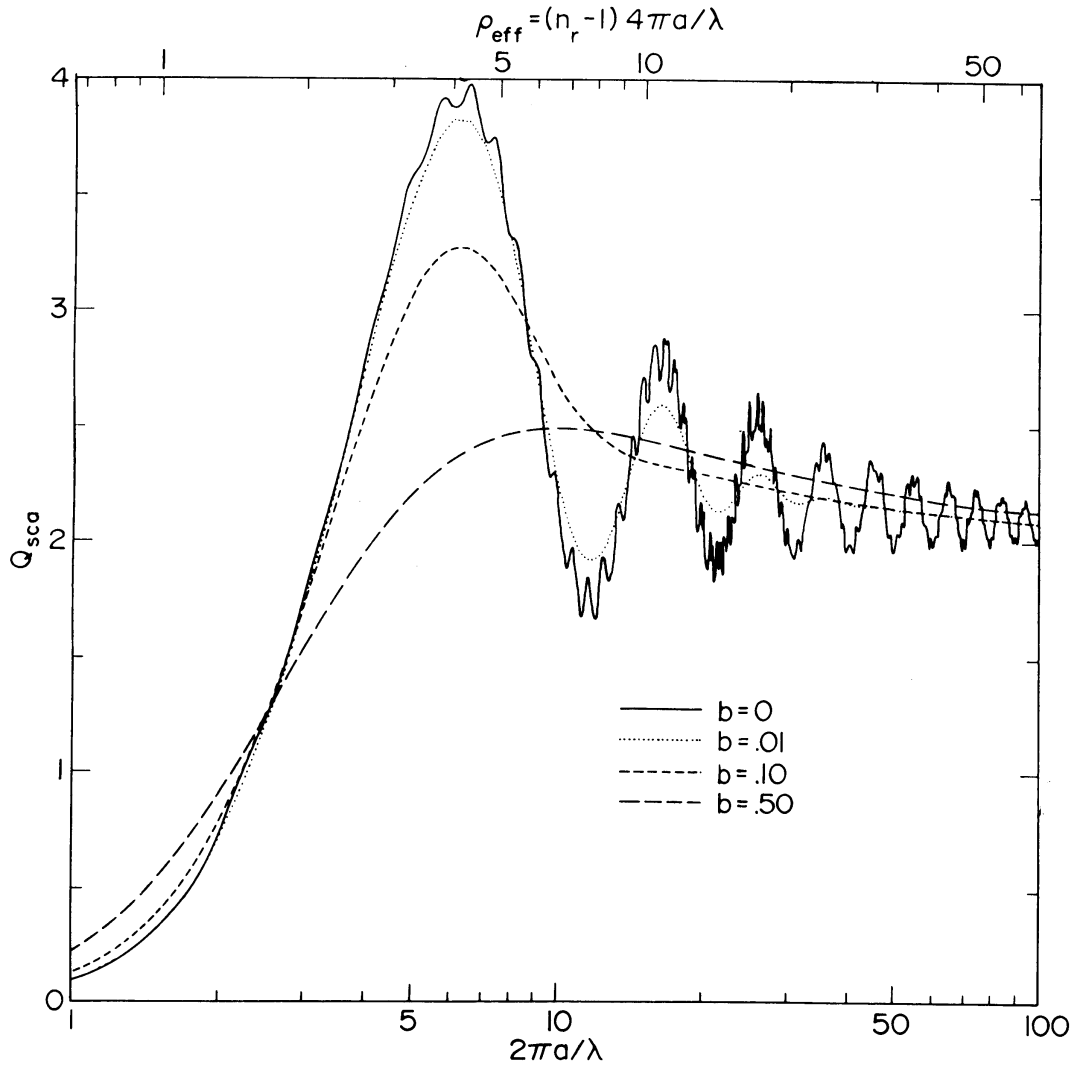

Fig. 8. Efficiency factor for scattering, Q_{sca}, as a function of the effective size parameter, $2\pi a/\lambda$. The standard size distribution (2.56) was used with four values of the effective variance b. For the case $b = 0$, $2\pi a/\lambda = 2\pi r/\lambda \equiv x$. The refractive index is $n_r = 1.33$, $n_i = 0$.

Figure 8 demonstrates that even a small dispersion of sizes* washes out the ripple in Q_{sca}. However the first major maximum persists to large values of b, so its effect must be noticeable in many cases. One example is an increase of atmospheric extinction with increasing wavelength ('anomalous extinction') which is sometimes observed (e.g., Porch *et al.*, 1973). This must be due to extinction by atmospheric aerosols with $\varrho_{eff} \sim 5$. The magnitude of the effect can serve as a rough measure of the width of the size distribution.

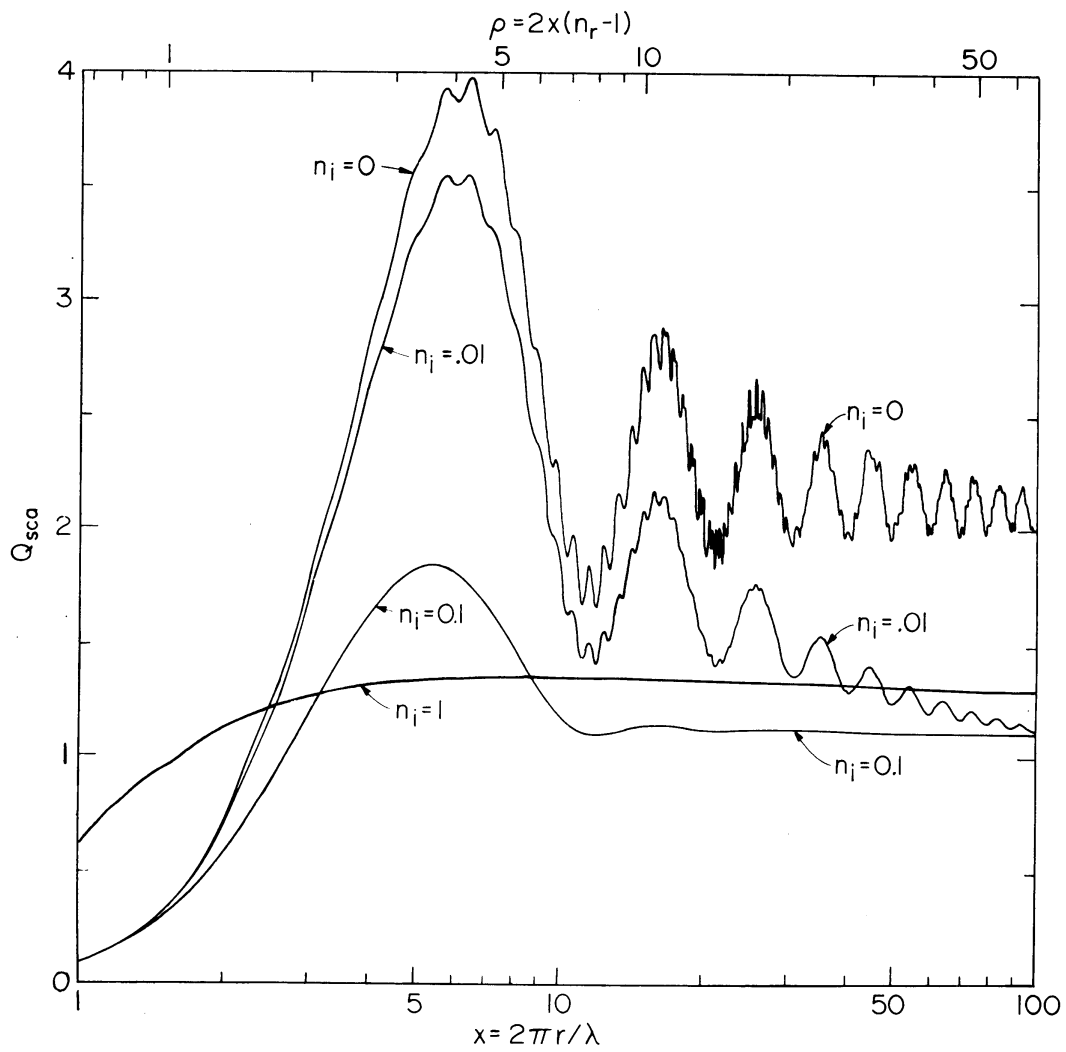Figure 9 illustrates that both the ripples and the major maxima and minima damp

Fig. 9.   Efficiency factor for scattering, Q_{sca}, as a function of the size parameter $x = 2\pi r/\lambda$. The refractive index is $n_r = 1.33$, with results shown for four values of n_i.

* v_{eff} is ~ 0.06–0.08 for the size distributions measured for particles in the stratosphere (the Junge layer) by Friend (1966) and Mossop (1965); it is ~ 0.10–0.20 for the distributions measured by Diem (1948) for water clouds, but values as large as ~ 0.5 were found by Weickmann and aufm Kampe (1953), whose measurements included larger particles than those sampled by Diem; v_{eff} is ~ 0.5–20 for the typical size distributions found by Junge (1963) for tropospheric aerosols.
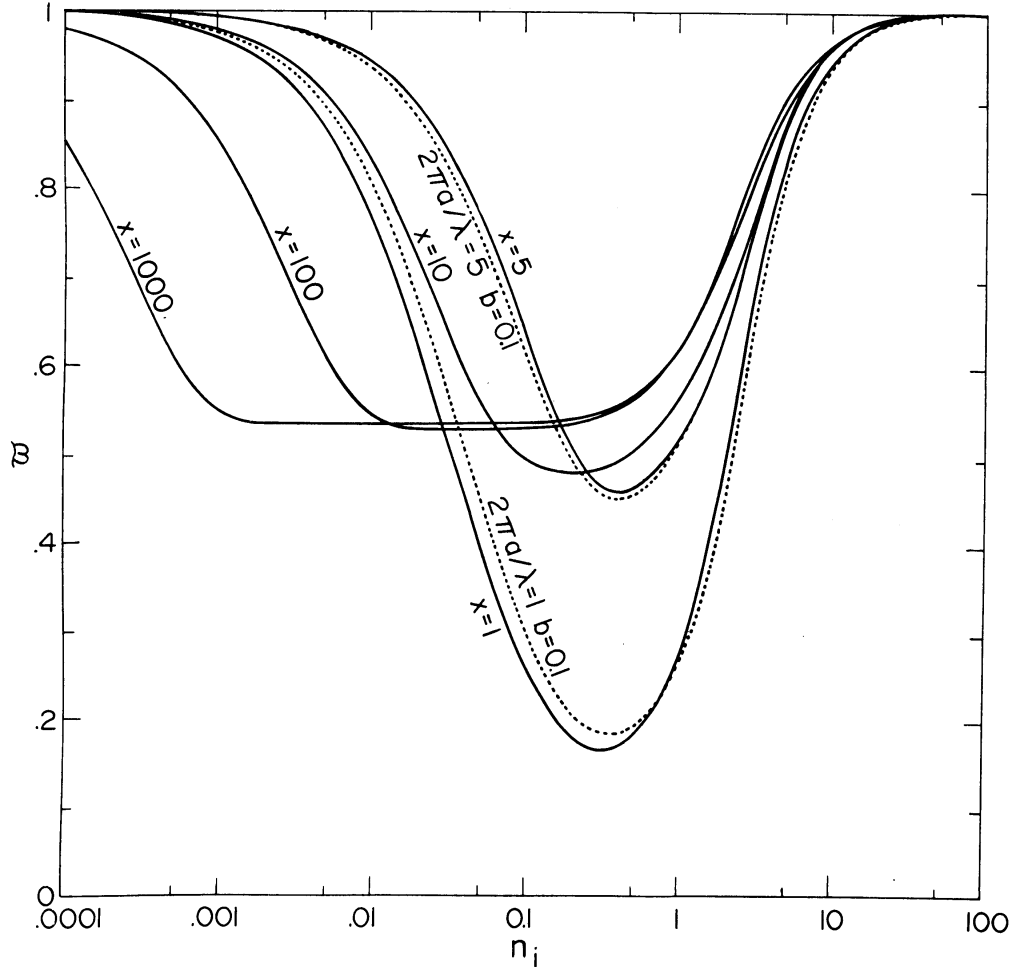
Fig. 10. Single scattering albedo, $\tilde{\omega}$, as a function of the imaginary part of the refractive index, n_i. The solid curves are for $b = 0$, corresponding to a single particle so $2\pi a/\lambda = 2\pi r/\lambda \equiv x$. The real refractive index is $n_r = 1.33$.

out as absorption within the particles increases. In geometrical optics the intensity of a light wave traversing a diameter of the sphere is decreased by the factor* e^{-4xn_i}, and thus the major maxima and minima are significantly damped for $4xn_i \sim 1$. The ripples damp out at a value of xn_i which is smaller, but not smaller by orders of magnitude. This is consistent with van de Hulst's (1957) model for the surface wave in which only a few circumvolutions of the sphere are involved.

Figure 9 also shows that as n_i increases Q_{sca} for large particles first decreases, reaches a minimum, and then increases. As n_i becomes large Q_{sca} approaches the value for a perfect reflector, i.e., $Q_{sca} \to 2$ (cf., 2.10).

The dependence of the single scattering albedo $\tilde{\omega}$ on x and n_i is illustrated in Figure 10 for $n_r = 1.33$. The solid curves are each for a single particle of a given size parameter.

* In traveling a distance z the amplitude of the electric field varies as $e^{-ikzn_c} = e^{-ikz(n_r - in_i)}$, and thus the intensity is proportional to e^{-2kzn_i}.

For large x and not too large n_i, $\tilde{\omega}$ approaches ~ 0.53. This can be understood from Figure 4; for $n_i = 0$ 50% of the scattered light is diffracted, 3.3% is reflected and the remainder is refracted into the particle. As long as n_i is small this division of the rays remains approximately correct, and for large particles the refracted light is absorbed within the particle even for small n_i. As x becomes small $\tilde{\omega}$ takes on values less than 0.5, a result of the fact that the Rayleigh region is being approached (cf., 2.19 and 2.20).

The dotted curves in Figure 10 are for a size distribution of significant width, $b = 0.10$ (cf., Figure 7). For $x = 1$ and $x = 5$ there is a non-negligible dependence of $\tilde{\omega}$ on b, as would be expected. However, for $x \geq 10$ $\tilde{\omega}$ is practically independent of the width of the size distribution. Thus for particles this large only one parameter, r_{eff}, is required to define the effect of the particle size distribution on $\tilde{\omega}$. This is a result of our choice of parameters; for example, it can be shown that two different distributions with the same mode radius or the same mean radius in general have considerably different values of $\tilde{\omega}$.

The asymmetry parameter $\langle \cos \alpha \rangle$ is graphed in Figure 11 as a function of $x_{\text{eff}} =$
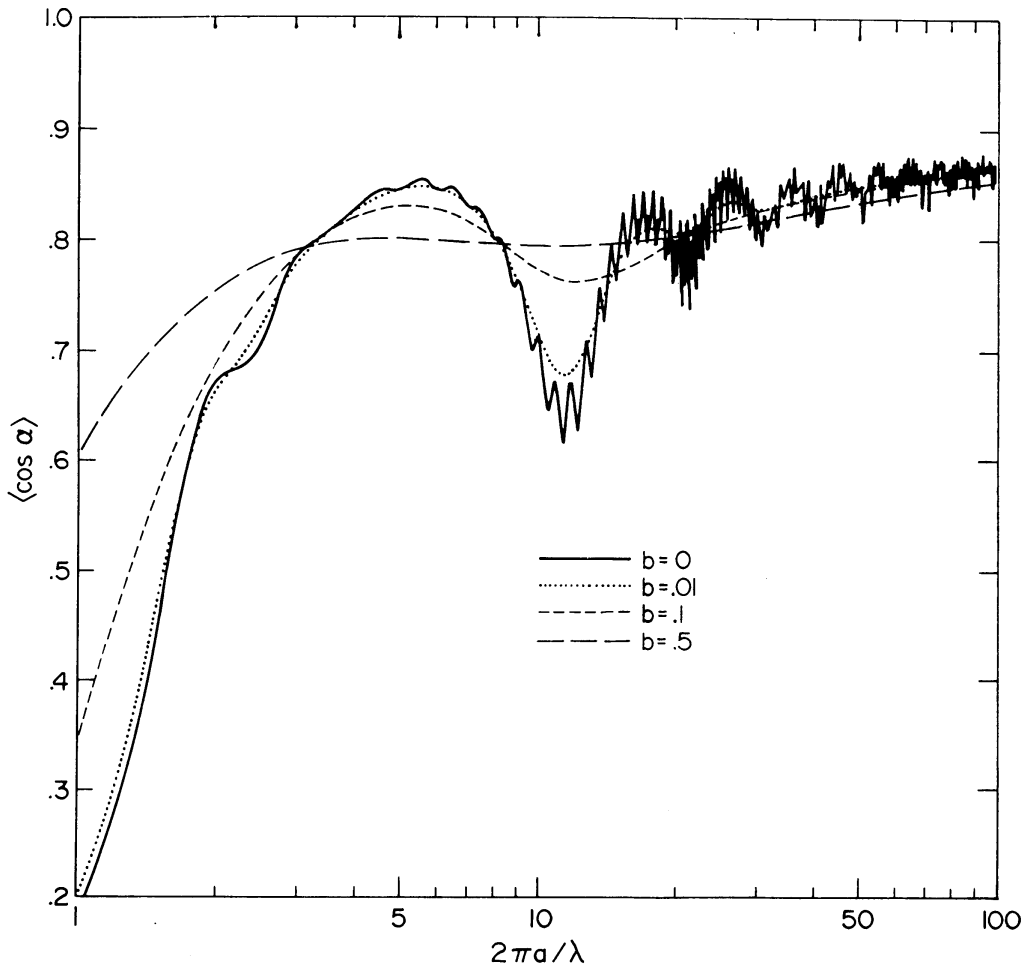

Fig. 11. Asymmetry parameter, $\langle \cos \alpha \rangle$, as a function of the effective size parameter, $2\pi a/\lambda$. The standard size distribution (2.56) was used with four values of the effective variance b. For the case $b = 0$, $2\pi a/\lambda = 2\pi r/\lambda \equiv x$. The refractive index is $n_r = 1.33$, $n_i = 0$.

$2\pi a/\lambda$ for the size distribution (2.56). The refractive index is $n_r = 1.33$. For small particles $\langle\cos\alpha\rangle$ approaches zero, the value obtained for Rayleigh scattering. For large x $\langle\cos\alpha\rangle$ approaches the result which is obtained with the geometrical optics phase function, ~ 0.87 (van de Hulst, 1957). The maxima and minima in $\langle\cos\alpha\rangle$ have the same physical origin as those in Q_{sca} discussed above. $\langle\cos\alpha\rangle$ is thus dependent on x_{eff} and v_{eff}. The dependence of $\langle\cos\alpha\rangle$ on higher moments is small provided $x_{eff} \geqslant 10$. For the range of v_{eff} typical of terrestrial clouds the dependence of $\langle\cos\alpha\rangle$ on v_{eff} is negligible, at least for the range of x_{eff} appropriate for the visible and near-infrared regions.

Figure 12 shows the asymmetry parameter for different real refractive indices. The size distribution is (2.56) with $b = 0.07$, which is sufficient to smooth out all maxima except the primary interference maximum (cf., Figure 8). This maximum in $\langle\cos\alpha\rangle$ corresponds to a maximum in Q_{sca}, since this feature is a result of constructive interference in the forward direction. For the larger values of refractive index $\langle\cos\alpha\rangle$
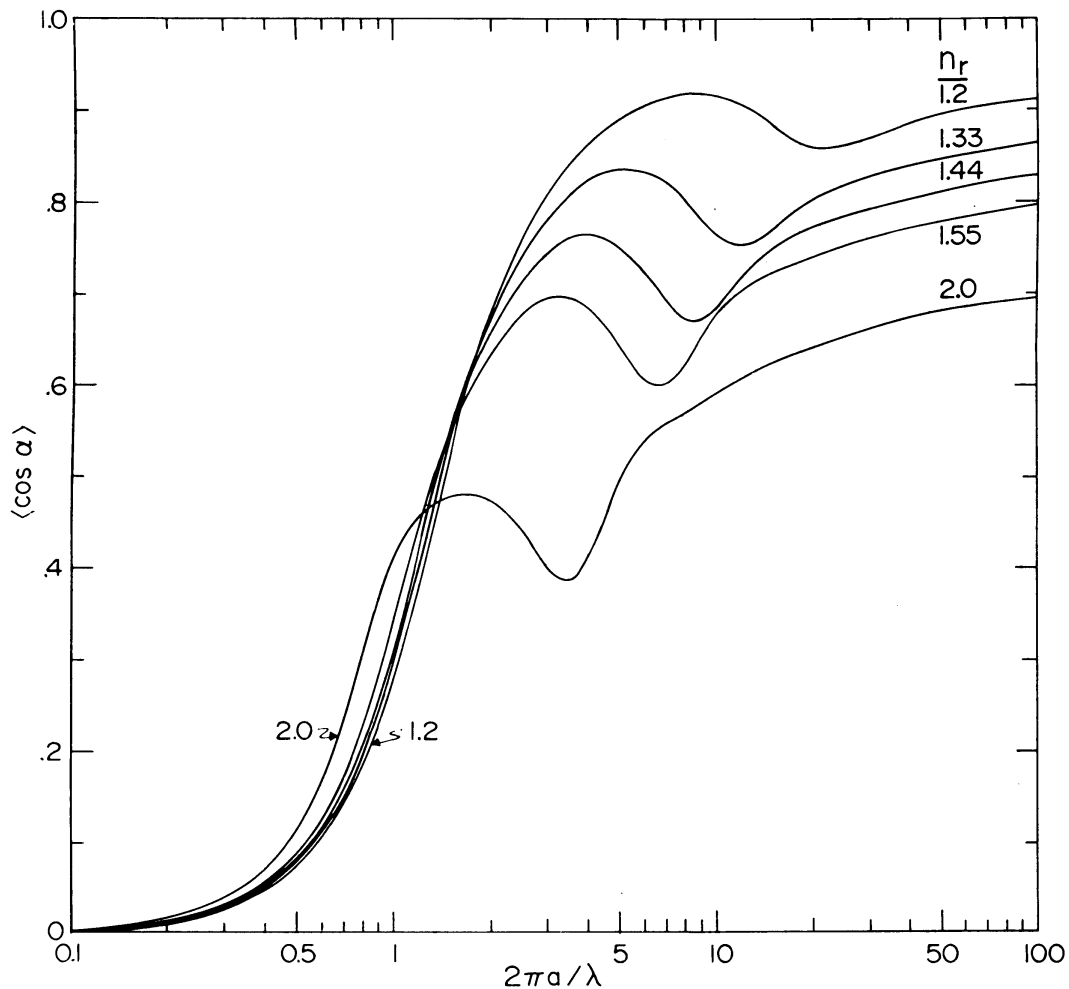

Fig. 12. Asymmetry parameter, $\langle\cos\alpha\rangle$, as a function of effective size parameter, $2\pi a/\lambda$. Results are shown for five values of the real refractive index, n_r, all with $n_i = 0$. The standard size distribution (2.56) was used with $b = 0.07$.

deviates more readily from its zero value for Rayleigh scattering, as expected. At $2\pi a/\lambda = 100$ the limit of $\langle \cos \alpha \rangle$ for geometrical optics has nearly been reached; e.g., for $n_r = 1.33$ the phase function for geometrical optics yields $\langle \cos \alpha \rangle \sim 0.87$. The gradual increase in $\langle \cos \alpha \rangle$ as it approaches its limiting value is due in large part to the decreasing width of the diffraction lobe of the phase function. As $n_r \to 1$, $\langle \cos \alpha \rangle \to 1$ for large $2\pi a/\lambda$, since $n_r = 1$ corresponds to no scattering at all. On the other hand, as $n_r \to \infty$, $\langle \cos \alpha \rangle \to 0.5$ for large $2\pi a/\lambda$, because half of the scattered radiation is diffracted in the forward direction and half is reflected isotropically (cf., 2.10).

Figure 13 illustrates the effect of the imaginary part of the refractive index on $\langle \cos \alpha \rangle$. For $x_{eff} = 1000$ as n_i increases $\langle \cos \alpha \rangle$ first increases from its geometrical optics value for $n_i = 0$ (~ 0.87); this increase is a result of absorption of rays refracted into the particle. At $n_i = 0.001$ the absorption of refracted rays is essentially complete since in traversing a particle diameter the reduction in intensity is the factor $e^{-4x n_i} = e^{-4}$. Thus only diffraction and reflection contribute and $\langle \cos \alpha \rangle$ $\sim 0.94 \times 1 + 0.06 \times \frac{1}{2} = 0.97$,
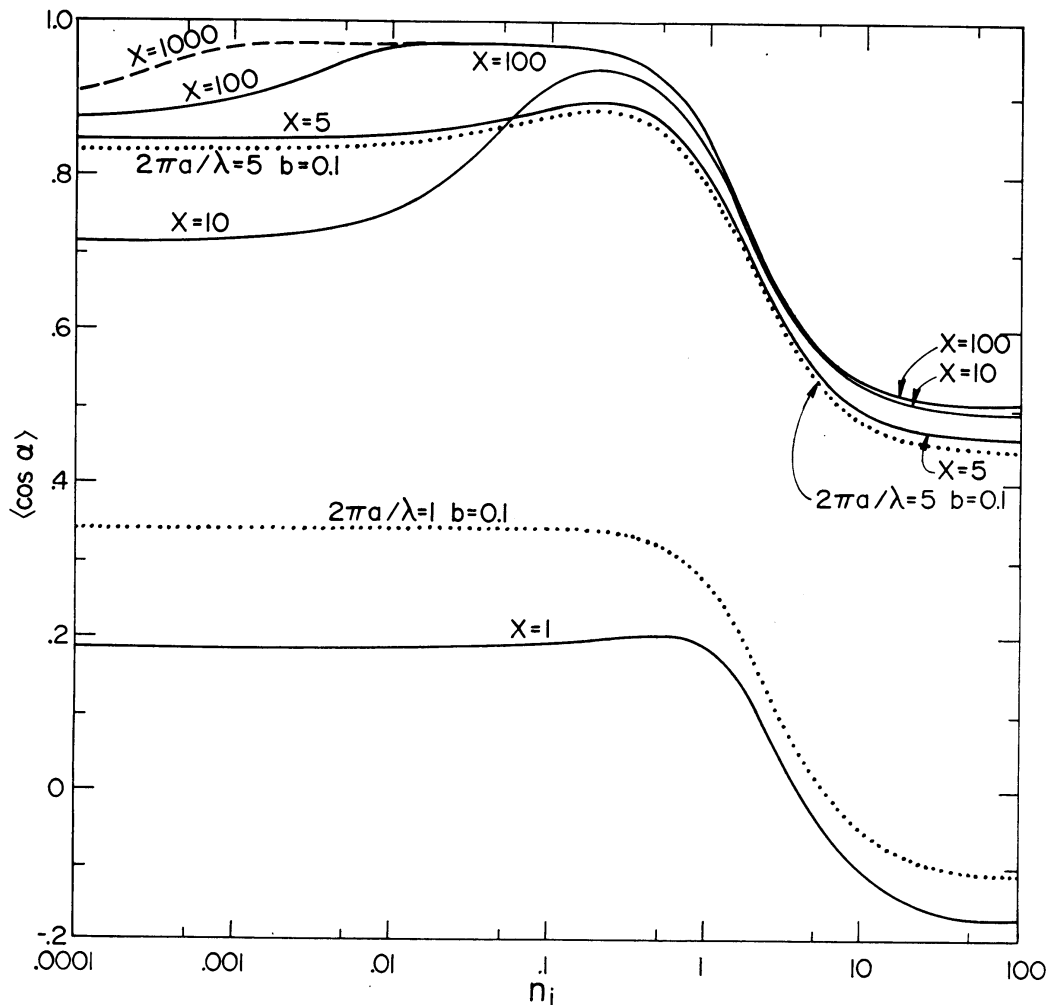

Fig. 13. Asymmetry parameter, $\langle \cos \alpha \rangle$, as a function of the imaginary part of the refractive index, n_i. The solid curves are for $b = 0$, corresponding to a single particle, so $2\pi a/\lambda = x$. The real refractive index is $n_r = 1.33$.

where 1 and $\frac{1}{2}$ are the approximate values of $\langle\cos\alpha\rangle$ for the diffracted and reflected components. For $x_{\text{eff}}=100$, n_i must be ~ 10 times larger for the transition to $\langle\cos\alpha\rangle$ ~ 0.97 to occur. As n_i increases further and becomes significant relative to n_r the amount and angular distribution of Fresnel reflection change, cf. (2.10), until finally $\langle\cos\alpha\rangle\to 0.5$ and $n_i\to\infty$, for the same reason as in the case $n_r\to\infty$.

For $x_{\text{eff}}=5$ and 10 $\langle\cos\alpha\rangle$ is qualitatively similar to the case of large particles, but the numerical values can not be reliably computed using geometrical optics. For $x_{\text{eff}}=1$ $\langle\cos\alpha\rangle$ is not far from the Rayleigh result, $\langle\cos\alpha\rangle=0$. For small n_i the significant terms in the Mie series in addition to the electric dipole term are all forward scattering, and thus $\langle\cos\alpha\rangle>0$ (van de Hulst, 1957, Section 10.3). However for large n_i the magnetic dipole term is large, and this gives primarily backward scattering. In the limit $x\to 0$ and $n_c\to\infty$, $\langle\cos\alpha\rangle\to -0.4$ (van de Hulst, 1957, Section 10.01).

The remaining graphs in this section are for elements of the phase matrix $\mathbf{P}(\alpha)$. $\mathbf{P}(\alpha)$ is generally more sensitive to the particle size distribution than the quantities Q_{sca}, $\tilde{\omega}$ and $\langle\cos\alpha\rangle$. Therefore we demonstrate in more detail the effect of the particle size distribution. We show that in many practical applications it is possible to adequately describe the size distribution with at most two parameters, the effective radius and the effective variance.

We illustrate the sensitivity of $\mathbf{P}(\alpha)$ to the shape of the size distribution with computations for four different distributions, the standard (gamma) distribution (2.56), the bimodal gamma distribution, the log-normal distribution and the power law distribution. For the bimodal distribution we use

$$n(r) = \frac{1}{2} \frac{r^{(1-3b)/b}e^{-r/(a_1 b)}}{(a_1 b)^{(1-2b)/b}\,\Gamma[(1-2b)/b]} + \frac{1}{2} \frac{r^{(1-3b)/b}e^{-r/(a_2 b)}}{(a_2 b)^{(1-2b)/b}\,\Gamma[(1-2b)/b]}$$

(2.59)

so that each of the two parts has the same value of b and contains half of the particles. For the log-normal distribution

$$n(r) = \frac{1}{(2\pi)^{1/2}\sigma_g}\frac{1}{r}\exp\left[-(\ln r - \ln r_g)^2/(2\sigma_g^2)\right],$$

where

$$\ln r_g = \int_0^\infty \ln r\, n(r)\, dr$$

(2.60)

and

$$\sigma_g^2 = \int_0^\infty (\ln r - \ln r_g)^2\, n(r)\, dr.$$

Finally, we choose the power law $\propto r^{-3}$, so

$$n(r) = \frac{2r_1^2 r_2^2}{r_2^2 - r_1^2}\, r^{-3}, \quad \text{for} \quad r_1 \leqslant r \leqslant r_2,$$

$$= 0, \qquad\qquad \text{otherwise}.$$

(2.61)

All of the distributions are normalized such that

$$\int_0^\infty n(r)\,dr = 1.$$ (2.62)

Figure 14 shows the single scattering intensity and polarization for all four distributions, with the computations being for refractive index $n_r = 1.33$, $n_i = 0$ and wavelength $\lambda = 0.55\mu$. The parameters in each distribution were chosen such that* $r_{\text{eff}} = 1\,\mu$ and
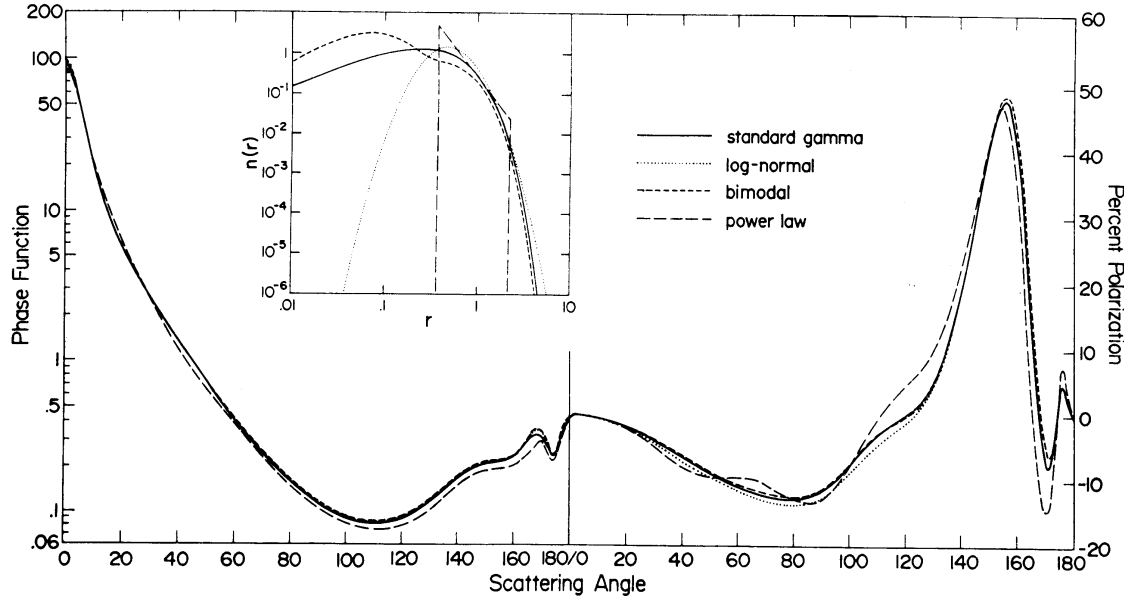

Fig. 14.   Phase function, P^{11}, and percent polarization, $-100P^{21}/P^{11}$, for single scattering of unpolarized incident light. Results are shown for the four size distributions illustrated in the inset, all of which have the same value for r_{eff} (1 μ) and v_{eff} (0.25), where r_{eff} is the effective radius and v_{eff} the effective variance. The calculations are for the real refractive index $n_r = 1.33$ and wavelength $\lambda = 0.55\,\mu$.

* For the log-normal distribution this required

$$r_g = r_{\text{eff}}/(1 + v_{\text{eff}})^{5/2} \sim 0.5724\mu,$$

$$\sigma_g^2 = \ln(1 + v_{\text{eff}}) \sim 0.4724.$$

For the power law distribution (2.61) r_1 and r_2 were obtained from

$$r_{\text{eff}} = \frac{r_2 - r_1}{\ln(r_2/r_1)},$$

$$v_{\text{eff}} = \frac{r_2 + r_1}{2(r_2 - r_1)} \ln(r_2/r_1) - 1,$$

which required $r_1 \sim 0.3620\,\mu$, $r_2 \sim 2.138\,\mu$. For the bimodal gamma distribution

$$r_{\text{eff}} = a_1 \left[\frac{1 + (a_2/a_1)^3}{1 - (a_2/a_1)^2}\right],$$

$$v_{\text{eff}} = \frac{[1 + (a_2/a_1)^4]\,[1 + (a_2/a_1)^2]}{[1 + (a_2/a_1)^3]^2}\,(1 + b) - 1.$$

We arbitrarily chose $a_2/a_1 = 5$, which then required $a_1 \sim 0.2063\,\mu$, $b \sim 0.2193$.

$v_{eff} = 0.25$, these numerical values being selected to yield a rather difficult test of how well the standard distribution represents the results for other distributions. For larger size parameters and/or smaller v_{eff} the different distributions usually yield results even closer than those in Figure 14.

In Figure 15 we have plotted results comparable to those in Figure 14, but with the parameters in each distribution selected such that the mean radius $\bar{r}$ (2.51) and the variance,

$$\sigma^2 = \frac{\int_0^\infty (r - \bar{r})^2 \, n(r) \, dr}{\int_0^\infty n(r) \, dr}, \tag{2.63}$$

are the same for all four distributions.* The results show significantly greater differences than in Figure 14. For the bimodal distribution the comparison is not entirely fair, because the smaller value of b for Figure 15 (which was required to obtain the appropriate value of σ^2) resulted in two very distinct modes in the size distribution. Nevertheless, Figures 14 and 15 are reasonably representative of the differences which are found between cases in which r_{eff} and v_{eff} are chosen to describe the size distribu-
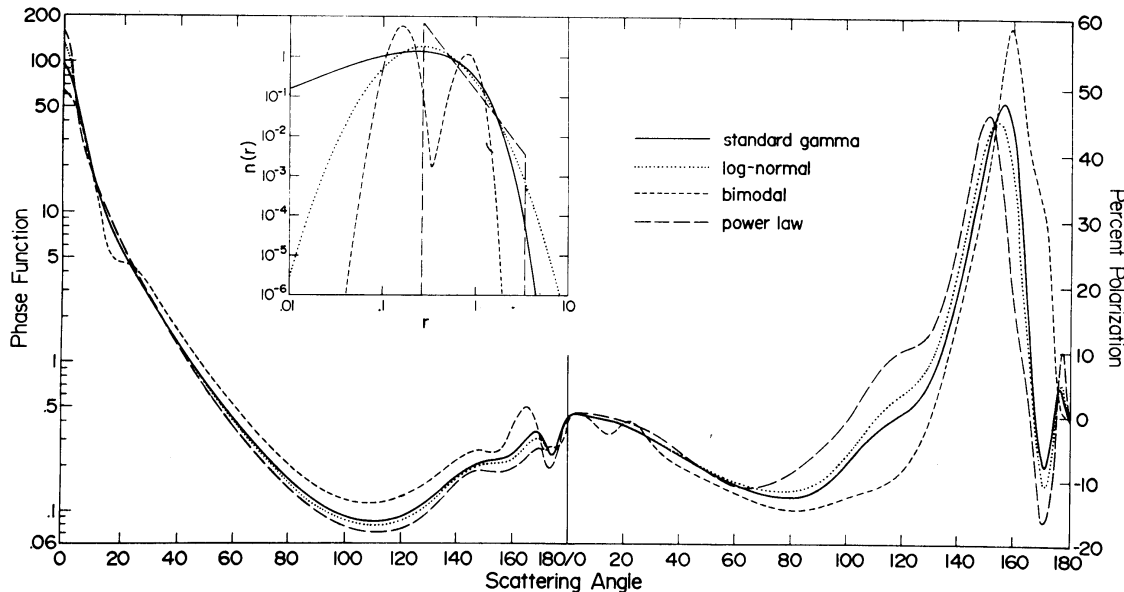

Fig. 15. Phase function, P^{11}, and percent polarization, $-100P^{21}/P^{11}$, for single scattering of unpolarized incident light. Results are shown for the four size distributions illustrated in the inset. The standard gamma distribution is the same as in Figure 14. All four distributions have $\bar{r} = 0.5 \, \mu$ and $\sigma^2 = 0.125 \, \mu^2$, where $\bar{r}$ is the mean radius and σ^2 the variance. The calculations are for the real refractive index $n_r = 1.33$ and wavelength $\lambda = 0.55 \, \mu$.

* For the gamma distribution $\bar{r} = a(1 - 2b)$ and $\sigma^2 = a^2 b(1 - 2b)$. Thus for $a = 1\mu$ and $b = 0.25$, $\bar{r} = 0.5 \, \mu$ and $\sigma^2 = 0.125 \, \mu^2$. The parameters in the other distributions were thus chosen such that $\bar{r}$ and σ^2 had these values. This required for the lognormal distribution $r_g = 0.4082 \, \mu$ and $\sigma_g = 0.6368$, for the bimodal distribution $a_1 = 0.1795$ and $b = 0.0357$, and for the power law distribution $r_1 = 0.2690$ and $r_2 = 3.535$. We took $a_2 = 5a_1$ for the bimodal distribution, as had been done for Figure 14.

tion and cases in which $\bar{r}$ and σ^2 are used. Thus if the simple moments, without the weight factor πr^2, are used to describe the size distribution, more than two moments are required to obtain results comparable to those in Figure 14. Of course if the mode radius is used to describe the size distribution the results are even much poorer than in Figure 15; i.e., different distributions with the same mode radius may have entirely different scattering properties.

We have shown that it is efficient to compare different size distributions by examining r_{eff}, v_{eff} and higher 'moments' if necessary. In the case of unimodal distributions, i.e., distributions with a single maximum, scattered radiation can be accurately defined by a small number of these characteristics. Thus, although it is impossible to
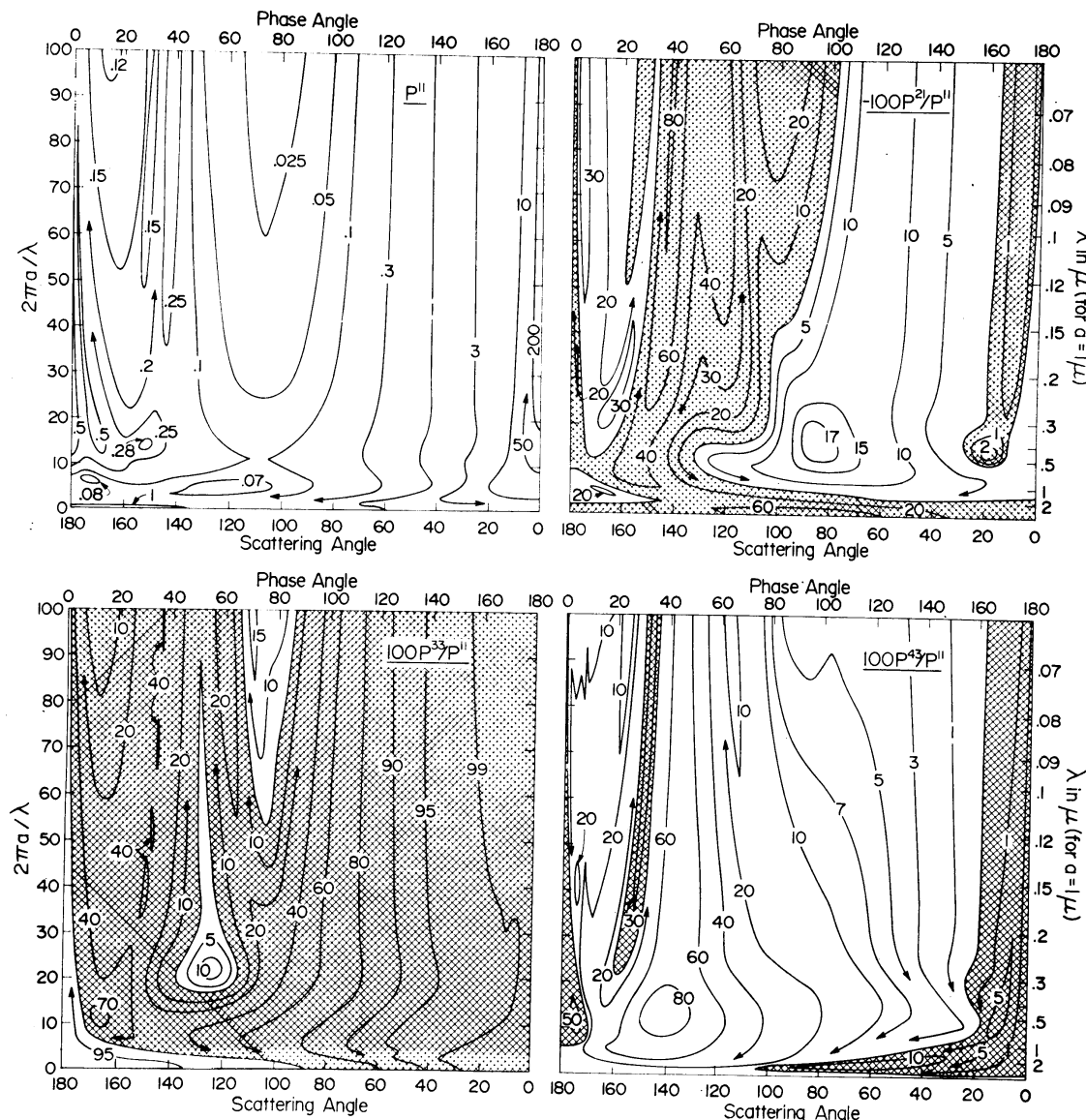

Fig. 16. Phase matrix for a size distribution of spheres with the real refractive index $n_r = 1.33$. The size distribution is given by (2.56) with $b = 0.07$. P^{11} is positive everywhere; for the other matrix elements positive regions are crosshatched.

extract the exact size distribution from measurements of scattered light, the major characteristics of the distribution can be obtained. This also allows the possibility of obtaining other information such as the particle refractive index.

Figures 16–20 are contour diagrams illustrating the dependence of the phase matrix on n_r, n_i, r_{eff} and v_{eff} for the range of these parameters that is important for light scattering in planetary atmospheres. The phase matrix elements are shown as a function of scattering angle (or its supplement, the phase angle) on the horizontal axis and as a function of the effective size parameter $2\pi a/\lambda$ on the vertical axis. By choosing any fixed value for a the vertical scale can be converted to a scale for λ. This is done on the right side of each figure for the choice $a = 1\mu$.

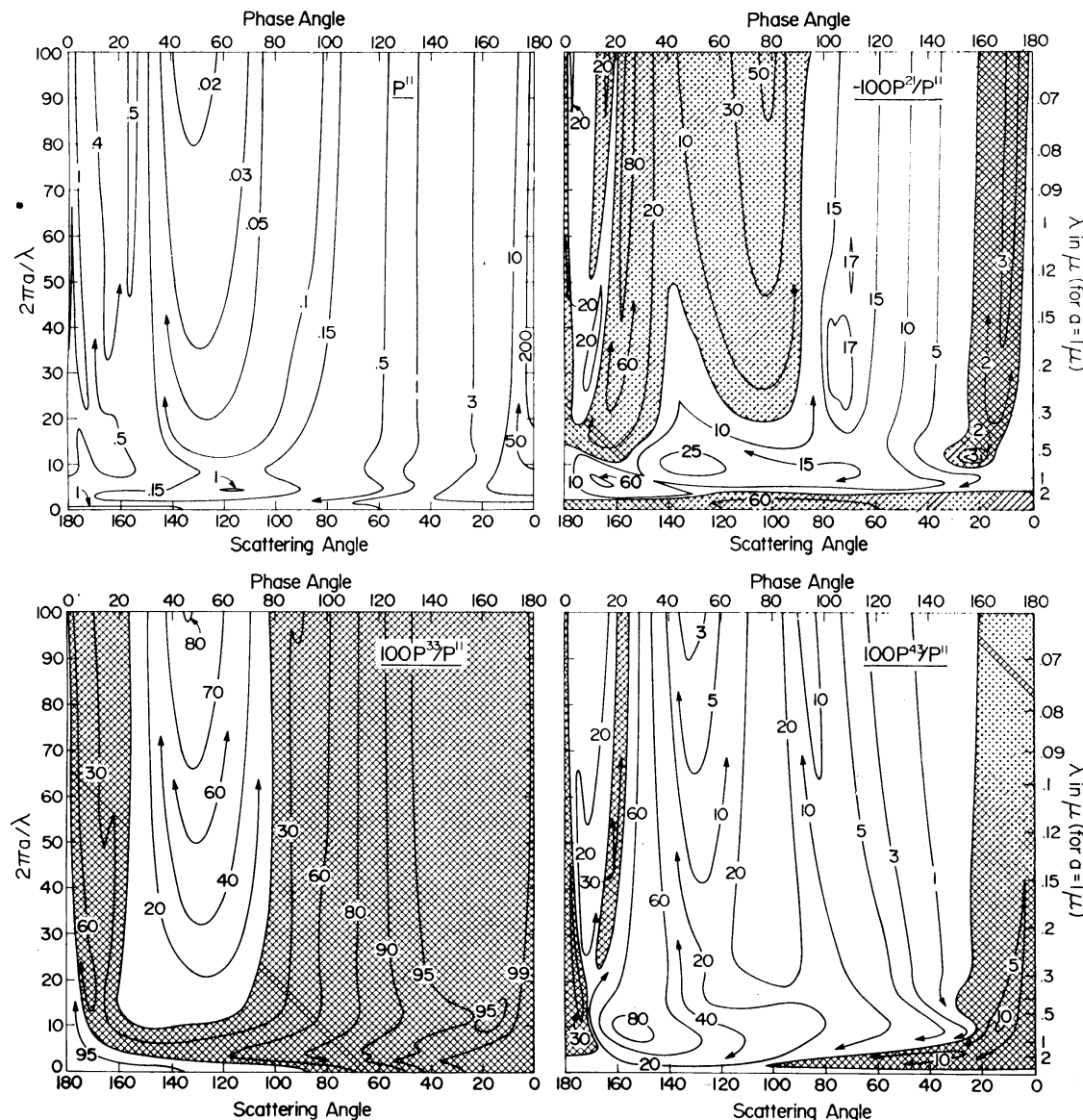Figures 16 and 17 illustrate the complete phase matrix for the real refractive indices

Fig. 17. Same as Figure 16, but for the real refractive index $n_r = 1.44$.

$n_r = 1.33$ and 1.44. P^{11} is the phase function and $-100\ P^{21}/P^{11}$ the percent linear polarization for single scattering of incident unpolarized light. The significance of the other two matrix elements is partially shown by Table I. Many of the features in these contour diagrams are most prominent in the linear polarization; thus in Figure 18 we have graphed the linear polarization for four additional real refractive indices in the range 1.25–2, for effective size parameters 0–50.

TABLE I

Stokes vectors of incident and scattered light for the case of scattering by spheres

Stokes vector of incident light	Polarization form of incident light	Stokes vector of light scattered by spheres in the plane of scattering
$\mathbf{I}_0 \propto (1, 0, 0, 0)$	unpolarized	$\mathbf{I} \propto (P^{11}, P^{21}, 0, 0)$
$\mathbf{I}_0 \propto (1, 1, 0, 0)$	linear, $\chi = 0°$	$\mathbf{I} \propto (P^{11} + P^{21}, P^{11} + P^{21}, 0, 0)$
$\mathbf{I}_0 \propto (1, 0, 1, 0)$	linear, $\chi = 45°$	$\mathbf{I} \propto (P^{11}, P^{21}, P^{33}, P^{43})$
$\mathbf{I}_0 \propto (1, 0, 0, 1)$	circular, right-handed	$\mathbf{I} \propto (P^{11}, P^{21}, -P^{43}, P^{33})$

The size distribution for Figures 16–18 is (2.56) with $b = v_{\mathrm{eff}} = 0.07$. This is broad enough to smooth out most of the interference maxima and minima which occur for a single particle, but not broader than most naturally occurring distributions. The integration over size parameter extended from $x_1 = 0$ to $x_2 = 300$, which is practically equivalent to the interval $(0, \infty)$.

For the smallest size parameters Rayleigh scattering occurs. Thus there is strong positive linear polarization, with the maximum linear polarization at scattering angle 90°. The Rayleigh scattering region is similar for different refractive indices, but it is more compressed for the larger values of n_r. This is understandable since the conditions for Rayleigh scattering are $x \ll 1$ and $|n_c x| \ll 1$.

For the largest size parameters the phase matrix approaches that for geometrical optics. At small scattering angles the phase function is large and the linear polarization is small because of the predominance of diffracted light. Other than diffraction, most of the light scattered into the forward hemisphere is due to rays passing through the particle with two refractions. This light has negative linear polarization, as follows from Fresnel's equations. Reflection from the outside of the particles contributes a positive linear polarization at all phase angles; although the intensity of these rays is small, it is sufficient to cause the long peninsula of positive linear polarization at scattering angles $\alpha \sim 15°$. This feature becomes stronger as n_r increases, because the Fresnel reflection coefficients increase with n_r.

The steep ridge and positive polarization maximum at scattering angles $\sim 150°$ (for $n_r = 1.33$) is the primary rainbow. This arises from rays internally reflected one time in spheres. These rays tend to be concentrated at a given scattering angle, as can be shown from geometrical optics. Similarly, the weaker feature at $\alpha \sim 120°$ (for

$n_r = 1.33$) is the second rainbow, due to rays undergoing two internal reflections. Still higher rainbows contain a negligible fraction of the scattered light, and they do not contribute any noticeable features. The location of the rainbows in scattering angle varies with n_r in accordance with Snell's law (cf., Liou and Hansen, 1971).

The sharp maximum in the backscattering direction ($\alpha \sim 180°$) is the glory. As mentioned above this is due in large part to incident edge rays and, for $\sqrt{2} \lesssim n_r \lesssim 2$, to rays internally reflected one time. The glory is focused into a region whose angular width is approximately inversely proportional to the effective size parameter.

For scattering angles $\sim 20°$ and size parameters ~ 15 (for $n_r = 1.33$) there is a hill of positive linear polarization, which nearly forms an island but is connected to the
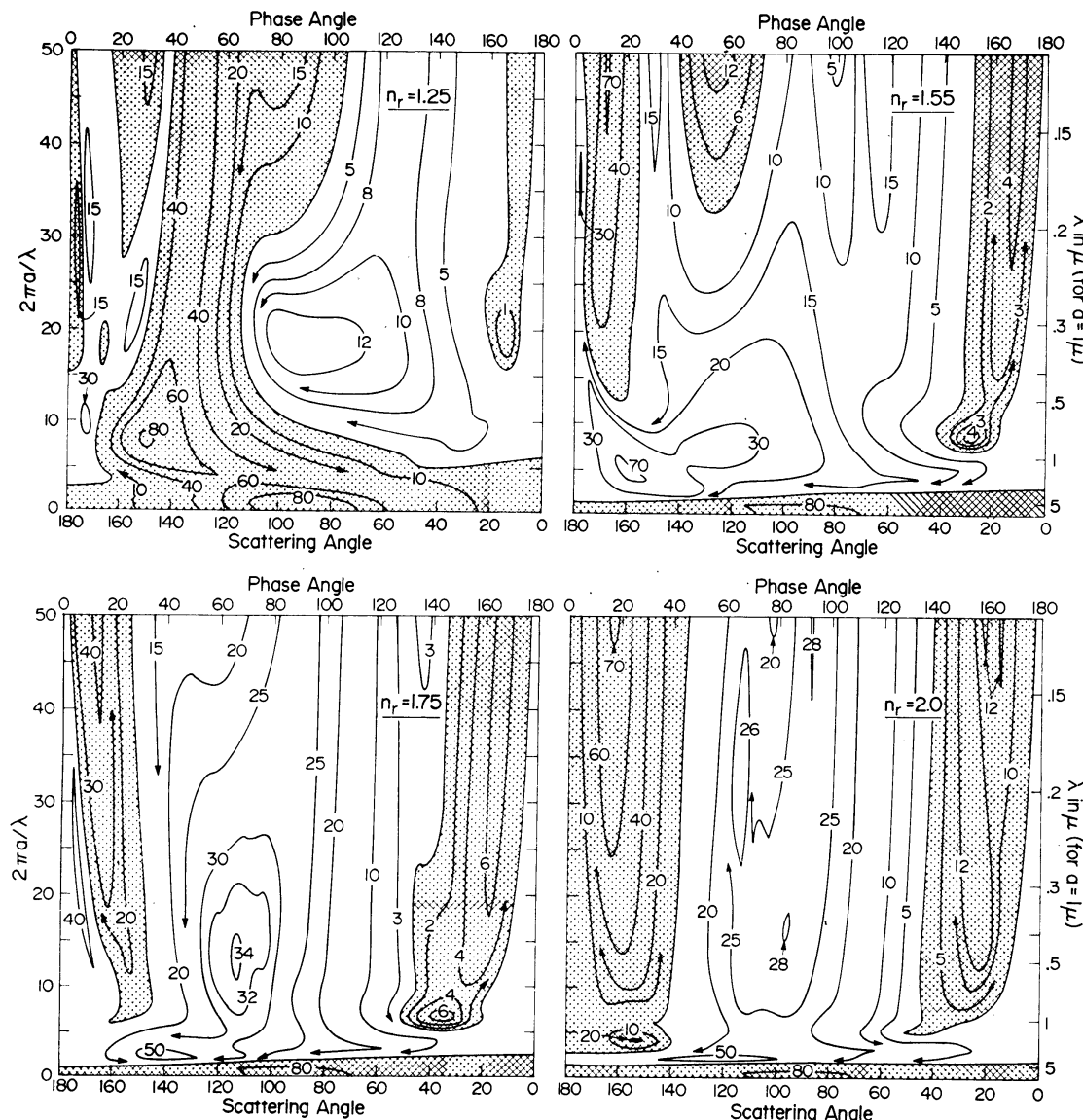

Fig. 18.   Percent polarization for single scattering of unpolarized incident light by a size distribution of spheres, $-100 P^{21}/P^{11}$, for the four indicated values of the real refractive index. The size distribution is given by (2.56) with $b = 0.07$. Positive regions are crosshatched.

peninsula of positive polarization for larger particles. This feature is a manifestation of what van de Hulst (1957) calls 'anomalous diffraction'. It is due to optical interference between diffracted light and light reflected and transmitted by the particle in the near forward direction. The phase shift of a ray traveling through the center of the sphere is $\varrho = 2x(n_r - 1)$, which accounts for the location of this feature in size parameter being $\propto 1/(n_r - 1)$.

In the transition region between large particle scattering and Rayleigh scattering the linear polarization is a complicated function of size parameter. As the size parameter decreases the degree to which the paths of separate light rays can be localized decreases. Thus the second rainbow, with a more detailed ray path, is lost from the polarization before the primary rainbow is. With decreasing size parameter the primary rainbow becomes blurred and its peak first moves toward larger scattering angles due to the asymmetric shape of the rainbow. For $n_r = 1.33$ the peak of the primary rainbow shifts to smaller scattering angles for size parameters $\lesssim 10$ and merges with Rayleigh scattering. This effect is less pronounced for the larger values of n_r because the Rayleigh region is more depressed and the rainbow is at a scattering angle further from the Rayleigh maximum. The negative linear polarization features for size parameters ~ 5 are due to edge rays and resulting surface waves, i.e., they are glory phenomena.

Figure 19 shows the linear polarization for $n_c = n_r = 1.40$ for the size distribution (2.56) with $b = 0, 0.01, 0.07$ and 0.25, the case $b = 0$ corresponding to a single particle. The integration limits on $2\pi a/\lambda$ were $(0, 300)$ for the other three cases, which was practically equivalent to $(0, \infty)$.

Figure 19 thus illustrates the effect of the width of the size distribution on the polarization. The case $b = 0$ appears as a field of maxima and minima, as a result of the optical interference phenomena for a single particle. Note that the rainbow, glory and Rayleigh regions are apparent even for a single particle.

The case $b = 0.01$ shows that even a very narrow size distribution is sufficient to smooth out most of the interference effects. The qualitative effect of broadening the distribution is easy to understand. It corresponds essentially to taking averages along vertical lines. Thus with increasing b hills tend to be smoothed out, holes are filled in, and corners are rounded off; straight vertical lines, however, remain almost unchanged.

The island at $2\pi a/\lambda \sim 10$, $\alpha \sim 20°$ for $b = 0.01$ is the major anomalous diffraction feature. The magnitude of this feature is sensitive to the particle size distribution. The maximum polarization decreases from $\sim 10\%$ to $\sim 3\%$ as b increases from 0.01 to 0.07 and the feature is absent for $b \gtrsim 0.12$. This is understandable since only a narrow distribution of sizes has the phase shift required for the interference feature.

The bridge of positive polarization formed by the merging of the primary rainbow and Rayleigh scattering is also strongly affected by the width of the size distribution. As b increases this bridge tends to be eroded away. Figure 19 illustrates that for $n_r = 1.40$ and $b = 0.25$ there is a large breach of negative polarization separating the regions of positive polarization. Figure 16 shows that for $n_r = 1.33$ no such breach

can exist for large b, because the polarization at $\alpha = 140°$ is positive for all values of $2\pi a/\lambda$.

Figure 20 illustrates the effect of the imaginary part of the refractive index on the phase function and percent polarization. n_r is 1.33 and n_i is 0.01 and 0.1, thus Figure 16 provides a comparison for $n_i = 0$. For small values of $2\pi a/\lambda$ $n_i = 0.01$ has little effect on the phase function or polarization (though of course it may have a major effect on the single scattering albedo, cf. 2.20). For large particles the absorption of refracted rays leads to a dominance of reflected rays and diffraction. Thus for $n_i = 0.1$ the phase function consists essentially of the diffraction peak in the forward direction and nearly
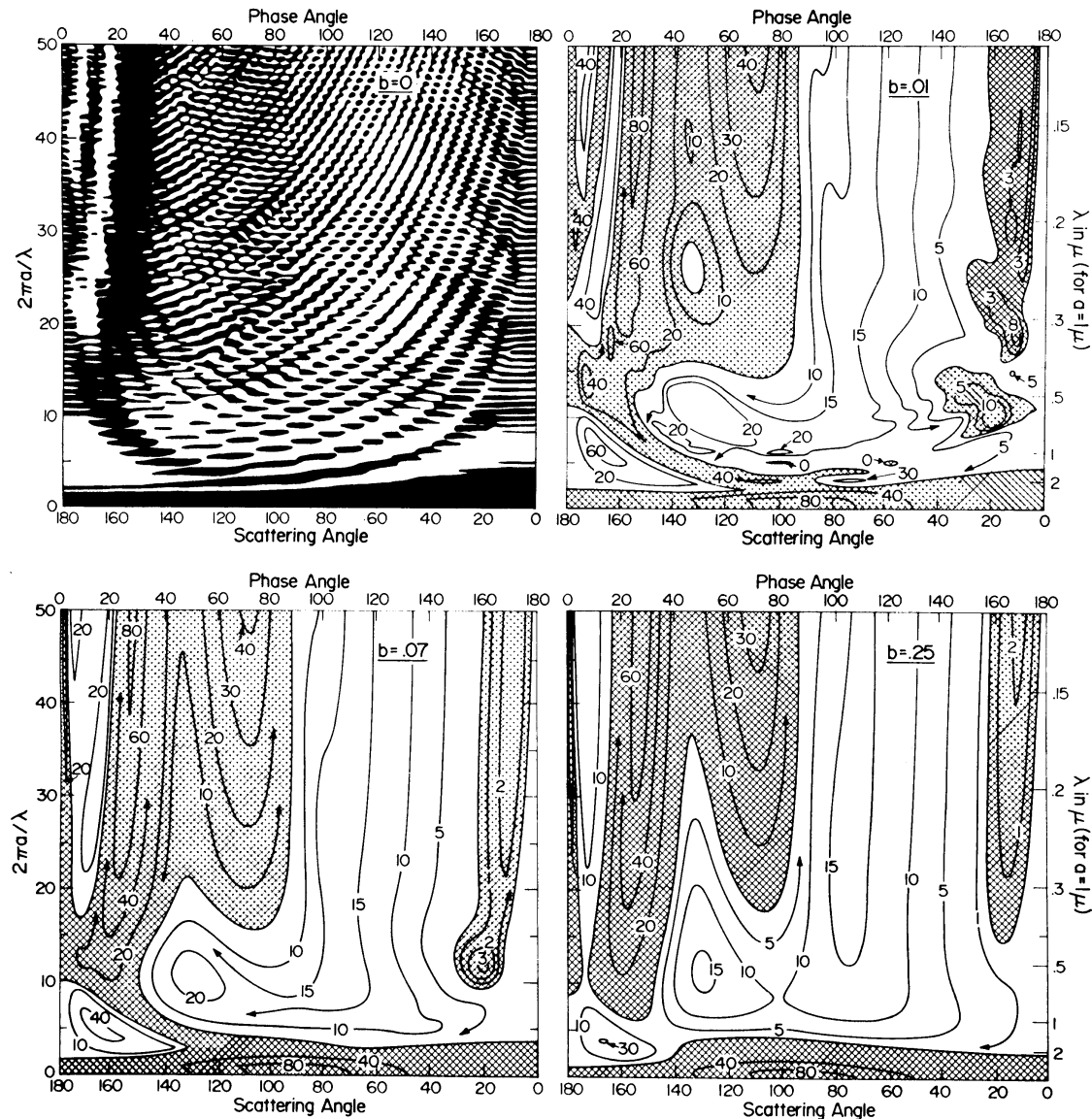

Fig. 19. Percent polarization for single scattering of unpolarized incident light by spheres, $-100P^{21}/P^{11}$, for the real refractive index $n_r = 1.40$. The size distribution is (2.56), with results shown for four values b. For $b = 0$, corresponding to a single particle, positive regions are blackened; for the other values of b positive regions are crosshatched.

isotropic scattering in the backward hemisphere. Note that the polarization is practically total at the Brewster angle, for which the phase angle is given by 2 arc tan 1.33 ~ 106°.

Polarization observations of Venus provide a striking example of how measurements of scattered light can be used to obtain the size distribution and refractive index of particles. Observations of Venus by Lyot (1929), Coffeen and Gehrels (1969) and Dollfus and Coffeen (1970) clearly show the rainbow, glory, anomalous diffraction and the breach of negative polarization between the rainbow and Rayleigh regions. Hansen and Hovenier (1974) have used these observations to derive accurate values for r_{eff}, v_{eff} and $n_r(\lambda)$ for the cloud particles on Venus.
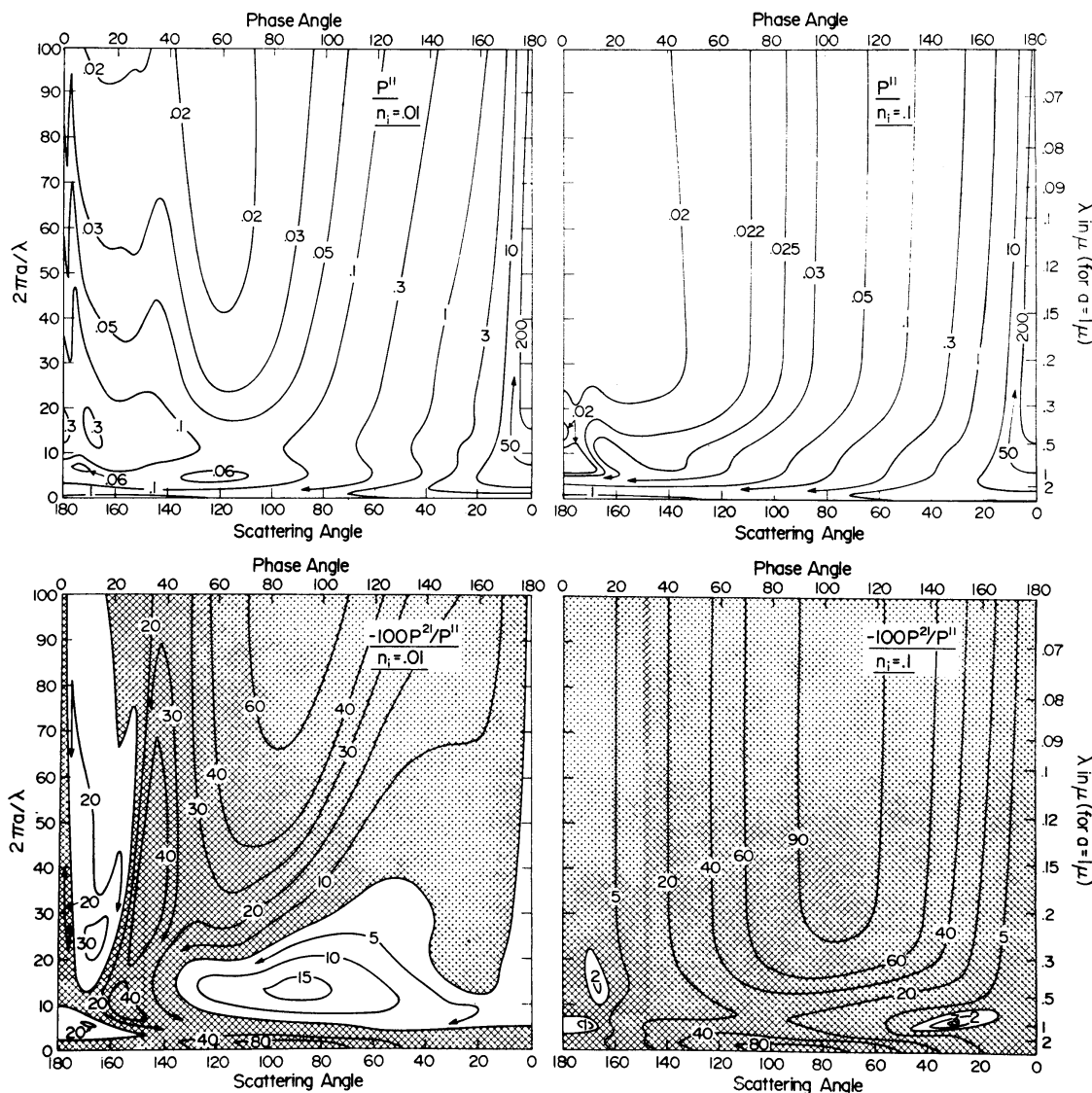

Fig. 20.   Phase function and percent polarization for single scattering of unpolarized incident light by a size distribution of spheres for the refractive index $n_r = 1.33$, $n_i = 0.01$ and 0.1. The size distribution is (2.56) with $b = 0.07$. For the percent polarization positive regions are crosshatched.

3. Multiple Scattering

A variety of techniques have been developed for computing the intensity and polarization of multiple scattered light. Our aims here are: (1) to demonstrate several of the computational methods which have proved particularly useful and show their close interrelationships, and (2) to illustrate the effects of multiple scattering on the information content in scattered radiation.

We present most of our graphs in Section 3.1 on the doubling method, because we have developed extensive programs for that method*. However, the same results could be obtained with many other methods. We also present graphical results in Section 3.2, because it is instructive to examine the contribution of successive orders of scattering to the intensity and polarization. Two methods for computing orders of scattering are presented: the classical method which involves successive integrations of the equation of transfer over optical depth, and a new method derived from an invariance principle. The method in Section 3.3, involving an iteration of the formal solution to the equation of transfer, is similar to the classical orders of scattering method; it converges faster but does not yield information on each order of scattering. The invariant imbedding method (Section 3.4) is based on an equation which gives the change in reflection when a very thin layer is added to the atmosphere; in contrast to the linear equation of transfer with boundary conditions, this method leads to a nonlinear initial value problem. In the method of X and Y functions (Section 3.5) the invariant imbedding equations are manipulated analytically to obtain certain integral equations, which are then solved numerically. In the method of discrete ordinates (Section 3.6) the equation of transfer is evaluated at N discrete zenith angles to obtain N equations for N unknowns; these may be solved numerically or, in some cases, analytically. The spherical harmonics method (Section 3.7) is very similar to the discrete ordinates method. The method of expansion in eigenfunctions (Section 3.8) has been of value in improving our understanding of the mathematics of idealized problems in radiative transfer, but it is too unwieldy for most practical applications. In contrast the Monte Carlo method (Section 3.9) treats multiple scattering as a simple stochastic process; thus this method is particularly useful because it can be easily applied to non-plane-parallel geometries.

The problem defined below for a plane-parallel atmosphere is sufficient to cover most applications for light scattering in planetary atmospheres. The scattering is assumed to be 'coherent' in the sense that no change of frequency occurs within the visible region (thus Raman scattering, for example, is excluded). Thermal emission is also excluded, but it can easily be added into the formalism.

Definitions. Most computations for multiple scattering in planetary atmospheres are made under the assumption that the atmosphere may be approximated as being composed of plane-parallel layers. In this case the location in the atmosphere can be specified by the optical depth,

---

* A program to compute the intensity is available from the authors.

$$\tau = \int\limits_{h}^{\infty} \kappa_{ext}\varrho \, dh' \,. \tag{3.1}$$

κ_{ext} is the extinction coefficient per unit mass and ϱ the atmospheric density at height h'. Thus we take $\tau = 0$ at the top of the atmosphere and $\tau = \tau_0$ at the bottom (Figure 21).

We use two systems to specify zenith angle:

(1) $u = $ cosine of angle with respect to direction of increasing τ (downward) range $+1$ (for the downward direction) to -1 (for the upward direction),

(2) $\mu = |u| = $ cosine of angle with respect to the outward normal, range $+1$ (for the normal direction) to 0 (for the grazing direction).
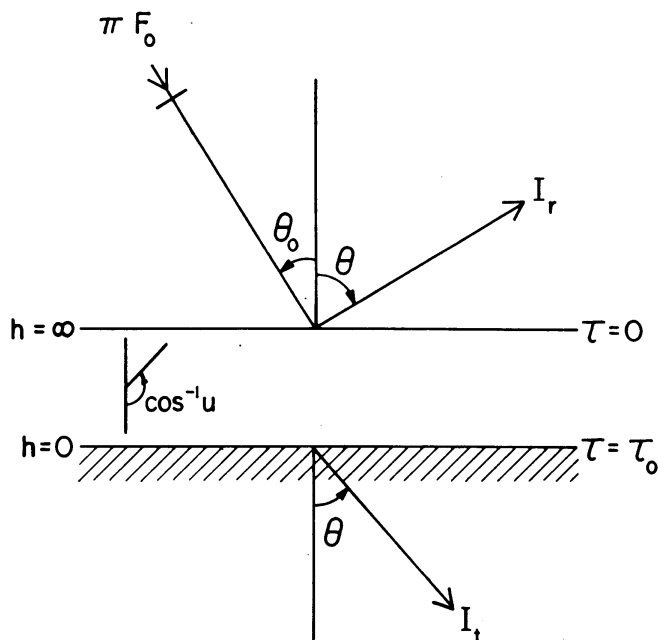
Fig. 21.   Definition of zenith angles and optical depth.

System 1 is used for the internal radiation field, i.e., within the atmosphere. System 2 is used for the reflected and transmitted radiation; the purpose of this second system is to avoid the appearance of a minus sign. We also let $\theta = \cos^{-1}\mu$, and for the zenith angle of radiation incident on the atmosphere we write $\theta_0 = \cos^{-1}\mu_0$ (Figure 21). Azimuth angle, ϕ, is measured counterclockwise looking downward.

The Stokes parameters of light incident on the top of the atmosphere are represented by the column vector,

$$\mathbf{I}_0 = \begin{Bmatrix} I_0 \\ Q_0 \\ U_0 \\ V_0 \end{Bmatrix}. \tag{3.2}$$

Similarly the Stokes parameters of the light diffusely reflected and transmitted by the atmosphere are $I_r(\mu, \phi)$ and $I_t(\mu, \phi)$, respectively. The units of $\mathbf{I}$ are those of photo-

metric brightness, say $\mathrm{erg\ s^{-1}\ cm^{-2}\ sterad^{-1}}$ (cf., footnote * of Section 2, p. 533).

It is convenient to express the solutions to the multiple scattering problem in terms of reflection and transmission matrices, each composed of four rows and four columns, such that

$$\mathbf{I}_r(\mu, \phi) = \frac{1}{\pi} \int\limits_0^1 \mu_0 \, d\mu_0 \int\limits_0^{2\pi} d\phi_0 \mathbf{R}(\mu, \mu_0, \phi - \phi_0) \mathbf{I}_0(\mu_0, \phi_0)$$

$$\mathbf{I}_t(\mu, \phi) = \frac{1}{\pi} \int\limits_0^1 \mu_0 \, d\mu_0 \int\limits_0^{2\pi} d\phi_0 \mathbf{T}(\mu, \mu_0, \phi - \phi_0) \mathbf{I}_0(\mu_0, \phi_0).$$

(3.3)

In many problems the quantity which is desired is the net flux of radiation, which is defined as

$$\pi\mathbf{F} = \int\limits_0^{2\pi} \int\limits_{-1}^1 I(u, \phi) \, u \, du \, d\phi = 2\pi \int\limits_{-1}^1 {}^0\mathbf{I}(u) \, u \, du,$$

(3.4)

where ${}^0\mathbf{I}(u)$ is the azimuth-independent term in a Fourier expansion of $\mathbf{I}(u, \phi)$. For a plane-parallel atmosphere the fraction of the incident flux which is reflected is called the local (or plane) albedo:

$$A(\mu_0) = 2 \int\limits_0^1 {}^0R^{11}(\mu, \mu_0) \mu \, d\mu,$$

(3.5)

where ${}^0R^{11}$ is the azimuth-independent part of the element in the first row and first column of $\mathbf{R}$. The spherical or Bond albedo is the ratio of the radiation reflected from a spherical but locally-plane-parallel atmosphere to the radiation incident from a distant source. For a locally-plane-parallel atmosphere.

$$A = 2 \int\limits_0^1 A(\mu_0) \mu_0 \, d\mu_0 = 4 \int\limits_0^1 \int\limits_0^1 {}^0R^{11}(\mu, \mu_0) \mu \, d\mu \, \mu_0 \, d\mu_0.$$

(3.6)

For most problems it is satisfactory to approximate incident sunlight as mono-directional i.e.,

$$\mathbf{I}_0 = \delta(\mu - \mu_0) \delta(\phi - \phi_0) \pi\mathbf{F}_0,$$

(3.7)

where δ is the Dirac delta function and $\pi\mathbf{F}_0$ is the incident flux per unit area perpendicular to the incident beam, say in $\mathrm{erg\ s^{-1}\ cm^{-2}}$. Thus in this case

$$\mathbf{I}_r(\mu, \phi) = \mu_0\mathbf{R}(\mu, \mu_0, \phi - \phi_0) \mathbf{F}_0$$
$$\mathbf{I}_t(\mu, \phi) = \mu_0\mathbf{T}(\mu, \mu_0, \phi - \phi_0) \mathbf{F}_0.$$

(3.8)

The reflection and transmission by a layer in general depend upon whether the layer is illuminated from above or below. We distinguish the case of illumination from

below with a superscript asterisk, thus

$$\mathbf{I}_r^* = \mu_0 \mathbf{R}^* (\mu, \mu_0, \phi - \phi_0) \mathbf{F}_0,$$
$$\mathbf{I}_t^* = \mu_0 \mathbf{T}^* (\mu, \mu_0, \phi - \phi_0) \mathbf{F}_0. \tag{3.9}$$

Although a planetary atmosphere is illuminated from above, the functions $\mathbf{R}^*$ and $\mathbf{T}^*$ are needed in some computations because a given layer can be illuminated by lower layers or a reflecting ground.

Symmetry relationships. For a homegenous plane-parallel atmosphere with a phase matrix of type (2.9) there are three pairs of independent symmetry relationships obeyed by the reflection and transmission matrices (Hovenier, 1969). First, the only difference between the cases of illumination from above and illumination from below is the sense in which the azimuth angle is reckoned; thus

$$\mathbf{R}^* (\mu, \mu_0, \phi - \phi_0) = \mathbf{R} (\mu, \mu_0, \phi_0 - \phi),$$
$$\mathbf{T}^* (\mu, \mu_0, \phi - \phi_0) = \mathbf{T} (\mu, \mu_0, \phi_0 - \phi). \tag{3.10}$$

Therefore, for a homogeneous layer, $\mathbf{R}^*$ and $\mathbf{T}^*$ never need to be computed if $\mathbf{R}$ and $\mathbf{T}$ are known.

A second pair of symmetry relationships involves the interchange of the rows and columns of the reflection and transmission matrices,

$$\mathbf{T} (\mu_0, \mu, \phi - \phi_0) = \mathbf{q}_3 \tilde{\mathbf{T}} (\mu, \mu_0, \phi - \phi_0) \mathbf{q}_3,$$
$$\mathbf{R} (\mu_0, \mu, \phi - \phi_0) = \mathbf{q}_4 \tilde{\mathbf{R}} (\mu, \mu_0, \phi - \phi_0) \mathbf{q}_4, \tag{3.11}$$

where the tilde indicates the transpose, and

$$\mathbf{q}_3 = \begin{Bmatrix} 1 & 0 & 0 & 0 \\ 0 & 1 & 0 & 0 \\ 0 & 0 & -1 & 0 \\ 0 & 0 & 0 & 1 \end{Bmatrix},$$

$$\mathbf{q}_4 = \begin{Bmatrix} 1 & 0 & 0 & 0 \\ 0 & 1 & 0 & 0 \\ 0 & 0 & 1 & 0 \\ 0 & 0 & 0 & -1 \end{Bmatrix}. \tag{3.12}$$

The relationships given by (3.11) are useful for checking computed results and for reducing the number of quantities computed.

The third pair of symmetry relationships is

$$\mathbf{R} (\mu, \mu_0, \phi_0 - \phi) = \mathbf{q}_3 \mathbf{q}_4 \mathbf{R} (\mu, \mu_0, \phi - \phi_0) \mathbf{q}_4 \mathbf{q}_3,$$
$$\mathbf{T} (\mu, \mu_0, \phi_0 - \phi) = \mathbf{q}_3 \mathbf{q}_4 \mathbf{T} (\mu, \mu_0, \phi - \phi_0) \mathbf{q}_4 \mathbf{q}_3. \tag{3.13}$$

This implies that the reflection and transmission matrices are each of the type

$$\begin{Bmatrix} c & c & s & s \\ c & c & s & s \\ s & s & c & c \\ s & s & c & c \end{Bmatrix}, \tag{3.14}$$

where c represents a matrix element which is an even function of $(\phi - \phi_0)$ and s represents an odd function of $(\phi - \phi_0)$. In a Fourier series expansion the even functions contain only cosine terms and the odd functions contain only sine terms.

The symmetry relationships (3.10), (3.11) and (3.13) follow from time reversal reciprocity (corresponding to interchange of the directions of incidence and emergence) and from the symmetry which exists with respect to the scattering plane for phase matrices of the type (2.9), cf., Hovenier (1969). For a homogeneous atmosphere all six relationships are valid. For an inhomogeneous atmosphere the second part of (3.11) and both parts of (3.13) are valid.

Phase matrix. The phase matrix in Section 2, $\mathbf{P}(\alpha)$, was defined with respect to the plane of scattering, with α the scattering angle. Since there are many different planes of scattering in multiple scattering problems, it is necessary to choose one common plane of reference for the Stokes parameters. For this purpose we use the local meridian plane, specified by the local normal ($u = 1$) and the direction of emergence (u, ϕ). As Chandrasekhar (1950) has shown, the phase matrix defined with respect to the local meridian plane may be obtained from $\mathbf{P}(\alpha)$ by means of appropriate rotations.

$$\mathbf{P}(u, u_0, \phi - \phi_0) = \begin{vmatrix} 1 & 0 & 0 & 0 \\ 0 & \cos 2i_2 & -\sin 2i_2 & 0 \\ 0 & \sin 2i_2 & \cos 2i_2 & 0 \\ 0 & 0 & 0 & 0 \end{vmatrix}$$

$$\mathbf{P}(\alpha) \begin{vmatrix} 1 & 0 & 0 & 0 \\ 0 & \cos 2i_1 & -\sin 2i_1 & 0 \\ 0 & \sin 2i_1 & \cos 2i_1 & 0 \\ 0 & 0 & 0 & 0 \end{vmatrix} \tag{3.15}$$

The rotation angles i_1 and i_2 for $0 < \phi - \phi_0 < \pi$ are given by

$$\cos i_1 = \frac{u(1 - u_0^2)^{1/2} - u_0(1 - u^2)^{1/2} \cos(\phi - \phi_0)}{(1 - \cos^2 \alpha)^{1/2}},$$

$$\cos i_2 = \frac{u_0(1 - u^2)^{1/2} - u(1 - u_0^2)^{1/2} \cos(\phi - \phi_0)}{(1 - \cos^2 \alpha)^{1/2}}, \tag{3.16}$$

where the scattering angle α is given by

$$\cos \alpha = u u_0 + (1 - u^2)^{1/2}(1 - u_0^2)^{1/2} \cos(\phi - \phi_0). \tag{3.17}$$

We introduce the notation

$$\mathbf{P}_r(\mu, \mu_0, \phi - \phi_0) \equiv \mathbf{P}(-\mu, \mu_0, \phi - \phi_0),$$
$$\mathbf{P}_t(\mu, \mu_0, \phi - \phi_0) \equiv \mathbf{P}(\mu, \mu_0, \phi - \phi_0),$$
$$\mathbf{P}_r^*(\mu, \mu_0, \phi - \phi_0) \equiv \mathbf{P}(\mu, -\mu_0, \phi - \phi_0),$$
$$\mathbf{P}_t^*(\mu, \mu_0, \phi - \phi_0) \equiv \mathbf{P}(-\mu, -\mu_0, \phi - \phi_0). \tag{3.18}$$

The phase matrix, if it is of the form (2.9), satisfies the symmetry relationships given above for the reflection and transmission matrices, i.e.,

$$
\begin{aligned}
\mathbf{P}_r^* (\mu, \mu_0, \phi - \phi_0) &= \mathbf{P}_r (\mu, \mu_0, \phi_0 - \phi), \\
\mathbf{P}_t^* (\mu, \mu_0, \phi - \phi_0) &= \mathbf{P}_t (\mu, \mu_0, \phi_0 - \phi),
\end{aligned}
\tag{3.19}
$$

$$
\begin{aligned}
\mathbf{P}_t (\mu_0, \mu, \phi - \phi_0) &= \mathbf{q}_3 \tilde{\mathbf{P}}_t (\mu, \mu_0, \phi - \phi_0) \mathbf{q}_3, \\
\mathbf{P}_r (\mu_0, \mu, \phi - \phi_0) &= \mathbf{q}_4 \tilde{\mathbf{P}}_r (\mu, \mu_0, \phi - \phi_0) \mathbf{q}_4,
\end{aligned}
\tag{3.20}
$$

and

$$
\begin{aligned}
\mathbf{P}_r (\mu, \mu_0, \phi_0 - \phi) &= \mathbf{q}_3 \mathbf{q}_4 \mathbf{P}_r (\mu, \mu_0, \phi - \phi_0) \mathbf{q}_4 \mathbf{q}_3, \\
\mathbf{P}_t (\mu, \mu_0, \phi_0 - \phi) &= \mathbf{q}_3 \mathbf{q}_4 \mathbf{P}_t (\mu, \mu_0, \phi - \phi_0) \mathbf{q}_4 \mathbf{q}_3.
\end{aligned}
\tag{3.21}
$$

These relationships are useful for checking purposes and for reducing the number of quantities computed. For example, it is sufficient to compute only the diagonal matrix elements of $\mathbf{P}_r$ and $\mathbf{P}_t$ and either the elements above the diagonal or those below the diagonal. With $\mathbf{P}_r$ and $\mathbf{P}_t$ computed for μ and μ_0 on the interval (0, 1) and $\phi - \phi_0$ on the interval (0, π) all other values for the phase matrix follow from the above relationships. Note that the phase matrix has the same division into odd and even functions as do the reflection and transmission matrices. Also $P^{41} = 0 = P^{14}$, as follows)from (2.9) and (3.15). Thus in this case $\mathbf{P} (\mu, \mu_0, \phi - \phi_0)$ is of the form

$$
\begin{Bmatrix}
c & c & s & 0 \\
c & c & s & s \\
s & s & c & c \\
0 & s & c & c
\end{Bmatrix}.
\tag{3.22}
$$

3.1. DOUBLING OR ADDING METHOD

The essence of the doubling or adding method is simple: if the reflection and transmission is known for each of two layers, the reflection and transmission from the combined layer can be obtained by computing the successive reflections back and forth between the two layers. If the two layers are chosen to be identical, the results for a thick homogeneous layer can be built up rapidly in a geometric (doubling) manner.

The principle for this method apparently goes back at least to Stokes (1862), who considered the reflection and transmission by a stack of glass plates. The theory was developed for gamma-ray transfer by Peebles and Plesset (1951), in a form somewhat resembling the method now used for multiple scattering problems. The adding method now commonly employed was developed by van de Hulst (1963), who also presented numerical results for isotropic scattering. Twomey et al. (1966) obtained numerical results for the intensity of light scattered by clouds. Hansen (1971a, b) and Hovenier (1971) extended the method to include polarization. Lacis and Hansen (1974) obtained results with the adding method for inhomogeneous model atmospheres, including the internal distribution of absorbed radiation. The procedure used by Grant and Hunt (1969) and Plass et al. (1973), called the matrix operator or star product method, is essentially the same as the adding method as far as actual computer computations are concerned.

Equations. Let τ_a and τ_b be the optical thickness of two layers to be added, with the subscripts a and b referring to the top and bottom layers, respectively (Figure 22). The recipe for the adding method is then[†]

$$\mathbf{Q}_1 = \mathbf{R}_a^* \mathbf{R}_b,$$

$$\mathbf{Q}_n = \mathbf{Q}_1 \mathbf{Q}_{n-1},$$

$$\mathbf{S} = \sum_{n=1}^{\infty} \mathbf{Q}_n,$$

$$\mathbf{D} = \mathbf{T}_a + \mathbf{S} \exp\left(- \tau_a/\mu_0\right) + \mathbf{S}\mathbf{T}_a,$$

$$\mathbf{U} = \mathbf{R}_b \exp\left(- \tau_a/\mu_0\right) + \mathbf{R}_b \mathbf{D},$$

$$\mathbf{R}\left(\tau_a + \tau_b\right) = \mathbf{R}_a + \exp\left(- \tau_a/\mu\right) \mathbf{U} + \mathbf{T}_a^* \mathbf{U},$$

$$\mathbf{T}\left(\tau_a + \tau_b\right) = \exp\left(- \tau_b/\mu\right) \mathbf{D} + \mathbf{T}_b \exp\left(- \tau_a/\mu_0\right) + \mathbf{T}_b \mathbf{D}. \tag{3.23}$$

The physical basis for this prescription can be inferred from Figure 22. The exponential terms refer to direct transmission through layer a or b without scattering; $\mathbf{T}$ is the diffuse transmission. Emerging from the bottom of the two layers is the diffuse trans-

$$R = R_1 + R_2 + R_3 + \cdots$$

$$U = U_1 + U_2 + U_3 + \cdots$$

$$D = D_1 + D_2 + D_3 + \cdots$$
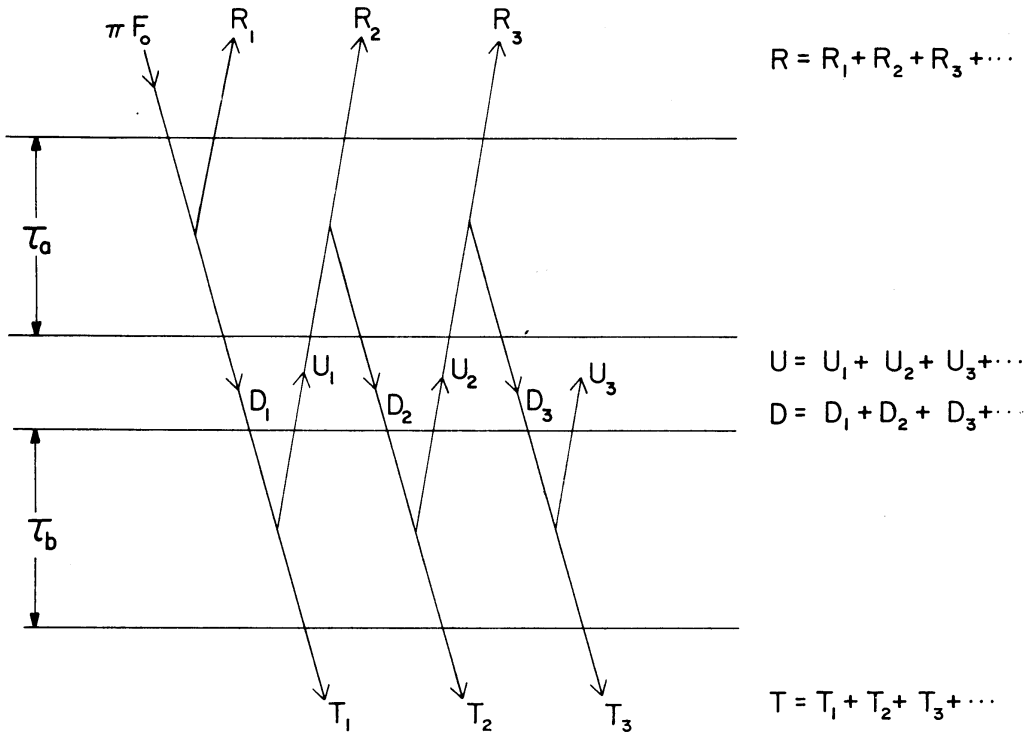
$$T = T_1 + T_2 + T_3 + \cdots$$

Fig. 22. Schematic representation of the adding method. The two layers of the atmosphere, of optical thickness τ_a and τ_b, are for convenience illustrated as if they were physically separated. In the computations, Equation (3.23), it is only necessary to make one summation.

[†] Sometimes the first three equations in (3.32) are combined by using a symbolic 'inverse operator' so that $\mathbf{S} = \mathbf{R}^*_a \mathbf{R}_b [1 - \mathbf{R}^*_a \mathbf{R}_b]^{-1}$; also the diffuse and direct transmission can be combined into one symbol. These changes are useful to abbreviate the recipe for adding, but the apparent simplifications are illusory since they do not simplify the actual computations.

mission $T(\tau_a + \tau_b)$ and the unscattered radiation of flux $\mu_0 \pi F_0 e^{-(\tau_a + \tau_b)/\mu_0}$ for horizontal areas. The transmission is explicitly divided into its diffuse and direct components because the appearance of a delta function in the total transmission makes it inappropriate for precise numerical integrations. D and U are, after multiplication by $\mu_0 F_0$, the diffuse intensities downward and upward at the dividing boundary between the two layers. The indicated summation is over the reflections between the two layers with $n-1$ indicating the number of times the radiation has crossed the dividing boundary going up. In practice this sum is terminated after a small number ($\lesssim 5$) of terms, depending on the accuracy desired. Furthermore, the omitted terms may be approximated by a geometric series because the ratio of successive terms approaches a constant value.

A prescription for computing R^* and T^*, analogous to (3.23), has been given by Lacis and Hansen (1974).

In (3.23) bold face symbols represent matrices of four rows and four columns. An arbitrary matrix of this type, say X, stands for

$$\mathbf{X} = X^{ij}(\mu, \mu_0, \phi - \phi_0), \qquad i, j = 1, 2, 3, 4, \tag{3.24}$$

where i and j are the indices for the rows and columns, respectively. The product of two matrices implies matrix multiplication and integration over the adjoining angles, an arbitrary $\mathbf{Z} = \mathbf{XY}$ being defined as

$$Z^{ij}(\mu, \mu_0, \phi - \phi_0) = \frac{1}{\pi} \int_0^1 \int_0^{2\pi} \left[\sum_{k=1}^4 X^{ik}(\mu, \mu', \phi - \phi') \, Y^{kj}(\mu', \mu_0, \phi' - \phi_0) \right] \mu' \, d\mu' \, d\phi'. \tag{3.25}$$

The numerical computations can be handled efficiently by means of a Fourier series expansion for the azimuth dependence and numerical quadrature for the μ' integrations. Formulae for the Fourier series expansions are given below. The adding Equations (3.23) remain valid for each Fourier component. Results are thus obtained for all values of $\phi - \phi_0$ and discrete values of μ and μ_0. The number of discrete zenith angles required depends on the anisotropy of the phase matrix and on the accuracy desired. This number of zenith angles can be kept at a moderate value, typically, 5–25, if the phase matrix is normalized for the discrete space of zenith angles (cf., Hansen, 1971b).

The doubling or adding method requires that the reflection and transmission matrices be known for the layers to be added. These can be obtained from analytic expressions for single scattering (cf., the following section on successive orders of scattering) with the initial optical thickness $\sim 2^{-20}$ or from any accurate multiple scattering method with a thicker initial layer. An efficient procedure is to compute successive orders of scattering for three orders and use an initial optical thickness $\sim 2^{-10}$.

In the formalism above we included polarization. However the adding method is also applicable as it stands to computations of the intensity with polarization neglected. It is only necessary that the matrices in (3.23) be interpreted as scalars; thus the superscripts in (3.24) and (3.25) may be omitted and there is no sum over k in

(3.25). The intensities computed with polarization neglected are approximations containing errors $\lesssim 10\%$ for Rayleigh scattering (Chandrasekhar, 1950) and errors $\lesssim 1\%$ for particles comparable to or larger than the wavelength in size (Hansen, 1971b).

Fourier series expansions. It is advantageous to expand the azimuth-dependent functions in Fourier series in $\phi - \phi_0$. Each term in the Fourier series may then be treated independently, allowing large savings in computer storage requirements. Furthermore, the behavior of different Fourier terms differs markedly and this behavior may be taken advantage of to reduce the computing time, as described below.

Let X represent the phase matrix or any of the matrices in (3.23). X may be expanded as

$$
X^{ij}(\mu, \mu_0, \phi - \phi_0) = {}^0X_c^{ij}(\mu, \mu_0) +
$$
$$
+ 2 \sum_{m=1}^{\infty} \left[{}^mX_c^{ij}(\mu, \mu_0) \cos m (\phi - \phi_0) + \right.
$$
$$
\left. + {}^mX_s^{ij}(\mu, \mu_0) \sin m (\phi - \phi_0) \right], \tag{3.26}
$$

where

$$
{}^mX_c^{ij}(\mu, \mu_0) = \frac{1}{2\pi} \int_0^{2\pi} X^{ij}(\mu, \mu_0, \phi') \cos m\phi' \, d\phi', \quad m = 0, 1, 2, \ldots, \tag{3.27}
$$

$$
{}^mX_s^{ij}(\mu, \mu_0) = \frac{1}{2\pi} \int_0^{2\pi} X^{ij}(\mu, \mu_0, \phi') \sin m\phi' \, d\phi', \quad m = 1, 2, \ldots. \tag{3.28}
$$

The rule for matrix multiplication, given by (3.25), becomes

$$
{}^0Z_c^{ij}(\mu, \mu_0) = 2 \int_0^1 \sum_{k=1}^4 {}^0X_c^{ik}(\mu, \mu') \, {}^0Y_c^{kj}(\mu', \mu_0) \mu' \, d\mu', \tag{3.29}
$$

$$
{}^mZ_c^{ij}(\mu, \mu_0) = 2 \int_0^1 \left\{ \sum_{k=1}^4 \left[{}^mX_c^{ik}(\mu, \mu') \, {}^mY_c^{kj}(\mu', \mu_0) - \right. \right.
$$
$$
\left. \left. - {}^mX_s^{ik}(\mu, \mu') \, {}^mY_s^{kj}(\mu', \mu_0) \right] \right\} \mu' \, d\mu', \tag{3.30}
$$

$$
{}^mZ_s^{ij}(\mu, \mu_0) = 2 \int_0^1 \left\{ \sum_{k=1}^4 \left[{}^mX_c^{ik}(\mu, \mu') \, {}^mY_s^{kj}(\mu', \mu_0) + \right. \right.
$$
$$
\left. \left. + {}^mX_s^{ik}(\mu, \mu') \, {}^mY_c^{kj}(\mu', \mu_0) \right] \right\} \mu' \, d\mu'. \tag{3.31}
$$

Most computations, including all numerical examples in this paper, are made for the special case in which the elements of the 4 by 4 phase matrix, $P^{ij}(\mu, \mu_0, \phi - \phi_0)$, are even functions of $\phi - \phi_0$ for the 2 by 2 submatrices ($ij = 11, 12, 21, 22$) and ($ij =$

$=33, 34, 43, 44$), and odd functions of $\phi - \phi_0$ for the submatrices $(ij=13, 14, 23, 24)$ and $(ij=31, 32, 41, 42)$. Thus in the following we omit the subscript s or c, since the superscript specifying the matrix element determines whether the function is odd or even.

Numerical examples. To illustrate the effect of multiple scattering on radiation reflected by a plane-parallel atmosphere we have made computations with four Mie scattering phase matrices. In each case for the real part of the refractive index we used $n_r = 1.44$; this happens to be approximately the value for the cloud particles on Venus (cf., Hansen and Hovenier, 1974), but the exact choice of n_r does not modify the general effects which we investigate. All four phase matrices are for the size distribution (2.56) with $a = 1\mu$ and $b = 0.07$, values which are also approximately correct for the Venus clouds. This effective radius of 1μ is large enough for features such as the rainbow and glory to exist at visible and near-infrared wavelengths.

TABLE II

Parameters defining the four Mie scattering phase matrices used for multiple scattering computations. In all four cases the real part of the refractive index was $n_r = 1.44$ and the particle size distribution was (2.56) with $a = 1 \mu$ and $b = 0.07$.

Case	n_i	λ	$\tilde{\omega}$	$\langle \cos \alpha \rangle$
1	0	0.55μ	1	0.7088
2	0.000024	0.55μ	0.999394	0.7090
3	0.000058	1μ	0.999408	0.7164
4	0.1	0.55μ	0.496827	0.9177

In Case 1 (Table II) we use $n_i = 0$ to obtain the maximum variation of reflected intensities with varying optical depth. In Cases 2 and 3 we choose small values of n_i such that the spherical albedo is 90% for $\tau = \infty$. Cases 2 and 3 differ in the wavelengths selected, 0.55μ and 1μ; this allows comparison of results for a case with the size parameter in the region with clear geometrical optics features and a case between the geometrical optics region and Rayleigh scattering. Case 4 has a substantial value of n_i, and thus serves as an example of results for absorbing particles. The complete phase matrices for these four cases are shown in Figure 23.

Figure 24 shows Fourier coefficients of the reflection matrix for the Case 1 phase matrix. These coefficients, computed for $\tau = 128$, are representative of results for a thick layer. $^m R^{11}$, which determines the intensity of reflected light for unpolarized incident light, usually is the largest of the matrix elements, at least for small m. $^m R^{21}$ and $^m R^{31}$ have comparable magnitudes, while $^m R^{41}$, which determines the circular polarization, is much smaller than the other matrix elements.

As suggested by Figure 24, the number of Fourier terms required to achieve a given relative accuracy depends strongly on μ and μ_0, but not so much on the matrix element. For Mie scattering the number of Legendre polynomials required to specify the

scattering functions S_1 and S_2 (2.42) is $\sim x$, as follows from the localization principle; thus the number of polynomials required to specify the phase matrix is $\sim 2x$ (cf. 2.41). It follows that in the most difficult case, when θ and θ_0 are both near grazing and single scattering dominates, the number of Fourier terms needed for an accurate result is $\sim 2x$. However, for many sets of θ and θ_0 the required number of Fourier terms is
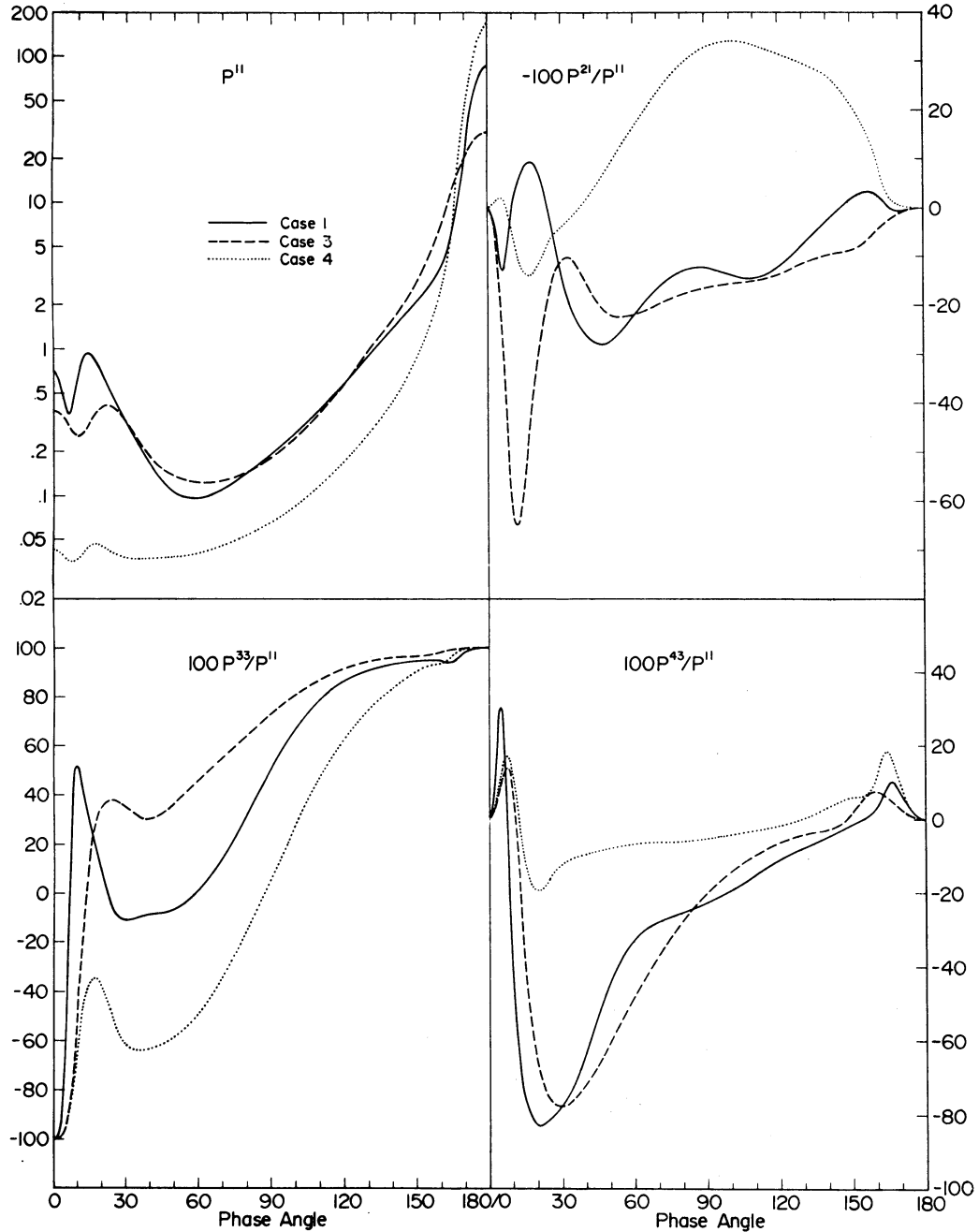
Fig. 23. Phase matrices for the four test cases (cf. Table II) used for multiple scattering computations. The phase matrix for Case 2 is indistinguishable from that which is illustrated for Case 1.
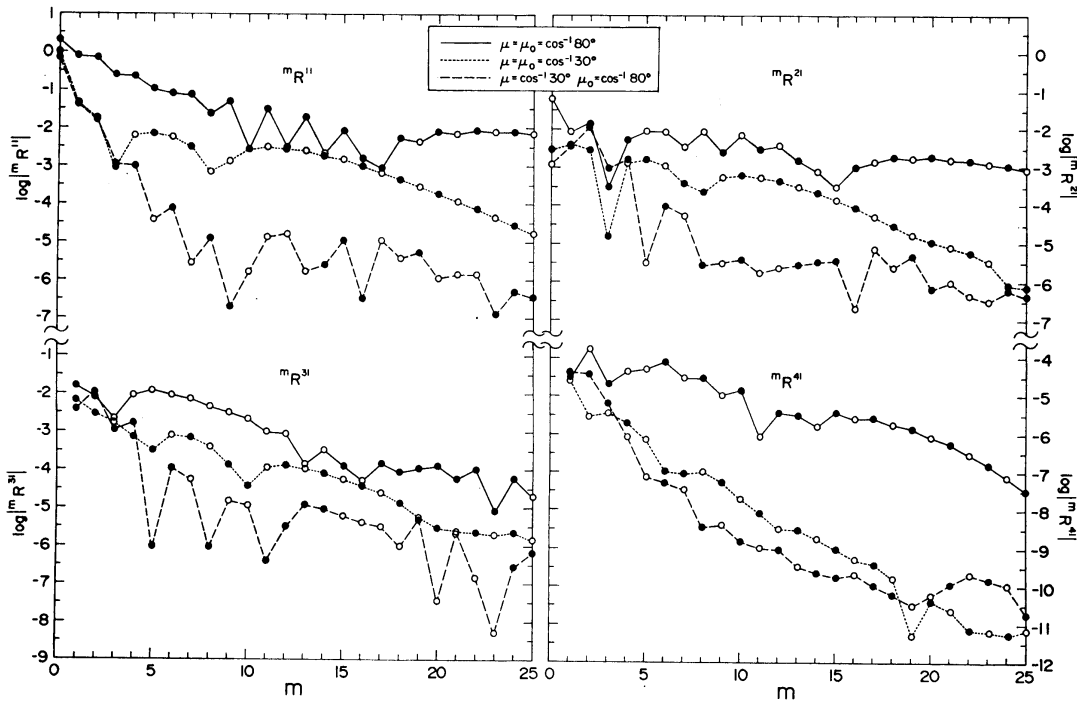
Fig. 24.   Fourier coefficients of the reflection matrix, for the Case 1 phase matrix with optical thickness 128. Filled circles indicate positive values and open circles negative values.

considerably less. Computing time can thus be reduced by terminating multiple scattering computations at some value of m which depends on μ and μ_0, as described by Hansen and Pollack (1970) and Dave and Gazdag (1970).

The number of terms which must be computed in the Fourier series can best be judged from graphs of the intensity summed over m. Examples of the reflection matrix for the Case 1 phase matrix are given in Figure 25 for $\tau = 128$. The results in the left half of Figure 25 are integrated over the disk of a spherical planet assuming a locally-plane-parallel atmosphere (cf. Horak, 1950). If the Stokes parameters U and V are integrated over a homogeneous planet they yield a null result for a phase matrix of the type (2.9); thus the integration for the circular polarization was extended only over the northern hemisphere for positive phase angles (which implies positive azimuth angles, cf. Horak, 1950). The circular polarization in the southern hemisphere has the same absolute value but the opposite sign; for negative phase angles all values must be multiplied by -1 (cf. Hansen, 1971c). The results in the right half of Figure 25 are the intensity as a function of $\phi - \phi_0$ for particular values of μ and μ_0.

For the Case 1 phase matrix $2x$ is ~ 23. However, for the light integrated over the planet 5 Fourier terms are already a good approximation and 15 terms give an accurate answer at most phase angles. This is partly due to the integration over the disk which averages the results over ϕ, but primarily it is due to the fact that only the sharpest features require the full number of Fourier terms. For $\theta = 30°$, $\theta_0 = 80°$ 5 Fourier terms give an accurate answer, while ~ 10 terms are required for $\theta = \theta_0 = 30°$ and ~ 20 terms for $\theta = \theta_0 = 80°$. Usually the required number of terms decreases as

θ and θ_0 decrease, because of the decreasing contribution of single scattering and the approach to the azimuth-independent situation, $\theta_0 = 0$. However, in Figure 25 the case $\theta = \theta_0 = 30°$ requires a substantial number of Fourier terms because in that case the scattering angle goes through the range 120–180°, which contains the rainbow and glory.

Thus it is not easy to give a recipe for the number of Fourier terms required for a given accuracy at a given angle. In practice, experience with computed results provides a good guide. Also, the Fourier coefficients for large values of m can be computed very rapidly, as described in the next section, and hence it is not essential that care be taken to terminate the series as quickly as possible.

The greatest number of Fourier terms is needed to define the diffraction peak. If accurate results are not required for scattering angles near 0° the number of Fourier terms which must be computed is considerably less than $2x$. However, in such a case the computational burden can be reduced even more by truncating the diffraction peak from the phase function and treating the photons scattered in the diffraction peak as if they were unscattered (cf. Hansen, 1969; Potter, 1970; Hansen and Pollack, 1970; Hansen, 1971b); this requires that $\tilde{\omega}$ and τ be appropriately scaled. The advantage of truncating the diffraction peak is that it considerably reduces the number of discrete zenith directions which must be used for the μ' integrations. The general forward
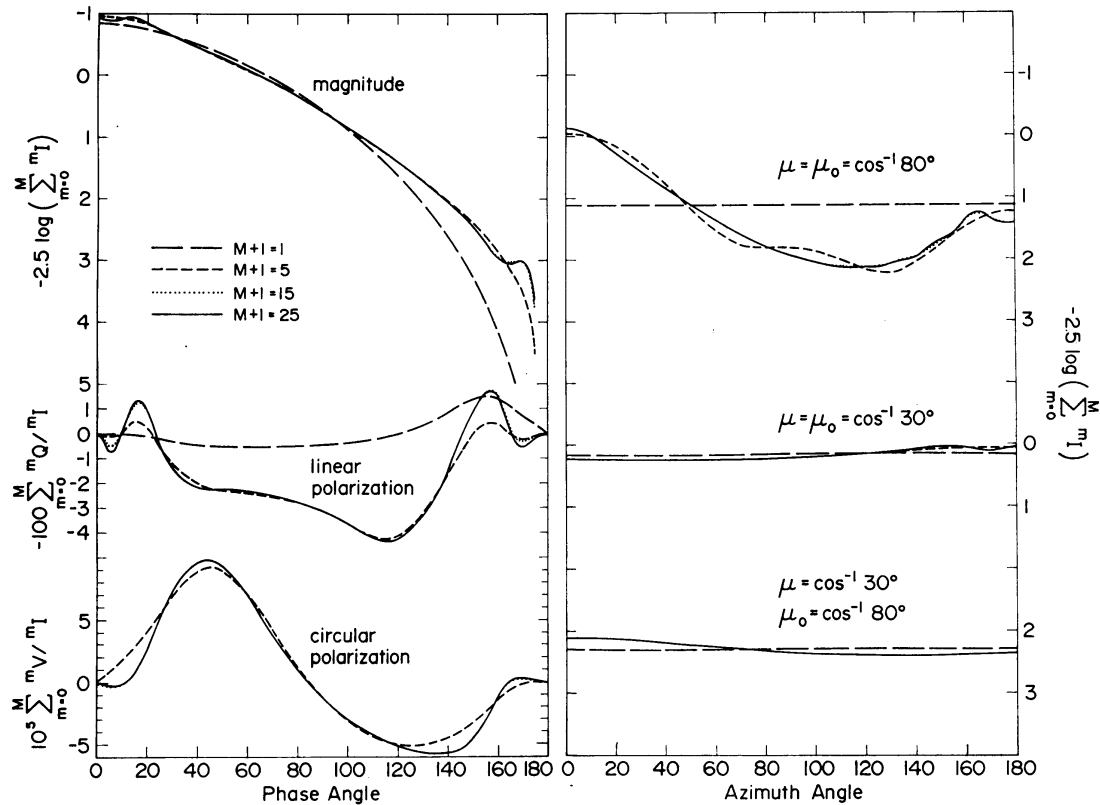

Fig. 25. Intensity, linear polarization and circular polarization of reflected sunlight for the Case 1 phase matrix with $\tau = 128$. $M + 1$ is the number of terms in the Fourier series. The incident solar flux is taken as π per unit area perpendicular to the incident beam.

scattering of the phase function, due to twice-refracted rays, is accurately described by 10–20 Fourier terms, depending on the value of the refractive index. However, rainbows and the glory may require more terms, because their sharpness increases as x increases. Respite from this difficulty is afforded by the rapid computation time for the high Fourier terms (cf. Section 3.2). Of course if only the flux or albedo is required, then only the $m=0$ term must be computed.

It is useful to examine the ratio of terms in the infinite series which occurs in the doubling method (3.23), including the dependence of the ratio on Fourier term. Let

$$^m\eta^{ij} \equiv \lim_{n \to \infty} {^mQ_n^{ij}}/{^mQ_{n-1}^{ij}}. \tag{3.32}$$

We find that $^m\eta^{ij}$ depends very little on matrix element (ij) and the dependence on μ, μ_0 which exists for $\tau \ll 1$ disappears as τ increases. Thus it is sufficient to plot $^m\eta^{11}$ as a function of m for several values of τ, as is done in Figure 26 for the Case 1 phase matrix.

For $m=0$ and $\tilde{\omega}=1$ $^m\eta^{ij}$ approaches unity as τ approaches infinity, an expected result since the flux is constant in an infinite conservatively scattering atmosphere. For large m, $^m\eta^{ij}$ is independent of τ. This indicates that the Fourier coefficients for large m are due to single scattering, which is a consequence of the fact that photons multiply scattered have a smoother distribution over angle. Hansen and Pollack (1970) took
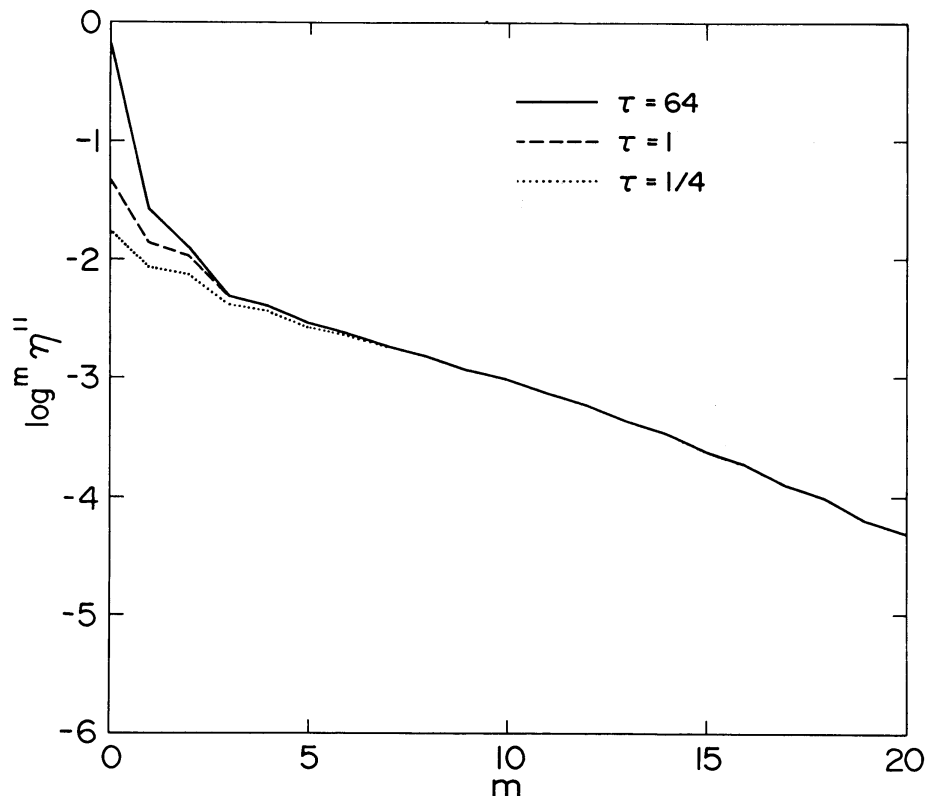

Fig. 26. $^m\eta^{11}$ as a function of the Fourier coefficient index m for the Case 1 phase matrix. $^m\eta^{11}$ is the limit of $^mQ_n^{11}/{^mQ_{n-1}^{11}}$ for large n, where $n-1$ is the number of times the light has passed the midlevel optical depth $(\tau/2)$ going up.

advantage of this fact to compute the high Fourier coefficients with the expression for single scattering. It is apparent that for intermediate values of m a few orders of scattering could be used to compute the Fourier coefficients. Since only the first few orders of scattering (say 3–5) contribute significantly for a layer with $\tau = 1/4$, Figure 26 suggests that only Fourier coefficients with $m \lesssim 5$ can not be obtained with a few orders of scattering. This expectation is basically borne out by computations in the next section.

In the remaining three graphs in this section we illustrate typical dependence of the intensity (Figure 27), linear polarization (Figure 28) and circular polarization (Figure 29) on τ, on particle size parameter and on particle absorption. The left halves of these figures are for the Case 1 phase matrix with four different values of τ. The right halves of the figures are for the Case 2, 3 and 4 phase matrices, all for $\tau = 128$, which in these cases is equivalent to $\tau = \infty$. For all three figures the Stokes parameters were integrated over a locally-plane-parallel spherical planet, but for the circular polarization the integration was only over the northern hemisphere.

Figure 27 shows that for small optical thicknesses features in the single scattering, such as the glory, rainbow and diffraction peak, can be readily identified in the intensity. However the features tend to be washed out for thick layers by the more isotropic multiple scattered light. Cases 2 and 3 have much different phase functions but values of $\tilde{\omega}$ such that the spherical albedo is 90% in both cases for $\tau \to \infty$. As a result the differences in the magnitude as a function of phase angle are minor between these two cases. Case 4 has a small value of $\tilde{\omega}$, due to $n_i = 0.1$, and thus the intensity is much less than in the other cases.
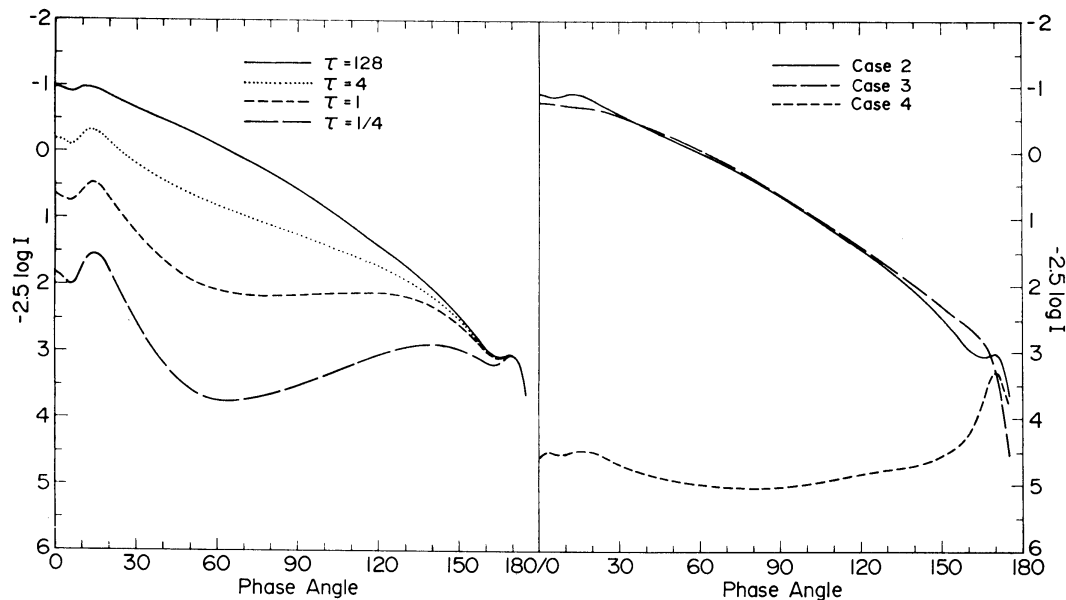

Fig. 27. Planetary magnitude, i.e. $-2.5 \log_{10} I$, as a function of phase angle. The left half of the figure is for the Case 1 phase matrix for four different values of the cloud optical thickness. The right half of the figure is for the Case 2, 3 and 4 phase matrices with $\tau = 128$. The incident solar flux is taken as π per unit area perpendicular to the incident beam.

Figure 28 illustrates that the linear polarization decreases with increasing optical depth. This is due to the fact that photons scattered several times tend to have little polarization, as shown more explicitly in the next section. Thus the neutral points (zero polarization) in the linear polarization do not move much with increasing τ, but the factor by which multiple scattering reduces the polarization is a strong function of phase angle. Since the linear polarization can be measured to an accuracy of $\sim 0.1\%$, the features in the angular distribution can be readily observed. The right half of Figure 28 illustrates that the polarization is sensitive to the variation in size parameter between Cases 2 and 3. In Case 4 the strong absorption in the particle ($n_i = 0.1$) results in the polarization of the scattered light being dominated by the positive polarization for Fresnel reflection. The small value of $\tilde{\omega}$ (~ 0.5) causes there to be little multiple scattering and thus the degree of linear polarization is large even for a thick atmosphere.

A review of applications of linear polarization to studies of planetary atmospheres has been given by Coffeen and Hansen (1974).

The circular polarization (Figure 29) also decreases with increasing optical depth for $\tau > 1/4$; as was the case for the linear polarization, this is due to the fact that photons scattered many times have low polarization. However, the circular polarization for single scattering is zero (cf. 3.22); thus the circular polarization is primarily due to the small polarization of photons scattered a few times, as graphically demonstrated in the following section. This explains the small magnitude of V/I for all τ and the fact that the neutral points move considerably with increasing τ. The right half of Figure 29 shows that the circular polarization is sensitive to particle size parameter and to
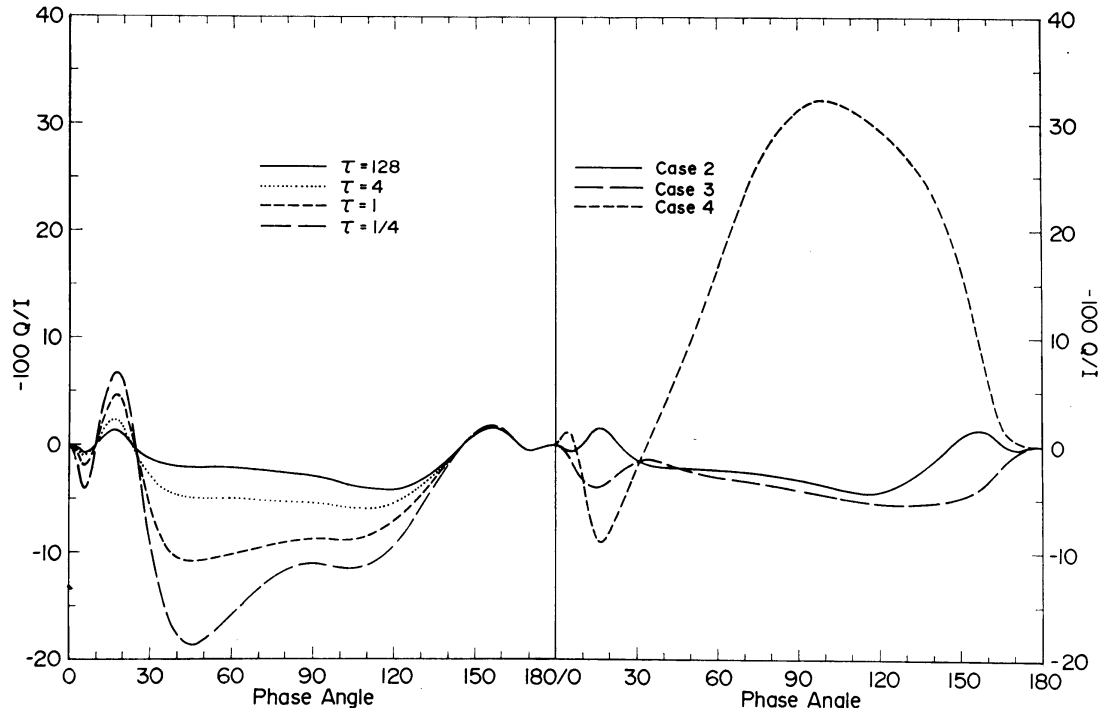

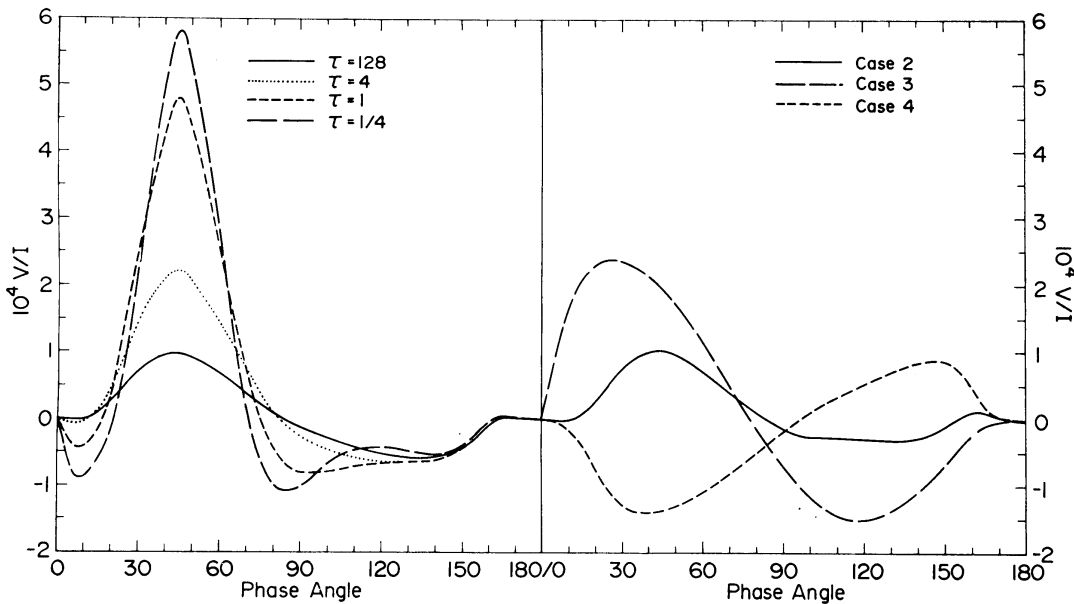Fig. 28. Same as Figure 27, but for the linear polarization, $-100Q/I$.

Fig. 29. Same as Figure 27, but for the circular polarization, $10^4 V/I$, and with the integration extended only over the northern hemisphere of the planet.

particle absorption. Note that the circular polarization is much greater for Case 3 ($x \sim 6$) than for Case 2 ($x \sim 11$), particularly for small phase angles, even though $V/I \to 0$ as $x \to 0$.

It is apparent that the circular polarization of reflected sunlight is a potentially valuable tool for remote analysis of cloud particle properties, particularly for the outer planets which can be observed over only a small range of phase angles from the Earth. Observations of Venus, for which the cloud particle properties are accurately known, would be useful to test the observational techniques and to verify the interpretation of the circular polarization for cloudy atmospheres. The capability for planetary circular polarization measurements has been proven by Kemp and associates (cf. Kemp *et al.*, 1971a, b; Kemp, 1974) and a thorough observational program seems warrented, including measurements from the ultraviolet to the near infrared at all available phase angles and measurements with a spatial resolution as high as practical. To extract the potential information contained in such observations it is essential that a detailed theoretical study be made of the influence of cloud particle parameters on the circular polarization and it is also essential that the observations of circular polarization be analyzed simultaneously with the linear polarization and intensity.

3.2. SUCCESSIVE ORDERS OF SCATTERING

The method of successive orders of scattering is one of the oldest and simplest in concept of the different solutions to multiple scattering problems. Several quite different methods of successive order scattering have been developed, but they have the common property that the intensity is computed individually for photons scattered once, twice, three times, etc., with the total intensity obtained as the sum over all

orders. Thus for the diffuse intensities we write

$$\mathbf{I}_r(\mu, \phi) = \sum_{n=1}^{\infty} \mathbf{I}_{r,n}(\mu, \phi),$$

$$\mathbf{I}_t(\mu, \phi) = \sum_{n=1}^{\infty} \mathbf{I}_{t,n}(\mu, \phi),$$

(3.33)

where n is the order of scattering. The reflection and transmission matrices are similarly decomposed

$$\mathbf{R}(\mu, \mu_0, \phi - \phi_0) = \sum_{n=1}^{\infty} \mathbf{R}_n(\mu, \mu_0, \phi - \phi_0),$$

$$\mathbf{T}(\mu, \mu_0, \phi - \phi_0) = \sum_{n=1}^{\infty} \mathbf{T}_n(\mu, \mu_0, \phi - \phi_0).$$

(3.34)

For cases in which a large number of scatterings are possible ($\tau \gtrsim 1$, $\tilde{\omega} \sim 1$) it might appear to be inefficient to solve for each order of scattering, since methods such as the adding method readily yield the reflection and transmission functions for the sum of all orders. However, there are several reasons why it is valuable to compute the intensities separately for at least a few orders, e.g.,

(1) In a Fourier series expansion of the intensity the high frequency terms arise from photons scattered a small number of times. Thus most of the Fourier terms may be accurately obtained by computing a few orders of scattering.

(2) In the doubling method a significant amount of computing time can be saved by taking an initial optical thickness $\sim 2^{-10}$ and computing 3 orders of scattering for that layer.

(3) For a homogeneous layer a solution for the intensity due to photons scattered n times with conservative scattering ($\tilde{\omega} = 1$) yields the solution for all other $\tilde{\omega}$, after multiplication by the factor $\tilde{\omega}^n$. In some cases this can be useful for computing absorption line profiles (cf. Belton *et al.*, 1968) or for computing heating rates, which involve an integration over frequency (cf. Lacis and Hansen, 1974).

(4) The results for successive orders provide insight useful for understanding multiple scattering results.

Classical method. The classical method for computing successive orders of scattering is based on the equation of transfer for the diffuse intensity

$$u \frac{d\mathbf{I}(\tau, u, \mu_0, \phi - \phi_0)}{d\tau} = -\mathbf{I}(\tau, u, \mu_0, \phi - \phi_0) + \mathbf{J}(\tau, u, \mu_0, \phi - \phi_0),$$

(3.35)

where

$$\mathbf{J}(\tau, u, \mu_0, \phi - \phi_0) \equiv \int_{-1}^{1} \int_{0}^{2\pi} \mathbf{P}(u, u', \phi - \phi') \mathbf{I}(\tau, u', \mu_0, \phi' - \phi_0) \, du' \, d\phi'$$

$$+ \frac{\tilde{\omega}}{4} e^{-\tau/\mu_0} \mathbf{P}(u, \mu_0, \phi - \phi_0) \mathbf{F}_0$$

(3.36)

is called the source function. The equation of transfer is subject to two-point boundary conditions, specifically at $\tau=0$ for $u>0$ and $\tau=\tau_0$ for $u<0$. For example, if the lower boundary is completely absorbing,

$$\begin{aligned}
\mathbf{I}(0, u, \phi) &= 0, & u &> 0 \\
\mathbf{I}(\tau_0, u, \phi) &= 0. & u &< 0
\end{aligned} \tag{3.37}$$

For these boundary conditions the 'formal' solution of the equation of transfer is

$$\mathbf{I}(\tau, u, \mu_0, \phi - \phi_0) = \int_0^\tau \mathbf{J}(\tau', u, \mu_0, \phi - \phi_0) \, e^{-(\tau - \tau')/u} \, d\tau'/u$$

$$(u = \mu > 0), \tag{3.38}$$

$$\mathbf{I}(\tau, u, \mu_0, \phi - \phi_0) = - \int_\tau^{\tau_0} \mathbf{J}(\tau', u, \mu_0, \phi - \phi_0) \, e^{(\tau' - \tau)/u} \, d\tau'/u$$

$$(u = -\mu < 0).$$

The second term on the right side of (3.36) is the source function due to the first scattering of the incident radiation,

$$\mathbf{J}_1(\tau, u, \mu_0, \phi - \phi_0) = \frac{\tilde{\omega}}{4} e^{-\tau/\mu_0} \mathbf{P}(u, \mu_0, \phi - \phi_0) \mathbf{F}_0. \tag{3.39}$$

Inserting (3.39) in the formal solution of the equation of transfer and integrating over τ we obtain the intensity due to photons scattered one time. For a homogeneous atmosphere the corresponding reflection and transmission matrices are

$$\begin{aligned}
\mathbf{R}_1(\mu, \mu_0, \phi - \phi_0) &\equiv \frac{\mathbf{I}_{r,1}(\mu, \mu_0, \phi - \phi_0)}{\mu_0 \mathbf{F}_0} = \\
&= \frac{\tilde{\omega}}{4(\mu + \mu_0)} \left\{ 1 - \exp\left[-\tau_0\left(\frac{1}{\mu} + \frac{1}{\mu_0}\right)\right]\right\} \times \\
&\quad \times \mathbf{P}(-\mu, \mu_0, \phi - \phi_0),
\end{aligned}$$

$$\begin{aligned}
\mathbf{T}_1(\mu, \mu_0, \phi - \phi_0) &\equiv \frac{\mathbf{I}_{t,1}(\mu, \mu_0, \phi - \phi_0)}{\mu_0 \mathbf{F}_0} = \\
&= \frac{\tilde{\omega}}{4(\mu - \mu_0)} \left[\exp\left(\frac{-\tau_0}{\mu}\right) - \exp\left(\frac{-\tau_0}{\mu_0}\right)\right] \times \\
&\quad \times \mathbf{P}(\mu, \mu_0, \phi - \phi_0), \tag{3.40}
\end{aligned}$$

and, from l' Hospital's rule, for $\mu = \mu_0$,

$$\mathbf{T}_1(\mu_0, \mu_0, \phi - \phi_0) = \frac{\tilde{\omega}\tau_0}{4\mu_0^2} \exp\left(\frac{-\tau_0}{\mu_0}\right) \mathbf{P}(\mu_0, \mu_0, \phi - \phi_0). \tag{3.41}$$

The source function for higher orders of scattering follows from

$$\mathbf{J}_{n+1}\left(\tau, u, \mu_0, \phi - \phi_0\right) = \frac{\tilde{\omega}}{4\pi} \int\limits_{-1}^{1} \int\limits_{0}^{2\pi} \mathbf{P}\left(u, u', \phi - \phi'\right) \times$$

$$\times \mathbf{I}_n\left(\tau, u', \mu_0, \phi' - \phi_0\right) du' d\phi' \qquad (3.42)$$

and the intensity from

$$\mathbf{I}_n\left(\tau, u, \mu_0, \phi - \phi_0\right) = \int\limits_{0}^{\tau} \mathbf{J}_n\left(\tau', u, \mu_0, \phi - \phi_0\right) e^{-(\tau - \tau')/u} d\tau'/u$$

$$(u = \mu > 0), \qquad (3.43)$$

$$\mathbf{I}_n\left(\tau, u, \mu_0, \phi - \phi_0\right) = -\int\limits_{\tau}^{\tau_0} \mathbf{J}_n\left(\tau', u, \mu_0, \phi - \phi_0\right) e^{(\tau' - \tau)/u} d\tau'/u$$

$$(u = -\mu < 0).$$

This method of successive order scattering has been used by van de Hulst (1948), Dave (1964), Irvine (1965) and others. With the integrations performed numerically this method has the advantage of being applicable to an inhomogeneous atmosphere. Disadvantages are large computing times and low accuracies for large optical thicknesses ($\tau \gtrsim 5$). Some respite is afforded by the fact that the ratio of successive terms, $I_{r,n}/I_{r,n-1}$ approaches a constant for large n (van de Hulst and Irvine, 1962), but the convergence to that constant is slow.

For a homogenous atmosphere a high accuracy can be achieved for all optical thicknesses by performing the τ integrations analytically. This has been done for second order scattering by Hovenier (1971) and for third order scattering by Travis (1974).

Invariance principle. For a homogeneous atmosphere the numerical τ integration can be avoided in a fashion somewhat more elegant than that described above. We derive here equations for successive orders of scattering which involve only μ integrations. The derivation is closely related to the invariant imbedding method described in Section 3.4. A similar derivation was also given by Uesugi and Irvine (1970); however, they did not include transmission or polarization and they considered only the special case $\tau = \infty$.

The reflection and transmission matrices for nth order scattering may be obtained from the same matrices for lower orders of scattering by using the following obvious 'invariance principle': *If a layer having the same optical properties is added to the top of a homogeneous layer, the reflection and transmission matrices are the same as they would be if the second layer were instead added to the bottom!*

If the added layer is so thin (optical thickness $\Delta\tau \ll 1$) that only single scattering occurs within it, then the events A, B, C and D in Figure 30 contribute to the nth order scattering. For $n = 2$ only events A, B and C occur. From the definition of the reflection
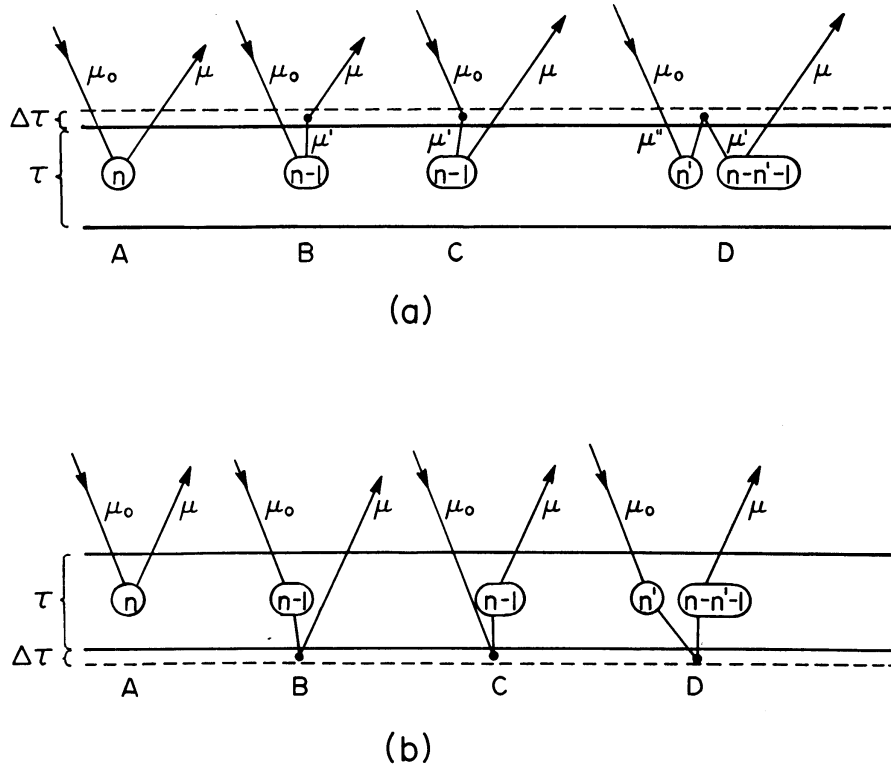
Fig. 30. Schematic representation of nth order diffuse reflection by a finite layer when an optically thin layer is added to the top (a) or bottom (b) of the main layer. There is at most one scattering in the thin layer.

matrix (3.3) and the single scattering expressions (3.40) we can write the reflection matrix for the layer of thickness $\tau + \Delta\tau$ as

$$
\mathbf{R}_n\left(\tau + \Delta\tau; \mu, \mu_0, \phi - \phi_0\right) = \left[1 - \frac{\Delta\tau}{\mu}\right]\mathbf{R}_n\left(\tau; \mu, \mu_0, \phi - \phi_0\right)\left[1 - \frac{\Delta\tau}{\mu_0}\right] +
$$

$$
+ \frac{1}{\pi}\int\limits_0^1\int\limits_0^{2\pi} \mu' \; \frac{\tilde{\omega}\Delta\tau}{4\mu'\mu} \mathbf{P}_t^*\left(\mu, \mu', \phi - \phi'\right) \mathbf{R}_{n-1}\left(\tau; \mu', \mu_0, \phi' - \phi_0\right) d\mu' \; d\phi' +
$$

$$
+ \frac{1}{\pi}\int\limits_0^1\int\limits_0^{2\pi} \mu' \; \mathbf{R}_{n-1}\left(\tau; \mu, \mu', \phi - \phi'\right) \frac{\tilde{\omega}\Delta\tau}{4\mu'\mu_0} \mathbf{P}_t\left(\mu', \mu_0, \phi' - \phi_0\right) d\mu' \; d\phi' +
$$

$$
+ \sum_{n'=1}^{n-2} \frac{1}{\pi}\int\limits_0^1\int\limits_0^{2\pi} \mu' \; \mathbf{R}_{n-n'-1}\left(\tau; \mu, \mu', \phi - \phi'\right) \times
$$

$$
\times \left[\frac{1}{\pi}\int\limits_0^1\int\limits_0^{2\pi} \mu'' \; \frac{\tilde{\omega}\Delta\tau}{4\mu'\mu''} \mathbf{P}_r^*\left(\mu', \mu'', \phi' - \phi''\right) \times \right.
$$

$$
\left. \times \mathbf{R}_{n'}\left(\tau; \mu'', \mu_0, \phi'' - \phi_0\right) d\mu'' \; d\phi''\right] d\mu' \; d\phi' . \tag{3.44}
$$

Similarly, for the case in which a layer of optical thickness $\Delta\tau$ is added to the bottom, (Figure 30b), we obtain

$$
\mathbf{R}_n(\tau + \Delta\tau; \mu, \mu_0, \phi - \phi_0) = \mathbf{R}_n(\tau; \mu, \mu_0, \phi - \phi_0) +
$$

$$
+ \frac{1}{\pi} \int_0^1 \int_0^{2\pi} \mu' e^{-\tau/\mu} \frac{\tilde{\omega}\Delta\tau}{4\mu'\mu} \mathbf{P}_r(\mu, \mu', \phi - \phi') \, \mathbf{T}_{n-1}(\tau; \mu', \mu_0, \phi' - \phi_0) \, \mathrm{d}\mu' \, \mathrm{d}\phi' +
$$

$$
+ \frac{1}{\pi} \int_0^1 \int_0^{2\pi} \mu' e^{-\tau/\mu_0} \mathbf{T}^*_{n-1}(\tau; \mu, \mu', \phi - \phi') \frac{\tilde{\omega}\Delta\tau}{4\mu'\mu_0} \mathbf{P}_r(\mu', \mu_0, \phi' - \phi_0) \, \mathrm{d}\mu' \, \mathrm{d}\phi' +
$$

$$
+ \sum_{n'=1}^{n-2} \frac{1}{\pi} \int_0^1 \int_0^{2\pi} \mu' \, \mathbf{T}^*_{n-n'-1}(\tau; \mu, \mu', \phi - \phi') \times
$$

$$
\times \left[\frac{1}{\pi} \int_0^1 \int_0^{2\pi} \mu'' \frac{\tilde{\omega}\Delta\tau}{4\mu'\mu''} \mathbf{P}_r(\mu', \mu'', \phi' - \phi'') \times \right.
$$

$$
\left. \times \mathbf{T}_{n'}(\tau; \mu'', \mu_0, \phi'' - \phi_0) \, \mathrm{d}\mu'' \, \mathrm{d}\phi'' \right] \mathrm{d}\mu' \, \mathrm{d}\phi' .
\tag{3.45}
$$

For $n = 2$ the last term on the right hand side of (3.44) and the last term on the right hand side of (3.45) should be omitted.

Subtracting Equation (3.45) from Equation (3.44) and neglecting terms of order $(\Delta\tau)^2$ we obtain

$$
\left(\frac{1}{\mu} + \frac{1}{\mu_0} \right) \mathbf{R}_n(\tau; \mu, \mu_0, \phi - \phi_0) =
$$

$$
= \frac{\tilde{\omega}}{4\pi\mu} \int_0^1 \int_0^{2\pi} \mathbf{P}^*_t(\mu, \mu', \phi - \phi') \, \mathbf{R}_{n-1}(\tau; \mu', \mu_0, \phi' - \phi_0) \, \mathrm{d}\mu' \, \mathrm{d}\phi' +
$$

$$
+ \frac{\tilde{\omega}}{4\pi\mu_0} \int_0^1 \int_0^{2\pi} \mathbf{R}_{n-1}(\tau; \mu, \mu', \phi - \phi') \, \mathbf{P}_t(\mu', \mu_0, \phi' - \phi_0) \, \mathrm{d}\mu' \, \mathrm{d}\phi' -
$$

$$
- \frac{\tilde{\omega} e^{-\tau/\mu_0}}{4\pi\mu_0} \int_0^1 \int_0^{2\pi} \mathbf{T}^*_{n-1}(\tau, \mu, \mu', \phi - \phi') \, \mathbf{P}_r(\mu', \mu_0, \phi - \phi_0) \, \mathrm{d}\mu' \, \mathrm{d}\phi' -
$$

$$
- \frac{\tilde{\omega} e^{-\tau/\mu}}{4\pi\mu} \int_0^1 \int_0^{2\pi} \mathbf{P}_r(\mu, \mu', \phi - \phi') \, \mathbf{T}_{n-1}(\tau, \mu', \mu_0, \phi' - \phi_0) \, \mathrm{d}\mu' \, \mathrm{d}\phi' +
$$

$$
+ \sum_{n'=1}^{n-2} \frac{\tilde{\omega}}{4\pi} \int_0^1 \int_0^{2\pi} \mathbf{R}_{n-n'-1}(\tau; \mu, \mu', \phi - \phi') \times
$$

$$\times \left[\frac{1}{\pi} \int_0^1 \int_0^{2\pi} \mathbf{P}_r^* \left(\mu', \mu'', \phi' - \phi'' \right) \mathbf{R}_{n'} \left(\tau; \mu'', \mu_0, \phi'' - \phi_0 \right) d\mu'' \, d\phi'' \right] d\mu' \, d\phi' -$$

$$- \sum_{n'=1}^{n-2} \frac{\tilde{\omega}}{4\pi} \int_0^1 \int_0^{2\pi} \mathbf{T}_{n-n'-1}^* \left(\tau; \mu, \mu', \phi - \phi' \right) \times$$

$$\times \left[\frac{1}{\pi} \int_0^1 \int_0^{2\pi} \mathbf{P}_r \left(\mu', \mu'', \phi' - \phi'' \right) \mathbf{T}_{n'} \left(\tau; \mu'', \mu_0, \phi'' - \phi_0 \right) d\mu'' \, d\phi'' \right] d\mu' \, d\phi' .$$

$$(3.46)$$

This is the desired equation for the nth order reflection matrix. For $n = 2$ the last two terms in Equation (3.46) should be omitted.

An equation for the nth order transmission matrix may be obtained in a similar manner. In Figure 30 the only difference is that the last leg in the photon history is downward. The resulting equation is

$$\left(\frac{1}{\mu} - \frac{1}{\mu_0} \right) \mathbf{T}_n \left(\tau; \mu, \mu_0, \phi - \phi_0 \right) =$$

$$= \frac{\tilde{\omega}}{4\pi\mu} \int_0^1 \int_0^{2\pi} \mathbf{P}_t \left(\mu, \mu', \phi - \phi' \right) \mathbf{T}_{n-1} \left(\tau; \mu', \mu_0, \phi' - \phi_0 \right) d\mu' \, d\phi' -$$

$$- \frac{\tilde{\omega}}{4\pi\mu_0} \int_0^1 \int_0^{2\pi} \mathbf{T}_{n-1} \left(\tau; \mu, \mu', \phi - \phi' \right) \mathbf{P}_t \left(\mu', \mu_0, \phi' - \phi_0 \right) d\mu' \, d\phi' +$$

$$+ \frac{\tilde{\omega} e^{-\tau/\mu_0}}{4\pi\mu_0} \int_0^1 \int_0^{2\pi} \mathbf{R}_{n-1}^* \left(\tau; \mu, \mu', \phi - \phi' \right) \mathbf{P}_r \left(\mu', \mu_0, \phi' - \phi_0 \right) d\mu' \, d\phi' -$$

$$- \frac{\tilde{\omega} e^{-\tau/\mu}}{4\pi\mu} \int_0^1 \int_0^{2\pi} \mathbf{P}_r^* \left(\mu, \mu', \phi - \phi' \right) \mathbf{R}_{n-1} \left(\tau; \mu', \mu_0, \phi' - \phi_0 \right) d\mu' \, d\phi' +$$

$$+ \sum_{n'=1}^{n-2} \frac{\tilde{\omega}}{4\pi} \int_0^1 \int_0^{2\pi} \mathbf{R}_{n-n'-1}^* \left(\tau; \mu, \mu', \phi - \phi' \right) \times$$

$$\times \left[\frac{1}{\pi} \int_0^1 \int_0^{2\pi} \mathbf{P}_r \left(\mu', \mu'', \phi' - \phi'' \right) \mathbf{T}_{n'} \left(\tau; \mu'', \mu_0, \phi'' - \phi_0 \right) d\mu'' \, d\phi'' \right] d\mu' \, d\phi' -$$

$$- \sum_{n'=1}^{n-2} \frac{\tilde{\omega}}{4\pi} \int_0^1 \int_0^{2\pi} \mathbf{T}_{n-n'-1} \left(\tau; \mu, \mu', \phi - \phi' \right) \times$$

$$\times \left[\frac{1}{\pi} \int\limits_0^1 \int\limits_0^{2\pi} \mathbf{P}_r^* \left(\mu', \mu'', \phi' - \phi'' \right) \mathbf{R}_{n'} \left(\tau; \mu'' \, \mu_0, \phi'' - \phi_0 \right) d\mu'' \, d\phi'' \right] d\mu' \, d\phi' .$$

$$(3.47)$$

Equations (3.46) and (3.47) can also be obtained from the invariant imbedding equations (Section 3.4) by expanding $\mathbf{R}$ and $\mathbf{T}$ in powers of $\tilde{\omega}$ and equating coefficients of $\tilde{\omega}^n$.

In a computer program it is efficient to omit $\tilde{\omega}$ from (3.46) and (3.47), i.e. to make computations for $\tilde{\omega} = 1$, and multiply $\mathbf{R}_n$ and $\mathbf{T}_n$ for each order of scattering by $\tilde{\omega}^n$ after all desired orders have been computed.

The azimuth dependence can be handled efficiently by means of Fourier expansions of $\mathbf{R}_n$, $\mathbf{T}_n$ and $\mathbf{P}$, as described above for the adding method. With such an expansion there are equations like (3.46) and (3.47) for each Fourier component, $\mathbf{R}_n^m$ and $\mathbf{T}_n^m$.

Note that (3.47) is indeterminate for $\mu = \mu_0$. Approximate results for that special case can be obtained by interpolation. Precise results, at least for second and third order scattering, can be obtained from the formulae obtained with the analytic τ integration described above.

Equations (3.46) and (3.47) give the nth order reflection and transmission in terms of all lower orders of scattering. Thus the lower orders must be retained individually. However for most of the applications described above the first three or four orders of scattering is sufficient. Thus the computation and storage problems are easily manageable.

Numerical examples. The results in this section were obtained employing (3.46) and (3.47), as described above except the totals for all orders of scattering which were computed with the doubling method. The graphs here suggest how an order of scattering approach can be used for rapid computations in certain cases and they illustrate the relative contributions of different orders of scattering to the intensity, linear polarization and circular polarization of reflected light.

Figure 31 shows how accurately the Fourier coefficients of the reflection matrix are approximated by the first four orders of scattering. These results are for the Case 1 phase matrix with $\tau = 128$ and $\theta = \theta_0 = 80°$, a set of angles which requires a large number of Fourier terms (cf. Figure 24). Two orders of scattering are sufficient to yield accurate results for terms with $m \gtrsim 20$. Except for the circular polarization (R^{41}), terms with $m \gtrsim 5$ are accurately obtained from four orders of scattering with an assumption of a geometric series for the higher orders of scattering. However, the improvement in the accuracy obtained by approximating the higher orders of scattering with a geometric series is moderate, even after four orders of scattering.

To determine the utility of the orders of scattering method it is useful to compare the computing time to that for the doubling method. In the infinite series in the doubling method three terms plus the assumption of a geometric series is sufficient for practically all Fourier terms (cf. Figure 26); thus the number of matrix multiplications in the doubling method (3.23) is ~ 7. First order scattering involves no matrix multiplications

and takes a negligible computing time. Second order scattering [(3.46) and (3.47)] involves eight matrix multiplications and third order scattering requires 14 additional matrix multiplications. Thus to compute the complete reflection and transmission matrices for the first three orders of scattering requires somewhat more time than that for three doublings. From test computations we find that the optimum combination of the doubling and orders of scattering methods is obtained: (a) for the low Fourier terms by doubling from an initial optical thickness $\sim 2^{-10}$ with the initial reflection and transmission matrices computed for three orders of scattering, (b) for the high Fourier terms by computing four orders of scattering (less for the highest terms) at the desired values of τ, with no doubling. Note that for the high Fourier terms the last order of scattering needs to be computed only for the first column of the reflection matrix and only for the particular values of θ and θ_0 for which results are desired.

Figure 32 shows the intensity for one, two, three, four and all orders of scattering for light integrated over a spherical but locally-plane-parallel atmosphere with $\tau = 128$. The results in the left half of the figure are for the Case 1 phase matrix and those in the right half for the Case 4 phase matrix. Figure 33 is the same except that it shows the
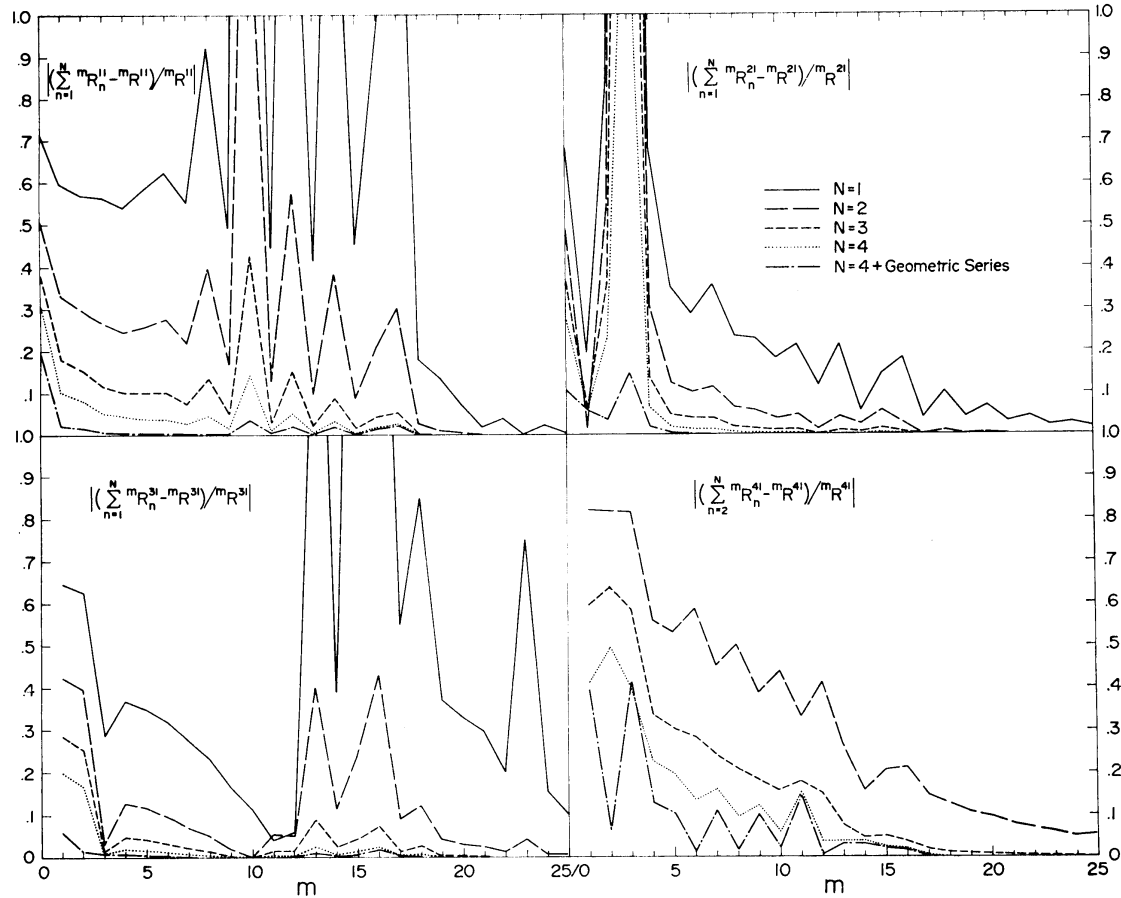

Fig. 31. Fractional error when the reflection matrix is approximated by a few orders of scattering. The calculations are for the Case 1 phase matrix with $\tau = 128$ and $\mu = \mu_0 = \cos^{-1} 80°$. The dash-dot curves were obtained by approximating orders of scattering above the fourth as a geometric series, i.e., with $^m R_4{}^{ij}/(1 - {}^m R_4{}^{ij}/{}^m R_3{}^{ij})$.

linear polarization. Figure 34 is the circular polarization for the same phase matrices, but obtained from an integration over only the northern hemisphere for positive phase angles (and thus positive $\phi - \phi_0$).

Figure 32 illustrates that for a thick atmosphere and high single scattering albedo four orders of scattering do not even qualitatively resemble the total intensity for all orders of scattering. Furthermore, approximating the higher orders of scattering with a geometric series does not help; for example, with that procedure the intensity obtained is about one (astronomical) magnitude too small for phase angles $\lesssim 30°$ and more than two magnitudes too large for phase angles $\sim 60°$. For the Case 4 phase matrix, which has $\tilde{\omega} \sim 0.5$, four orders of scattering are a fair approximation to the total intensity. With the addition of a geometric series for the higher orders of scattering an accuracy within a few percent can be achieved. Of course for an optically thin layer $(\tau \lesssim 1)$ it is always possible to obtain the intensity accurately with four orders of scattering plus a geometric series.

In Figures 33 and 34 note that the total intensity is used while the other Stokes parameters are summed over N orders of scattering. This is an effective way to illustrate the polarization due to higher orders of scattering. It is also of potential application because it is possible to rapidly compute the intensity with an accuracy of better than 1% (for particles larger than or comparable to the wavelength in size) by neglecting polarization (cf., Hansen, 1971b). The accuracy of using the total intensity along with orders of scattering computations for the other Stokes parameters has been tested for
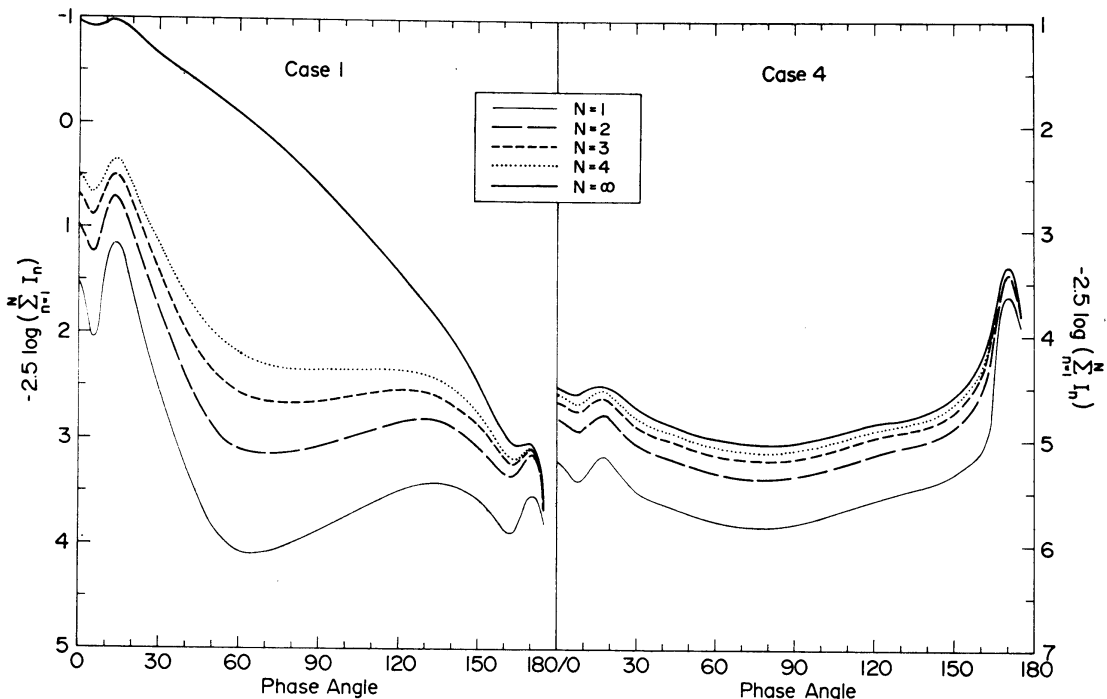

Fig. 32.   Planetary magnitude for one, two, three, four and all orders of scattering. The left half of the figure is for the Case 1 phase matrix and the right half for the Case 4 phase matrix. The cloud optical thickness is 128 in both cases.
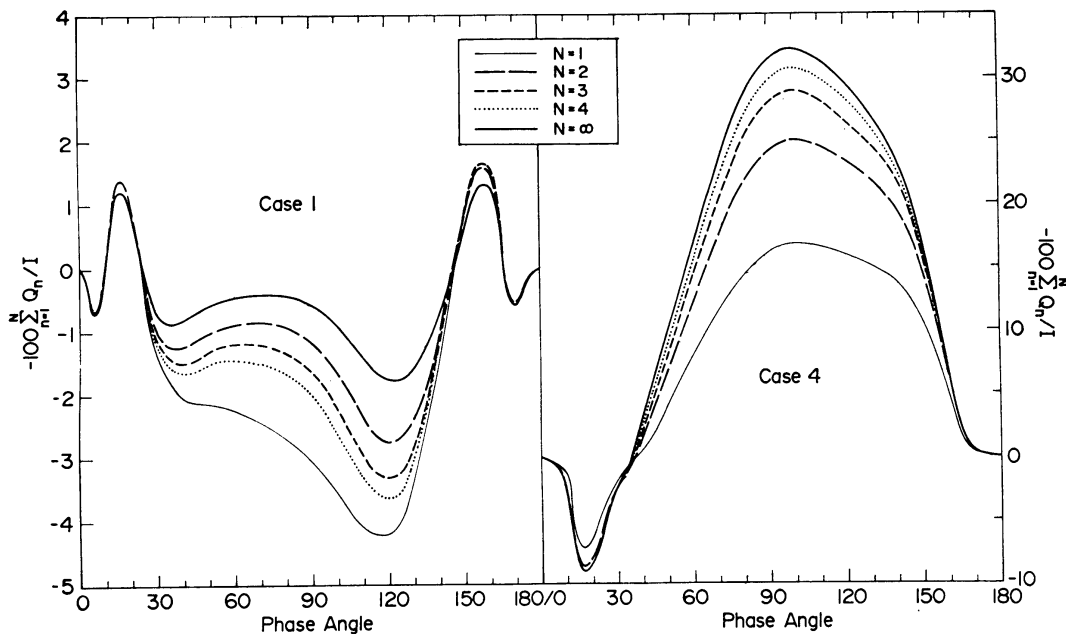
Fig. 33. Same as Figure 32, but for the linear polarization.

two orders of scattering by Hansen and Hovenier (1971). Hovenier (1971) has suggested that the accuracy could be greatly improved by computing a few orders of scattering and approximating the omitted terms with a geometric series.

Figure 33 shows that at some phase angles there is still a significant contribution to the linear polarization from fourth and higher orders of scattering. Much of the polarization of high order scattering arises from photons which have their first few scatterings in the forward direction, after which they are still nearly unpolarized and moving approximately in the direction of incidence, and their last scattering at a large phase angle. This has been demonstrated by Hansen (1971b), who uses this behavior to obtain an improved 'single scattering' approximation.

If the approximation of a geometric series is added to the $N = 4$ result the agreement with the linear polarization for $N = \infty$ is substantially improved, with the maximum difference in Figure 33 being $\lesssim 0.2\%$ polarization. Thus Q_n approaches a geometric series much more rapidly than does I_n. This was previously noted by Hovenier (1971) from calculations for first and second order scattering.

Figure 34 indicates that four orders of scattering do not provide a good approximation for the circular polarization. This is true even for the Case 4 phase matrix which has $\tilde{\omega} \sim 0.5$; for example, at small phase angles the circular polarization for four orders of scattering has the opposite sign of that for all orders of scattering. Furthermore it only makes matters worse to approximate higher orders of scattering as a geometric series; indeed, at many phase angles the ratio V_4/V_3 is greater than unity, so the resulting approximation fluctuates wildly with phase angle and would be off scale if graphed in Figure 34.

It is easy to qualitatively understand the different behavior of the intensity, linear
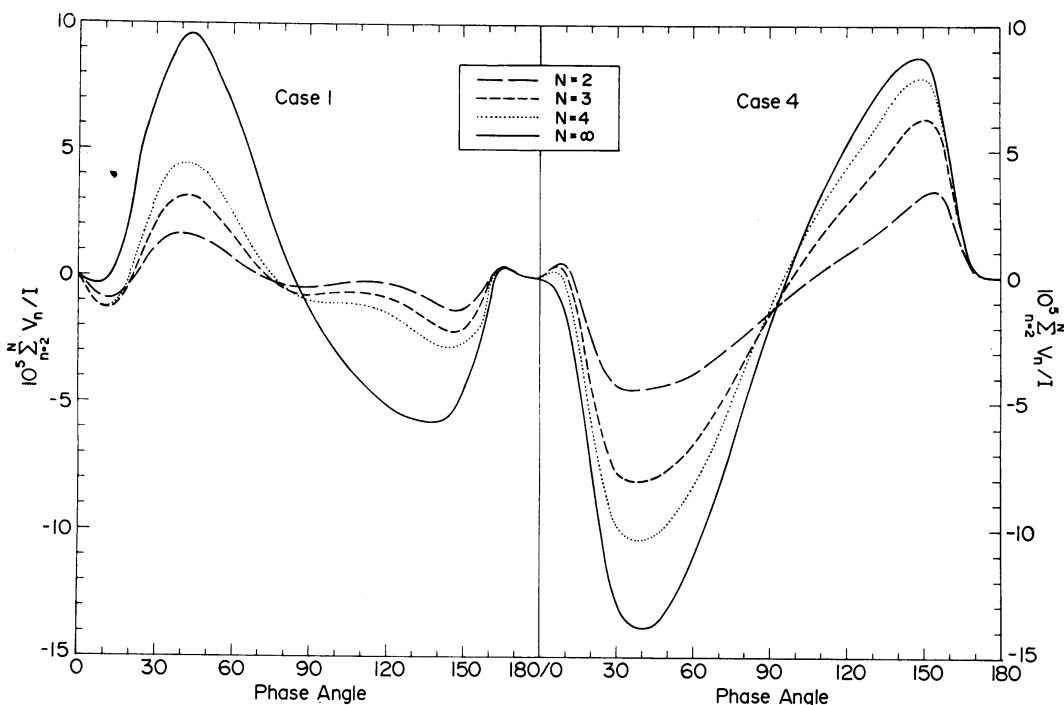
Fig. 34. Same as Figure 32, but for the circular polarization, and with the integration extended only over the northern hemisphere of the planet.

polarization and circular polarization. For a thick layer with large $\tilde{\omega}$ there obviously must be many orders of scattering which contribute to the intensity. However, photons scattered several times in effect lose memory of their initial direction; thus for them no preferred plane is defined and the value of the linear polarization for photons scattered several times is small. A similar consideration applies to the circular polarization, but since the circular polarization arises only from multiple scattering the relative contribution remains important for many orders of scattering.

We have not attempted a more theoretical investigation of the behavior of the Stokes parameters with the order of scattering. The main practical conclusions are: (1) for Fourier coefficients of the reflection matrix with $m \gtrsim 5$ a good accuracy for the Stokes parameters I, Q and U can be obtained from four orders of scattering and the assumption of a geometric series, (2) all Fourier coefficients of the Stokes parameters Q and U can be computed rather accurately with four orders of scattering and the assumption of a geometric series, (3) at least several terms in the Fourier expansion of V require computations with the full four-by-four phase matrix* with a method accounting for all orders of scattering.

3.3. Iteration of formal solution

The 'formal' solution to the equation of transfer (3.38) and the definition of the source function (3.36) do not actually represent a solution for I, but only an integral re-

---

* The first three Stokes parameters can be obtained with an accuracy about 10^{-5} by working with only three-by-three matrices (cf., Hansen, 1971b).

lationship. However, if the optical thickness is not too large these equations are amenable to solution by standard numerical procedures. Herman and Browning (1965) showed that a simple (Gauss-Seidel) iterative technique for two-point boundary value problems converges to an accurate solution in the case of Rayleigh scattering. Dave (1970), cf. also Dave and Gazdag (1970), used the same method to obtain solutions for Mie scattering.

The basis of this method is the following. Let the atmosphere be divided into a number of layers each of optical thickness $\Delta\tau$. According to (3.38) the downward intensity at a level $i+1$ is given approximately, in terms of quantities at levels i and $i-1$, by

$$\mathbf{I}^{i+1}(\tau, \mu, \mu_0, \phi - \phi_0) \sim \mathbf{I}^{i-1}(\tau, \mu, \mu_0, \phi - \phi_0) \, e^{-2\Delta\tau/\mu} + (1 - e^{-2\Delta\tau/\mu}) \times$$
$$\bar{\mathbf{J}}^i(\tau, \mu, \mu_0, \phi - \phi_0), \qquad (3.48)$$

where $\bar{\mathbf{J}}^i$ is an average value for the source function within the ith layer. $\bar{\mathbf{J}}^i$ is calculated by inserting $\mathbf{I}^i$, obtained from the preceding step, in (3.36) and numerically evaluating the integral over angle; the starting condition at $\tau=0$ is $\mathbf{I}(+\mu)=0$, according to the boundary condition (3.37). Herman and Browning (1965) evaluated both the μ and ϕ integrations numerically, while Dave (1970) expanded the azimuth dependence in a Fourier series.

In the first computation of the downward intensity the upward intensity is assumed to be zero in obtaining $\bar{\mathbf{J}}$. After the level $\tau=\tau_0$ is reached $\mathbf{I}(-\mu)$ is computed in upward progression from

$$\mathbf{I}^{i-1}(\tau, -\mu, \mu_0, \phi - \phi_0) \sim \mathbf{I}^{i+1}(\tau, -\mu, \mu_0, \phi - \phi_0) \, e^{-2\Delta\tau/\mu} +$$
$$+ (1 - e^{-2\Delta\tau/\mu}) \, \bar{\mathbf{J}}^i(\tau, -\mu, \mu_0, \phi - \phi_0), \qquad (3.49)$$

with $\bar{\mathbf{J}}^i$ obtained by inserting $\mathbf{I}^i$ in (3.36) and evaluating the integrals over angle. When the level $\tau=0$ is reached the first estimate for $\mathbf{I}$ has been obtained. The process is then repeated with the values of $\bar{\mathbf{J}}^i$ computed from the most recent values of $\mathbf{I}$. The iterations are continued until $\mathbf{I}$ converges to a constant, or slightly fluctuating, value.

This method is very similar to the orders of scattering method with τ integration. The method described in this section has the advantage of faster convergence; according to J. V. Dave (private communication) it is about 50% faster than the classical orders of scattering method. Of course the method of this section has the disadvantage of not yielding the result for the individual orders of scattering. An advantage of both of these iterative methods is that they are easily applicable to inhomogeneous atmospheres. Their primary limitation is that they become very inefficient for thick atmospheres (say $\tau \gtrsim 5$).

3.4. INVARIANT IMBEDDING

The invariant imbedding equations are differential equations giving the change in the reflection and transmission matrices when an optically thin layer is added to the atmosphere. In concept this method is thus a special case of the adding method. In

addition, the physical derivation of the invariant imbedding equations which we give is closely related to the derivation we gave for the orders of scattering Equations, (3.46) and (3.47). However, the computer programming and numerical behavior of results for invariant imbedding are different from these other methods. Therefore invariant imbedding is actually an additional method for multiple scattering computations.

Consider a layer of optical thickness τ, which may be inhomogeneous, and add a thin layer $(\Delta\tau \ll 1)$ with any optical properties to the top side. The reflection matrix for the combined layer, of optical thickness $\tau + \Delta\tau$, is [cf., Figure 35 and the definition of $\mathbf{R}$, (3.3)]

$$
\mathbf{R}\left(\tau + \Delta\tau; \mu, \mu_0, \phi - \phi_0\right) = \left[1 - \frac{\Delta\tau}{\mu}\right]\mathbf{R}\left(\tau; \mu, \mu_0, \phi - \phi_0\right)\left[1 - \frac{\Delta\tau}{\mu_0}\right] +
$$

$$
+ \frac{\tilde{\omega}\Delta\tau}{4\mu\mu_0}\mathbf{P}_r\left(\mu, \mu_0, \phi - \phi_0\right) + \frac{1}{\pi}\int\limits_0^1\int\limits_0^{2\pi}\mu'\,\frac{\tilde{\omega}\Delta\tau}{4\mu'\mu}\mathbf{P}_t^*\left(\mu, \mu', \phi - \phi'\right) \times
$$

$$
\times\,\mathbf{R}\left(\tau; \mu', \mu_0, \phi' - \phi_0\right)\mathrm{d}\mu'\,\mathrm{d}\phi' +
$$

$$
+ \frac{1}{\pi}\int\limits_0^1\int\limits_0^{2\pi}\mu'\mathbf{R}\left(\tau; \mu, \mu', \phi - \phi'\right)\frac{\tilde{\omega}\Delta\tau}{4\mu'\mu_0}\mathbf{P}_t\left(\mu', \mu_0, \phi' - \phi_0\right)\mathrm{d}\mu'\,\mathrm{d}\phi' +
$$

$$
+ \frac{1}{\pi}\int\limits_0^1\int\limits_0^{2\pi}\mu'\mathbf{R}\left(\tau; \mu, \mu', \phi - \phi'\right) \times
$$

$$
\times\left[\frac{1}{\pi}\int\limits_0^1\int\limits_0^{2\pi}\mu''\,\frac{\tilde{\omega}\Delta\tau}{4\mu'\mu''}\mathbf{P}_r^*\left(\mu', \mu'', \phi' - \phi''\right) \times\right.
$$

$$
\times\,\mathbf{R}\left(\tau; \mu'', \mu_0, \phi'' - \phi_0\right)\mathrm{d}\mu''\,\mathrm{d}\phi''\Bigg]\mathrm{d}\mu'\,\mathrm{d}\phi', \tag{3.50}
$$

or

$$
\frac{\partial\mathbf{R}\left(\tau; \mu, \mu_0, \phi - \phi_0\right)}{\partial\tau} = -\left(\frac{1}{\mu} + \frac{1}{\mu_0}\right)\mathbf{R}\left(\tau; \mu, \mu_0, \phi - \phi_0\right) + \frac{\tilde{\omega}}{4\mu\mu_0} \times
$$

$$
\times\,\mathbf{P}_r\left(\mu, \mu_0, \phi - \phi_0\right) + \frac{\tilde{\omega}}{4\pi\mu}\int\limits_0^1\int\limits_0^{2\pi}\mathbf{P}_t^*\left(\mu, \mu', \phi - \phi'\right) \times
$$

$$
\times\,\mathbf{R}\left(\tau; \mu', \mu_0, \phi' - \phi_0\right)\mathrm{d}\mu'\,\mathrm{d}\phi' + \frac{\tilde{\omega}}{4\pi\mu_0}\int\limits_0^1\int\limits_0^{2\pi}\mathbf{R}\left(\tau; \mu, \mu', \phi - \phi'\right) \times
$$

$$
\times\,\mathbf{P}_t\left(\mu', \mu_0, \phi' - \phi_0\right)\mathrm{d}\mu'\,\mathrm{d}\phi' + \frac{\tilde{\omega}}{4\pi}\int\limits_0^1\int\limits_0^{2\pi}\mathbf{R}\left(\tau; \mu, \mu', \phi - \phi'\right) \times
$$

$$\times \left[\frac{1}{\pi} \int\limits_{0}^{1} \int\limits_{0}^{2\pi} \mathbf{P}_r^*\left(\mu', \mu'', \phi' - \phi''\right) \mathbf{R}\left(\tau; \mu'', \mu_0, \phi'' - \phi_0\right) d\mu'' \, d\phi'' \right] \times$$

$$\times d\mu' \, d\phi' \,. \tag{3.51}$$

This is the invariant imbedding equation for $\mathbf{R}$; it is essentially the same as Equation (29) p. 169 of Chandrasekhar (1950). Note that in this method τ is measured from the ground up. For an inhomogeneous atmosphere $\mathbf{P}$ is also a function of τ.

In the invariant imbedding method, (3.51) is used for numerical computations to build an atmosphere from the ground up. Thus reflection from a planetary atmosphere is treated as an initial value problem with the initial condition

$$\mathbf{R}\left(0; \mu, \mu_0, \phi - \phi_0\right) = \mathbf{R}_g\left(\mu, \mu_0, \phi - \phi_0\right),$$

where $\mathbf{R}_g$ is the ground reflectivity, ranging from $R_g = 0$ for a completely absorbing ground to $R_g = 1$ for a conservatively reflecting Lambert surface. (3.51) yields the increment in $\mathbf{R}$ due to an added layer of thickness $\Delta\tau$. Several numerical methods for difference equations have been used to solve (3.51), the simplest being $\mathbf{R}\left(\tau + \Delta\tau\right) = = \mathbf{R}(\tau) + \Delta\tau \times \partial\mathbf{R}/\partial\tau$. Larger step sizes ($\Delta\tau \sim$ a few times 10^{-2}) can be taken with one of the Runge-Kutta methods or a predictor-corrector method (cf., Hamming, 1973; Mingle, 1973); these represent approximations of $\mathbf{R}(\tau)$ in terms of polynomials. Mathews *et al.* (1967) have given a difference equation procedure based upon ex-
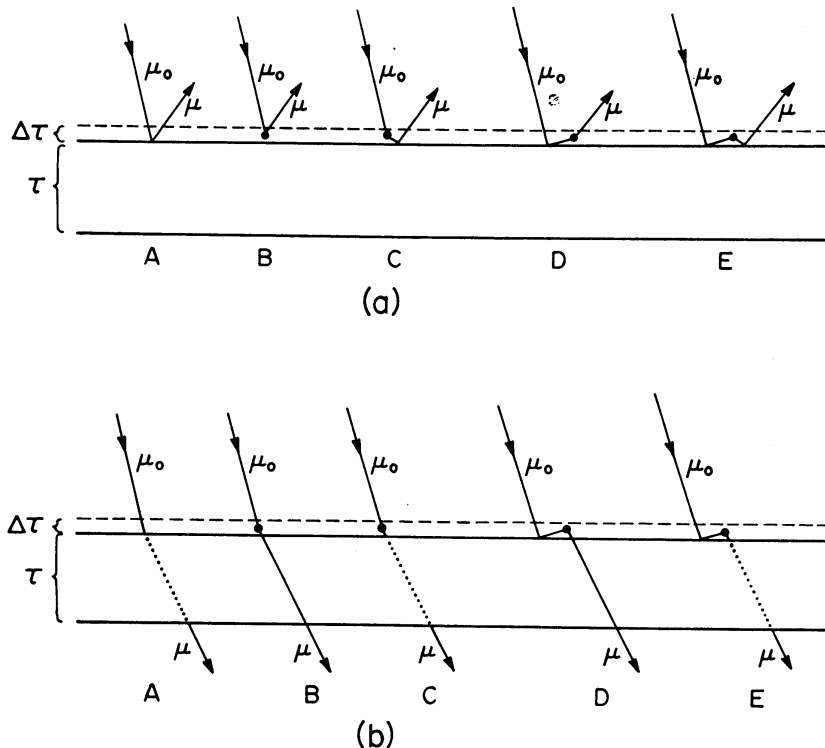

Fig. 35. Schematic representation of reflection (a) and transmission (b) by a plane-parallel layer when a very thin layer ($\Delta\tau \ll 1$) is added to the top of the main layer. There is at most one scattering in the thin layer. A dotted line represents diffuse transmission.

ponentials rather than polynomials; this choice is based on the asymptotic behavior of **R** and **T** and thus presumably allows a larger step size for a thick atmosphere.

In the numerical computations it is efficient to treat the azimuth dependence with a Fourier expansion in $\phi - \phi_0$ and to use discrete quadrature points for μ, e.g., the Gauss divisions for the interval (0, 1). Internal sources, such as thermal emission, can easily be added into the invariant imbedding equation (e.g., see Bellman *et al.*, 1967).

Invariant imbedding has been used in planetary applications mainly for computations of reflection, but an equation for $\partial \mathbf{T}/\partial \tau$ may also be easily obtained. By inspection (cf., Figure 35b) we see that the change in the transmission matrix upon addition of a thin layer to the top of the atmosphere is

$$\frac{\partial \mathbf{T}}{\partial \tau} = -\frac{1}{\mu_0}\mathbf{T} + \frac{\tilde{\omega}e^{-\tau/\mu}}{4\mu\mu_0}\mathbf{P}_t + \frac{\tilde{\omega}}{4\pi\mu_0}\int \mathbf{T}\mathbf{P}_t \, d\Omega' + \frac{\tilde{\omega}e^{-\tau/\mu}}{4\pi\mu}\int \mathbf{P}_r^*\mathbf{R} \, d\Omega' +$$

$$+ \frac{\tilde{\omega}}{4\pi}\int \mathbf{T}\left[\frac{1}{\pi}\int \mathbf{P}_r^*\mathbf{R} \, d\Omega''\right] d\Omega' . \tag{3.52}$$

For brevity we have omitted the functional arguments and combined the integration symbols, e.g., $d\Omega' = d\mu' \, d\phi'$. The different terms in (3.52) represent the ways in which diffuse transmission may occur with no more than one scattering in the layer of optical thickness $\Delta\tau$. Thus the possibility of direct transmission through one, but not both, of the layers is accounted for.

The invariant imbedding equation for $\partial\mathbf{T}/\partial\tau$ involves **R** as well as τ. Thus (3.51) must be computed along with (3.52) to find **T**. Furthermore, (3.52) is less stable for numerical computations than (3.51); thus to obtain a given accuracy it is necessary to take smaller step sizes $\Delta\tau$ in computing $\partial\mathbf{T}/\partial\tau$ than in computing $\partial\mathbf{R}/\partial\tau$.

By adding a thin layer to the bottom of the atmosphere, we obtain two additional invariant imbedding equations for **R** and **T**.

$$\frac{\partial \mathbf{R}}{\partial \tau} = \frac{\tilde{\omega}}{4\mu\mu_0}\mathbf{P}_r \exp\left[-\tau\left(\frac{1}{\mu} + \frac{1}{\mu_0}\right)\right] + \frac{\tilde{\omega}}{4\pi\mu}\int \mathbf{P}_r\mathbf{T} \, d\Omega' + \frac{\tilde{\omega}}{4\pi\mu_0}\int \mathbf{T}^*\mathbf{P}_r \, d\Omega' +$$

$$+ \frac{\tilde{\omega}}{4\pi}\int \mathbf{T}^*\left[\frac{1}{\pi}\int \mathbf{P}_r\mathbf{T}^* \, d\Omega''\right] d\Omega' , \tag{3.53}$$

and

$$\frac{\partial \mathbf{T}}{\partial \tau} = -\frac{1}{\mu}\mathbf{T} + \frac{\tilde{\omega}e^{-\tau/\mu_0}}{4\mu\mu_0}\mathbf{P}_t + \frac{\tilde{\omega}}{4\pi\mu}\int \mathbf{P}_t\mathbf{T} \, d\Omega' + \frac{\tilde{\omega}e^{-\tau/\mu_0}}{4\pi\mu_0}\int \mathbf{R}^*\mathbf{P}_r \, d\Omega' +$$

$$+ \frac{\tilde{\omega}}{4\pi}\int \mathbf{R}^*\left[\frac{1}{\pi}\int \mathbf{P}_r\mathbf{T} \, d\Omega''\right] d\Omega' . \tag{3.54}$$

Equations (3.51)–(3.54) are essentially Equations (29)–(32) in Chandrasekhar's book (1950, pp. 169–170). Chandrasekhar subtracted (3.53) from (3.51) and (3.54) from (3.52), obtaining two integral equations for **R** and **T**. Those equations are the basis for the method of X and Y functions (Section 3.5).

Ambartsumian (1942, 1958) was the first to obtain invariant imbedding equations. He used the equations in essentially the same way as Chandrasekhar, as described in Section 3.5.

The direct numerical attack on the differential equations, for which we reserve the terminology invariant imbedding, became practical with the advent of high-speed digital computers. This approach was published most extensively by Bellman, Kalaba, Ueno, Wing and associates (e.g., Bellman *et al.*, 1960; Wing, 1962). Tables of numerical results for isotropic scattering were given by Bellman *et al.* (1963).

The only major disadvantage of the invariant imbedding approach is the relatively long computation time, in comparison, for example, to the doubling method. However, if the phase function is normalized for the discrete space of zenith angles (e.g., Hansen, 1971b), the computing time is feasible for most phase functions in the case of reflection calculations. The primary advantage of the invariant imbedding method is that it does not become less efficient for an inhomogeneous atmosphere. In addition, it is easy to obtain invariant imbedding equations for a spherical atmosphere (e.g., Bellman *et al.*, 1969), a horizontally inhomogeneous atmosphere (e.g., Bellman *et al.*, 1963a) or time dependent problems (e.g., Bellman *et al.*, 1963b). However the additional variables in these problems make computations very slow, and there have been few numerical results.

Although the invariant imbedding method has not played a major role in planetary applications, it has the potential to be useful for computing reflection by an inhomogeneous atmosphere. In order for the method to be efficient it is important that advantage be taken of the behavior of **R** with increasing τ. For example, the high Fourier terms could be computed beginning near the top of the atmosphere (perhaps at $\tau \sim 1$–2), since only a few scatterings contribute to those terms. Even the azimuth-independent term could be computed for only the top part of the atmosphere, provided that an approximation were included for the reflection function of the atmosphere beneath the starting level.

3.5. METHOD OF X AND Y FUNCTIONS

The method of 'X and Y' functions involves the determination of certain integral equations for functions which depend upon only one angle and are directly related to R and T. The integral equations are solved numerically, so the method can not properly be termed an analytic approach; however, a great deal of algebraic manipulation may indeed be employed in obtaining the integral equations. These integral equations are completely specified by means of a factor Ψ in the kernel. Ψ depends on the particular phase function or phase matrix and is called the characteristic function.

The method of X and Y functions thus involves three essential steps: (1) determination of the characteristic function $\Psi(\mu)$, (2) solution of the integral equations for for $X(\mu)$ and $Y(\mu)$, and (3) computation of R and T from X and Y. For $\tau = \infty$ $Y(\mu) = = 0$, and the notation $H(\mu)$ is generally used for $X(\mu)$ in this special case.

We illustrate the method of X and Y functions for the simple case of isotropic

scattering. References to results for more complicated phase functions and for polarization are given below.

By subtracting the two invariant imbedding equations for $\partial R/\partial \tau$, (3.51) and (3.53), we obtain

$$
\left(\frac{1}{\mu} + \frac{1}{\mu_0}\right) R\left(\mu, \mu_0, \phi - \phi_0\right) = \frac{\tilde{\omega}}{4\mu\mu_0} \, P_r\left(\mu, \mu_0, \phi - \phi_0\right) \times
$$

$$
\times \left\{1 - \exp\left[-\tau\left(\frac{1}{\mu} + \frac{1}{\mu_0}\right)\right]\right\} + \frac{\tilde{\omega}}{4\pi\mu} \left\{\int P_t^*\left(\mu, \mu', \phi - \phi'\right) \times\right.
$$

$$
\times R\left(\mu', \mu_0, \phi' - \phi_0\right) d\Omega' - \int P_r\left(\mu, \mu', \phi - \phi'\right) \times
$$

$$
\left. \times T\left(\mu', \mu_0, \phi' - \phi_0\right) d\Omega'\right\} + \frac{\tilde{\omega}}{4\pi\mu_0} \left\{\int R\left(\mu, \mu', \phi - \phi'\right) \times\right.
$$

$$
\times P_t\left(\mu', \mu_0, \phi' - \phi_0\right) d\Omega' - \int T^*\left(\mu, \mu', \phi - \phi'\right) \times
$$

$$
\left. \times P_r\left(\mu', \mu_0, \phi' - \phi_0\right) d\Omega'\right\} + \frac{\tilde{\omega}}{4\pi} \left\{\int R\left(\mu, \mu', \phi - \phi'\right) \times\right.
$$

$$
\times \left[\frac{1}{\pi}\int P_r^* \times \left(\mu', \mu'', \phi' - \phi''\right) R\left(\mu'', \mu_0, \phi'' - \phi_0\right) d\Omega''\right] d\Omega' -
$$

$$
- \int T\left(\mu, \mu', \phi - \phi'\right) \left[\frac{1}{\pi}\int P_r\left(\mu', \mu'', \phi' - \phi''\right) \times\right.
$$

$$
\left. \times T\left(\mu'', \mu_0, \phi'' - \phi_0\right) d\Omega''\right] d\Omega'\right\} \tag{3.55}
$$

which is valid for a general phase matrix. Separation of the variables μ and μ_0 is trivial for isotropic scattering: in this special case (3.55) becomes

$$
4\left(\mu + \mu_0\right) R\left(\mu, \mu_0\right) = \tilde{\omega} \left[X\left(\mu\right) X\left(\mu_0\right) - Y\left(\mu\right) Y\left(\mu_0\right)\right], \tag{3.56}
$$

where

$$
X\left(\mu\right) \equiv 1 + 2\mu \int_0^1 R\left(\mu, \mu'\right) d\mu', \tag{3.57}
$$

$$
Y\left(\mu\right) \equiv e^{-\tau/\mu} + 2\mu \int_0^1 T\left(\mu, \mu'\right) d\mu'. \tag{3.58}
$$

Similarly, subtracting the two invariant imbedding equations for $\partial T/\partial \tau$ and considering the case of isotropic scattering yields

$$
4\left(\mu - \mu_0\right) T\left(\mu, \mu_0\right) = \tilde{\omega} \left[Y\left(\mu\right) X\left(\mu_0\right) - X\left(\mu\right) Y\left(\mu_0\right)\right]. \tag{3.59}
$$

Inserting (3.56) and (3.59) into (3.57) and (3.58) we obtain the integral equations for X and Y:

$$X(\mu) = 1 + \mu \int_0^1 \frac{\Psi(\mu')}{(\mu + \mu')} [X(\mu) X(\mu') - Y(\mu) Y(\mu')] \, d\mu', \qquad (3.60)$$

$$Y(\mu) = e^{-\tau/\mu} + \mu \int_0^1 \frac{\Psi(\mu')}{(\mu - \mu')} [Y(\mu) X(\mu') - X(\mu) Y(\mu')] \, d\mu', \qquad (3.61$$

where

$$\Psi(\mu) = \frac{\tilde{\omega}}{2}. \qquad (3.62)$$

Chandrasekhar (1950) used an iteration procedure to solve the above non-linear integral equations for X and Y. This yields correct results as has been shown by comparisons with results of other multiple scattering methods. However, for $\tilde{\omega} = 1$ special care is required to obtain the physically correct solution (cf., Chandrasekhar, 1950). Actually, it has been shown that it is possible to encounter incorrect (unphysical) solutions of (3.60) and (3.61) for any value of $\tilde{\omega}$, unless appropriate constraints are applied; the constraints required to obtain the physically correct solution are discussed in an extensive mathematical exercise by Mullikin (e.g., Carlstedt and Mullikin, 1966) and with a simplified physical interpretation by Pahor and Kuščer (1966).

Extensive tables of $X(\mu)$ and $Y(\mu)$ for conservative and nonconservative isotropic scattering and many values of $\tau \leqslant 3.5$ are given by Carlstedt and Mullikin (1966) along with asymptotic formulae for larger τ. Results for $\tau = \infty$ (H functions) are given by Stibbs and Weir (1959) and Abhyankar and Fymat (1971).

For anisotropic phase functions the method of X and Y functions can be considerably more involved. By expanding P, R and T in Fourier series the azimuth dependence can be handled readily; (3.55) and the equation obtained by subtracting (3.52) and (3.54) separate immediately into independent equations for each set of Fourier components, R^m and T^m. However, separation of the variables μ and μ_0 is more difficult. Chandrasekhar (1950) gave ad hoc treatments for a few simple phase functions, but these involved a great deal of algebraic manipulation. Already for a three term phase function the bookkeeping is enormous (cf. Horak and Chandrasekhar, 1961). For more general phase functions it is more promising to use a systematic bookkeeping for the reduction to H functions or X and Y functions (cf. van de Hulst, 1970; Sobolev, 1974); the prescriptions and polynomials involved are based in part on work of Kuščer (1955) and Busbridge (1960, 1967).

Chandrasekhar (1950) and Sobolev (1974) give tables of H, X and Y functions for several anisotropic phase functions with as many as three terms; most of the tables are for $\tilde{\omega} = 1$ and for coarse increments in μ. More extensive tables of H functions are given by Lenoble (1970) for the Rayleigh phase function and by Kolesov and Smotkii (1972) for phase functions with as many as four terms. Extensive tables of X and Y functions are given by Sweigart (1970) for the Rayleigh phase function.

The method of X and Y functions has been extended to include polarization in the simple case of Rayleigh scattering. This problem yielded to the ad hoc treatment of Chandrasekhar (1950), essentially because the Fourier components of the phase matrix could easily be factored into the product of a matrix dependent only on μ and a matrix dependent only on μ_0. The method of X and Y functions has not been successfully extended to a more general case, such as Mie scattering, although considerable effort (e.g. Sekera, 1966) has been expended with that goal in mind.

The relevant H functions for Rayleigh scattering are given by Chandrasekhar (1950), Lenoble (1970) and Abhyankar and Fymat (1971); the latter two references include results for $\tilde{\omega} < 1$. X and Y functions for $\tilde{\omega} = 1$ are given by Sekera and Kahle (1966); results in terms of the Stokes parameters are given by Coulson et al. (1960) for optical thicknesses not exceeding unity. Bond and Siewert (1971) give some H functions for the case in which the phase matrix is a linear combination of isotropic and Rayleigh scattering.

The main attraction of the method of X and Y functions is the reduction of the solution to functions of a single angle. The primary drawback of the method is the extensive amount of algebra which has been employed for most phase functions and phase matrices. A useful extension to general phase matrices has not been demonstrated.

3.6. Discrete ordinate method

In the discrete ordinate method the equation of transfer (3.35) is attacked by expanding the phase function in Legendre polynomials and replacing the integral over u' with a finite sum, i.e., the quadrature is performed using $2n$ discrete u' (n discrete μ). The limit $n = 1$ is a two stream approximation, with one upward direction and one downward direction. For large n the method in principle becomes arbitrarily accurate. By taking the limit $n \to \infty$ the method of eigenvalue expansions (Section 3.8) is obtained.

The origins of the discrete ordinate method date at least to the two-stream method of Schuster (1905) and Schwarzschild (1906). Wick (1943) and Chandrasekhar (1944, 1950) developed the method with n discrete ordinates.

We sketch the discrete ordinate method here for the problem in which the intensity is computed with polarization neglected, because that is the realm in which the method has been applied. The phase function is expanded in, or approximated by, a finite number of Legendre polynomials,

$$P(\cos \alpha) = \sum_{l=0}^{L} c_l P_l(\cos \alpha), \tag{3.63}$$

where the coefficients c_l are constants. By the addition theorem of spherical harmonics

$$P(u, \mu_0, \phi - \phi_0) = \sum_{m=0}^{L} (2 - \delta_{0,m}) \sum_{l=m}^{L} c_l^m P_l^m(u) P_l^m(\mu_0) \cos m (\phi - \phi_0),$$

where
$$\tag{3.64}$$

$$c_l^m = c_l \frac{(l-m)!}{(l+m)!}, \qquad \delta_{0,m} = \begin{cases} 1 & \text{if} \quad m = 0 \\ 0 \text{ move over} \end{cases}, \tag{3.65}$$

and the P_l^m are the associated Legendre functions. Thus the intensity is also expanded in the form

$$I(\tau, u, \phi) = \sum_{m=0}^{L} I^m(\tau, u) \cos m(\phi - \phi_0), \qquad (3.66)$$

and the equation of transfer splits up into $L+1$ independent equations for the I^m,

$$u_i \frac{dI_i^m}{d\tau} = -I_i^m + \frac{\tilde{\omega}}{2} \sum_{l=m}^{L} c_l^m P_l^m(u_i) \sum_{j=-n}^{n} w_j I_j^m P_l^m(u_j) +$$

$$+ \frac{\tilde{\omega} F_0 e^{-\tau/\mu_0} (2 - \delta_{0,m})}{4} \sum_{l=m}^{L} c_l^m P_l^m(u_i) P_l^m(\mu_0), \qquad (3.67)$$

where the integral over u' has been replaced with a sum over j, with ordinates u_j and weights w_j. Usually Gauss quadrature is employed. i and j take on the values ± 1, $\pm 2, \ldots \pm n$ in the nth approximation. Thus (3.67) represents $2n$ linear equations for each, m, $m = 0, 1, \ldots L$. n is taken as any number satisfying $4n - 1 > 2L$.

The solution of the nonhomogeneous differential Equation (3.67) is the sum of a solution of the homogeneous part of the equation, which must have the form

$$\frac{e^{-k_m}}{1 + u_i k_m} \sum_{l=m}^{L} c_l^m \zeta_l^m P_l^m(u_i) \qquad (3.68)$$

and a particular integral of (3.67), for which one form is

$$\frac{(2 - \delta_{0,m}) F_0 e^{-\tau/\mu_0}}{4} \sum_{l=m}^{L} c_l^m \gamma_l^m \frac{P_l^m(u_i)}{1 + u_i/\mu_0}. \qquad (3.69)$$

Relations for determining the constants k_m, ζ_l^m, γ_l^m and c_l^m are obtained by substituting these solutions into the equation of transfer and by using the boundary conditions on I_i^m.

For simple cases, involving as many as three terms in the expansion of the phase function in Legendre polynomials, Chandrasekhar (1950) has done the algebra to analytically approach the solution. However, numerical computations are still required in the end.

Determination of the constants in the discrete ordinate method can be handled systematically, thus allowing numerical computations in principle for any order of approximation n. Descriptions of appropriate procedures and quantitative results have been given, for example, by Lenoble (1956), Samuelson (1969) and Liou (1973).

An advantage of the discrete ordinate method is that it yields the internal field as well as the reflection and transmission. A disadvantage is that considerable algebra

is required prior to numerical computations. However, at least for the azimuth-independent term, the discrete ordinate method can give rather accurate results (within a percent or so) already for $n=3$ or 4, so it is an efficient procedure when accuracies of that order are sufficient (cf. Weinman and Guetter, 1972; Liou, 1973). Liou (1974) has given a quasi-analytic solution for $n=2$ (4-stream approximation) which may be sufficiently accurate for computations of the flux in many applications.

3.7. SPHERICAL HARMONICS METHOD

The spherical harmonics method, which is also known as the 'P_L-approximation', is very similar to the discrete ordinates method. The spherical harmonics method also begins with the equation of transfer, but the intensity is immediately expanded into a finite number of spherical harmonics (Davison, 1958; Lenoble, 1961). The mth azimuthal component of the intensity is thus of the form

$$I^m(\tau, u) = \sum_{l=m}^{L} (2l + 1)\, d_l^m(\tau)\, P_l^m(u) \tag{3.70}$$

and the phase function is expanded in Legendre polynomials as in (3.63). The P_l^m are the associated Legendre functions and the d_l^m are coefficients to be determined. By taking L sufficiently large the intensity can in principle be obtained to an arbitrary accuracy.

If (3.70) is substituted into the equation of transfer a system of $L+1-m$ simultaneous first order linear differential equations is obtained. This system must be solved subject to the boundary conditions on the equation of transfer. For finite L the boundary conditions can not be exactly satisfied for all u. Thus there is some arbitrariness in the choice of conditions applied to the system of simultaneous equations. Usually either Marshak's (1947) or Mark's (1944) boundary conditions are used; the relative merits are discussed by Davison (1958).

The system of simultaneous equations obtained in the spherical harmonics method is described in detail by Davison (1958) and Case and Zweifel (1967). Quantitative applications of the method have been made by Deuze *et al.* (1973), who use a quasi-analytic approach, and by Dave and Canosa (1974), who use a direct numerical procedure. The latter approach can easily be extended to an inhomogeneous atmosphere. Dave and Armstrong (1974) describe a scheme to numerically smooth fluctuations in the intensity which normally exist in the spherical harmonics solution for finite L.

The practical applicability of the spherical harmonics method is similar to the discrete ordinates method. Indeed, for the azimuth independent part of the intensity, $I^0(\tau, u)$, the equations are exactly the same in the two methods (cf. Davison, 1958; Kofink, 1967). A useful characteristic of the spherical harmonics method is that, like the discrete ordinate method, it can yield a reasonable accuracy for low order approximations. With appropriate modifications the spherical harmonics method is in principle applicable to geometries other than a plane-parallel atmosphere (cf. Davison, 1958).

3.8. EXPANSION IN EIGENFUNCTIONS

The method of expansion in eigenfunctions is based on a standard mathematical technique for solving differential equations. The solution of the equation of transfer is obtained as an expansion in a series of solutions to the homogeneous part of the equation,

$$u \frac{dI(\tau, u, \phi)}{d\tau} = -I(\tau, u, \phi) + \frac{\tilde{\omega}}{4\pi} \int_{-1}^{1} \int_{0}^{2\pi} P(u, u', \phi - \phi') \times$$
$$\times I(\tau, u', \phi') \, du' \, d\phi', \qquad (3.71)$$

in which the dependence of I on μ_0 is implicit. Particular solutions of (3.71) can be found in the form

$$e^{-\tau/\nu} \phi_\nu^m (u) (1 - u^2)^{m/2} \cos m\phi, \qquad (3.72)$$

where ϕ_ν^m is called the eigenfunction and ν is the corresponding eigenvalue. The method thus consists essentially of: (1) finding the eigenfunctions of (3.71), (2) proving that the eigenfunctions form a complete set, and (3) expanding the solution of the complete equation of transfer in terms of these eigenfunctions using the appropriate boundary conditions.

Very extensive mathematical manipulation is required to actually work out this method of expansion in eigenfunctions. Even then the recipe for numerical computations is extremely complicated. This method was worked out for isotropic scattering by Case (1960) and, in a paper containing more than 100 equations, for a phase function consisting of an arbitrary number of polynomials by McCormick and Kuščer (1966). It is found that there is a continuous set of eigenvalues in the range $-1 < \nu < 1$, corresponding to a continuous set of singular eigenfunctions, and a discrete set of eigenvalues outside the range $(-1, 1)$. The singular eigenfunctions do not lead to any essential difficulties because the final solution involves integrals over them. The solutions for I can be expressed in terms of H functions, moments of H functions and certain polynomials. In general these functions and the coefficients of the polynomials must be computed numerically. The most ambitious numerical results are apparently those of Kaper et al. (1970) for the azimuthally-symmetric case and Feinstein et al. (1972) for the azimuth-dependent case.

A more detailed description of the method of expansion in eigenfunctions can be obtained from the above references, Mika (1961), Case (1967), Case and Zweifel (1967), McCormick and Kuščer (1973) and Kuščer and McCormick (1974); the latter reference contains a particularly clear presentation of the method.

The method of expansion in eigenfunctions provides a rigorous mathematical treatment of the equation of transfer, but is apparently too complicated to compete with other methods described in this review for numerical applications to planetary atmospheres. In particular, extensions to nonhomogeneous atmospheres and non-plane-parallel geometries, though possible in principle, would apparently not be practical for obtaining quantitative results. However, even if the method of expansion in

eigenfunctions is not used for numerical computations it has some relevance to planetary problems, e.g., (1) the largest discrete eigenvalue v and the corresponding eigenfunction give the diffusion exponent and the diffusion pattern deep within a thick atmosphere (van de Hulst, 1970), and (2) extensions of the theory for expansions in eigenfunctions can be used to obtain polynomials occurring in the method of X and Y functions (cf. van de Hulst, 1970; Pahor, 1966, 1967).

3.9. MONTE CARLO METHOD

The Monte Carlo method takes advantage of the fact that the scattering of an individual photon is essentially a stochastic process, with the phase function being the probability density function for scattering at a given angle. Photons are thus allowed to play a game of change in a computer and by recording the history of a sufficient number of photons the radiation field can in principle be determined to an arbitrary accuracy. The basic simplicity of this method allows great flexibility, and hence it can be applied to complicated problems which would be virtually insoluble by the methods described above.

The Monte Carlo method was used for computer simulation of multiple scattering problems at least as early as the 1940's and the basic precept of stochastic trials has much earlier origins (cf. Hammersley and Handscomb, 1964). Several additional books on the Monte Carlo method are available, e.g., Cashwell and Everett (1959), Shreider (1966) and Spanier and Gelbard (1969). A useful review paper has been given by House and Avery (1969). Many applications to plane-parallel planetary atmospheres have been made, e.g., by Collins and Wells (1965), Plass and Kattawar (1968, 1971) and Danielson et al. (1969). Van Blerkom (1971) and Appleby and van Blerkom (1974) have used this method to compute reflection from clouds with horizontal striations, while McKee and Cox (1974) have used it for application to finite cubic clouds. Kattawar et al. (1973) have used the Monte Carlo method for computing the radiation field in a plane-parallel atmosphere-ocean system. Marchuk and Mikhailov (1967a, b), Kattawar and Adams (1971) and Collins et al. (1972) have applied the method to spherical atmospheres. Kastner (1964) has used it to include a redistribution of photon frequencies in L_α scattering.

In the Monte Carlo method a system of coordinates and boundaries are defined appropriate for the atmosphere being considered. Photons are successively 'released' from the source, which may be, for example, sunlight incident from a given direction or thermal radiation distributed through the atmosphere. A given photon suffers its first interaction (scattering or absorption) after traveling an optical distance

$$l = l_0 \ln (1/r), \tag{3.73}$$

where l_0 is the mean free photon path,

$$l_0 = 1/\sigma_{ext} \tag{3.74}$$

and r is a random number in the interval (0, 1). The new direction of the photon can

be obtained by taking ϕ from

$$\phi = 2\pi r \tag{3.75}$$

and θ from

$$r = \frac{\displaystyle\int_0^\theta P(\theta')\sin\theta'\,d\theta'}{\displaystyle\int_0^\pi P(\theta')\sin\theta'\,d\theta'}, \tag{3.76}$$

where in each case r is a new number on $(0, 1)$. Bookkeeping is maintained of the number of photons crossing unit area at each location at which the intensity is desired.

In an optimized computer program a simulated photon history is not terminated by absorption or escape from the atmosphere. Instead a weight W is associated with each photon and appropriately reduced at each interaction. Thus W may be multiplied by $\tilde{\omega}[1 - \exp(-\tau_e)]$ at each scattering, where τ_e is the optical distance to the boundary of the atmosphere in the direction of the photon path, and the location of the next interaction is restricted to lie on the pathlength within the atmosphere. In this way the start-up time required to inject new photons into the atmosphere is minimized. A given photon history is terminated after its weight reaches an assigned lower limit. The optimum value for this lower limit can best be determined from experience; Plass and Kattawar (1971) use the value 10^{-5}.

Additional biasing schemes may be used to prevent over-processing of photons which contribute to an easily defined aspect of the radiation field. With any biasing scheme the probability distribution for a particular event is distorted to force the selection of random variable into a favorable category. The physics of the situation is maintained by appropriately weighting the photon. Biasing schemes are valuable for reducing computer time, but they must be used with care to avoid introduction of spurious results.

The variety of biasing procedures is one of the reasons that there are many different Monte Carlo codes. The different options available within the general Monte Carlo method make it difficult to document precisely, and thus the reliability of the results depends considerably on the practitioner. However, the same problem exists to some extent with all the numerical methods for multiple scattering.

The major advantage of the Monte Carlo method is the ease with which it can be applied to many complicated problems, particularly to non-plane-parallel atmospheres. The only real disadvantage of the method is the limited accuracy obtained with moderate computer time. Most results which have been presented possess statistical fluctuations of at least a few percent, and these errors decrease in magnitude only as the square root of the number of photons processed. However, computers are likely to continue to improve in their speed and storage capabilities and there is likely to be an increased need for solving problems with non-plane-parallel atmospheres. Thus the Monte Carlo method should play a majorrale in future planetary applications.

Acknowledgements

References

Abhyankar, K. D. and Fymat, A. L.: 1971, *Astrophys. J. Suppl.* **23**, 35.
Allen, C. W.: 1963, *Astrophysical Quantities*, Athlone Press, London, 291 pp.
Ambartsumian, V. A.: 1942, *Astr. Zh. (Russ.)* **19**, 30.
Ambartsumian, V. A.: 1958, *Theoretical Astrophysics*, Pergamon Press, New York, 645 pp.
Appleby, J. F. and van Blerkom, D. J.: 1974, submitted to *Icarus*.
Bellman, R., Kagiwada, H., Kalaba, R., and Ueno, S.: 1967, *Icarus* **7**, 365.
Bellman, R. E., Kagiwada, H. H., Kalaba, R. E., and Ueno, S.: 1969, *Icarus* **11**, 417.
Bellman, R. E., Kalaba, R. E., and Prestrud, M. C.: 1963, *Invariant Imbedding and Radiative Transfer in Slabs of Finite Thickness*, American Elsevier, New York, 346 pp.
Bellman, R., Kalaba, R., and Ueno, S.: 1963a, *Icarus* **1**, 297.
Bellman, R., Kalaba, R., and Ueno, S.: 1963b, *J. Math. Anal. Appl.* **7**, 310.
Bellman, R., Kalaba, R., and Wing, G. M.: 1960, *J. Math. Phys.* **1**, 280.
Belton, M. J. S., Hunten, D. M., and Goody, R. M.: 1968, in J. C. Brandt and M. B. McElroy (eds.), *The Atmospheres of Venus and Mars*, Gordon and Breach, New York, 288 pp.
Bond, G. R. and Siewert, C. E.: 1971, *Astrophys. J.* **164**, 97.
Born, M. and Wolf, E.: 1959, *Principles of Optics*, Pergamon Press, New York, 803 pp.
Bryant, H. C. and Cox, A. J.: 1966, *J. Opt. Soc. Amer.* **56**, 1529.
Bryant, H. C. and Jarmie, N.: 1974, *Sci. Amer.* **231**, 60.
Busbridge, I. W.: 1960, *The Mathematics of Radiative Transfer*, Cambridge Univ. Press, Cambridge, 143 pp.
Busbridge, I. W.: 1967, *Astrophys. J.* **149**, 195.
Cabannes, J.: 1929, *La Diffusion Moléculaire de la Lumière*, Les Presses Universitaires de France, Paris, 326 pp.
Carlstedt, J. L. and Mullikin, T. W.: 1966, *Astrophys. J. Suppl.* **12**, 449.
Case, K. M.: 1960, *Ann. Phys.* **9**, 1.
Case, K. M.: 1967, in E. Inönü and P. F. Zweifel (eds.), *Developments in Transport Theory*, Academic Press, New York, 381 pp.
Case, K. M. and Zweifel, P. F.: 1967, *Linear Transport Theory*, Addison-Wesley, Reading, Mass., 342 pp.
Cashwell, E. D. and Everett, C. J.: 1959, *Monte Carlo Method*, Pergamon Press, New York, 153 pp.
Chandrasekhar, S.: 1944, *Astrophys. J.* **100**, 76.
Chandrasekhar, S.: 1950, *Radiative Transfer*, Oxford Univ. Press, 393 pp.
Coffeen, D. L. and Gehrels, T.: 1969, *Astron. J.* **74**, 433.
Coffeen, D. L. and Hansen, J. E.: 1974, in T. Gehrels (ed.), *Planets, Stars and Nebulae Studied With Photopolarimetry*, Univ. Arizona Press, Tucson, p. 518.
Collins, D. G. and Wells, M. B.: 1965, REP. RRA-T54 (Radiation Research Associates, Inc., Ft. Worth, Texas), Vols. 1 and 2.
Collins, D. G., Blattner, W. G., Wells, M. B., and Horak, H. G.: 1972, *Appl. Opt.* **11**, 2684.
Coulson, K. L., Dave, J. V., and Sekera, Z.: 1960, *Tables Related to Radiation Emerging From a Planetary Atmosphere with Rayleigh Scattering*, Univ. of Calif. Press, Berkeley, 584 pp.
Danielson, R. E., Moore, D. R., and van de Hulst, H. C.: 1969, *J. Atmospheric Sci.* **26**, 1078.
Dave, J. V.: 1964, *Astrophys. J.* **140**, 1292.
Dave, J. V.: 1969, *Appl. Opt.* **8**, 155.
Dave, J. V.: 1970, *Appl. Opt.* **9**, 2673.
Dave, J. V. and Armstrong, B. H.: 1974, submitted to *J. Atmospheric Sci.*
Dave, J. V. and Canosa, J.: 1974, *J. Atmospheric Sci.* **31**, 1089.
Dave, J. V. and Gazdag, J.: 1970, *Appl. Opt.* **9**, 1457.
Davison, B.: 1958, *Neutron Transport Theory*, Oxford Univ. Press, London, 450 pp.

Deirmendjian, D.: 1964, *Appl. Opt.* **3**, 187.

Deirmendjian, D.: 1969, *Electromagnetic Scattering on Spherical Polydispersions*, American Elsevier, New York, 290 pp.

Deuze, J. L., Devaux, C., and Herman, M.: 1973, *Nouv. Rev. Optique* **4**, 307.

de Vaucouleurs, G.: 1951, *Ann. Phys.* **6**, 211.

Diem, M.: 1948, *Meteor. Rund.* **1**, 261.

Dollfus, A. and Coffeen, D. L.: 1970, *Astron. Astrophys.* **8**, 251.

Feinstein, D. L., Butler, F. E., Piech, K. R., and Leonard, A.: 1972, *Phys. Fluids* **15**, 1641.

Friend, J. P.: 1966, *Tellus* **18**, 465.

Grant, I. P. and Hunt, G. E.: 1969, *Proc. Roy. Soc. London* A **313**, 183.

Hammersley, J. M. and Handscomb, D. C.: 1964, *Monte Carlo Methods*, John Wiley, New York, 178 pp.

Hamming, R. W.: 1973, *Numerical Methods For Scientists and Engineers*, McGraw-Hill, New York, 721 pp.

Hansen, J. E.: 1969, *J. Atmospheric Sci.* **26**, 478.

Hansen, J. E.: 1971a, *J. Atmospheric Sci.* **28**, 120.

Hansen, J. E.: 1971b, *J. Atmospheric Sci.* **28**, 1400.

Hansen, J. E.: 1971c, *J. Atmospheric Sci.* **28**, 1515.

Hansen, J. E. and Hovenier, J. W.: 1971, *J. Quant. Spectr. Radiat. Transfer* **11**, 809.

Hansen, J. E. and Hovenier, J. W.: 1974, *J. Atmospheric Sci.* **31**, 1137.

Hansen, J. E. and Pollack, J. B.: 1970, *J. Atmospheric Sci.* **27**, 265.

Herman, B. M. and Browning, S. R.: 1965, *J. Atmospheric Sci.* **22**, 559.

Horak, H. G.: 1950, *Astrophys. J.* **112**, 445.

Horak, H. G. and Chandrasekhar, S.: 1961, *Astrophys. J.* **134**, 45.

House, L. L. and Avery, L. W.: 1969, *J. Quant. Spectr. Radiat. Transfer* **9**, 1579.

Hovenier, J. W.: 1969, *J. Atmospheric Sci.* **26**, 488.

Hovenier, J. W.: 1971, *Astron. Astrophys.* **13**, 7.

Irvine, W. M.: 1963, *Bull. Astron. Inst. Neth.* **17**, 176.

Irvine, W. M.: 1965, *Astrophys. J.* **142**, 1563.

Junge, C. E.: 1963, *Air Chemistry and Radiochemistry*, Academic Press, New York, 382 pp.

Kaper, H. G., Shultis, J. K., and Veninga, J. G.: 1970, *J. Comp. Phys.* **6**, 288.

Kastner, S. O.: 1964, Goddard Space Flight Center rept. TMX-55062, 12 pp.

Kattawar, G. W. and Adams, C. N.: 1971, *Astrophys. J.* **167**, 183.

Kattawar, G. W. and Plass, G. N.: 1967, *Appl. Opt.* **6**, 1377.

Kattawar, G. W., Plass, G. N., and Guinn, J. A.: 1973, *J. Phys. Ocean.* **3**, 353.

Kemp, J. C.: 1974, in T. Gehrels (ed.), *Planets, Stars and Nebulae Studied with Photopolarimetry*, Univ. Arizona Press, Tucson, p. 607.

Kemp, J. C., Swedlund, J. B., Murphy, R. E., and Wolstencroft, R. D.: 1971a, *Nature* **231**, 169.

Kemp, J. C., Wolstencroft, R. D., and Swedland, J. B.: 1971b, *Nature* **232**, 165.

Kendall, M. G. and Stuart, A.: 1963, *The Advanced Theory of Statistics,* Vol. 1, *Distribution Theory*, Hafner Publ. Com., New York, 433 pp.

Kerker, M.: 1969, *The Scattering of Light*, Academic Press, New York, 666 pp.

Khrgian, A. Kh.: 1961, *Cloud Physics*, Israel Prog. Scien. Trans., Jerusalem, 392 pp.

Kofink, W.: 1967, in E. Inönü and P. F. Zweifel (eds.), *Developments in Transport Theory*, Academic Press, New York, 381 pp.

Kolesov, A. K. and Smotkii, O. I.: 1972, *Soviet Astron. A. J.* **15**, 802.

Kuščer, I.: 1955, *J. Math. Phys.* **34**, 256.

Kuščer, I. and McCormick, N. J.: 1974, *UCLA International Conference on Radiation and Remote Probing of the Atmosphere,* Western Periodicals, North Hollywood, 506 pp.

Lacis, A. A. and Hansen, J. E.: 1974, *J. Atmospheric Sci.* **31**, 118.

Lenoble, J.: 1956, *Rev. Opt.* **35**, 1.

Lenoble, J.: 1961, *Compt. Rend. Acta. Sci.* **252**, 2087.

Lenoble, J.: 1970, *J. Quant. Spectr. Radiat. Transfer* **10**, 533.

Liou, K. N.: 1973, *J. Atmospheric Sci.* **30**, 1303.

Liou, K. N.: 1974, *J. Atmospheric Sci.,* **31**, 1473.

Liou, K. N. and Hansen, J. E.: 1971, *J. Atmospheric Sci.* **28**, 995.

Lorenz, L.: 1898, *Oeuvres Scientifiques*, Vol. 1, Lehman and Stage, Copenhagen, p. 405.

Lyot, B.: 1929, *Ann. Obs. Paris (Meudon)* **8**, 161.

Marchuk, G. I. and Mikhailov, G. A.: 1967a, *Izv. Atmospheric Ocean. Phys.* **3**, 258.

Marchuk, G. I. and Mikhailov, G. A.: 1967b, *Izv. Atmospheric Ocean. Phys.* **3**, 394.

Mark, J. C.: 1944, Nat. Res. Coun. Canada, Atomic Energy Project report MT 92.

Marshak, R. E.: 1947, *Phys. Rev.* **71**, 443.

Mathews, D. R., Hansen, K. F., and Mason, E. A.: 1967, *Nucl. Sci. Eng.* **27**, 263.

McCormick, N. J. and Kuščer, I.: 1966, *J. Math. Phys.* **7**, 2036.

McCormick, N. J. and Kuščer, I.: 1973, in E. J. Henley and J. Lewins (eds.), *Advances in Nuclear Science and Technology* **7**, p. 181, Academic Press, New York, 379 pp.

McKee, T. B. and Cox, S. K.: 1974, submitted to *J. Atmospheric Sci.*

Mie, G.: 1908, *Ann. Phys.* **25**, 377.

Mika, J. R.: 1961, *Nucl. Sci. Eng.* **11**, 415.

Mingle, J. D.: 1973, *The Invariant Imbedding Theory of Nuclear Transport*, American Elsevier, New York, 131 pp.

Mossop, S. C.: 1965, *Geochim. Cosmochim. Acta* **29**, 201.

Pahor, S.: 1966, *Nucl. Sci. Eng.* **26**, 192.

Pahor, S.: 1967, *Nucl. Sci. Eng.* **29**, 248.

Pahor, S. and Kuščer, I.: 1966, *Astrophys. J.* **143**, 888.

Peebles, G. H. and Plesset, M. S.: 1951, *Phys. Rev.* **81**, 430.

Penndorf, R.: 1957, *J. Opt. Soc. Amer.* **47**, 176.

Plass, G. N. and Kattawar, G. W.: 1968, *Appl. Opt.* **7**, 415.

Plass, G. N. and Kattawar, G. W.: 1971, *J. Atmospheric Sci.* **28**, 1187..

Plass, G. N., Kattawar, G. W., and Catchings, F. E.: 1973, *Appl. Opt.* **12**, 314.

Pollack, J. B.: 1967, *Icarus* **7**, 42.

Porch, W. M., Ensor, D. S., Charlson, R. J., and Heintzenberg, J.: 1973, *Appl. Opt.* **12**, 34

Potter, J. F.: 1970, *J. Atmospheric Sci.* **27**, 943.

Rayleigh, Lord (J. W. Strutt): 1871, *Phil. Mag.* **41**, 107, 274 and 477.

Rayleigh, Lord (J. W. Strutt): 1918, *Phil. Mag.* **35**, 373.

Samuelson, R. E.: 1969, *Icarus* **10**, 258.

Schuster, A.: 1905, *Astrophys. J.* **21**, 1.

Schwarzschild, K.: 1906, *Göttinger Nachrichten*, 41.

Sekera, Z.: 1966, Memorandums RM-4951-PR and RM-5056-PR, Rand Corporation, Santa Monica.

Sekera, Z. and Kahle, A. B.: 1966, Memorandum R-452-PR, Rand Corporation, Santa Monica.

Shreider, Y. A.: 1966, *The Monte Carlo Method*, Pergamon Press, New York, 381 pp.

Shurcliff, W. A.: 1962, *Polarized Light*, Harvard Univ. Press, Cambridge, 207 pp.

Sobolev, V. V.: 1974, *Light Scattering in Planetary Atmospheres*, Pergamon Press, New York (in press).

Spanier, J. and Gelbard, E. M.: 1969, *Monte Carlo Principles and Neutron Transport Problems*, Addison-Wesley, Reading, Mass., 234 pp.

Stibbs, D. W. N. and Weir, R. E.: 1959, *Monthly Notices Roy. Astron. Soc.* **119**, 512.

Stokes, G. G.: 1862, *Proc. Roy. Soc. (London)* **11**, 545.

Sweigart, A. V.: 1970, *Astrophys. J. Suppl.* **22**, 1.

Travis, L. D.: 1974, in preparation.

Twomey, S., Jacobowitz, H., and Howell, H. B.: 1966, *J. Atmospheric Sci.* **23**, 289.

Uesugi, A. and Irvine, W. M.: 1970, *Astrophys. J.* **159**, 127.

van Blerkom, D. J.: 1971, *Astrophys. J.* **166**, 235.

van de Hulst, H. C.: 1948, *Astrophys. J.* **107**, 220.

van de Hulst, H. C.: 1957, *Light Scattering by Small Particles*, Wiley, New York, 470 pp.

van de Hulst, H. C.: 1963, Tech. Rept., Inst. Space Studies, NASA, New York, 81 pp.

van de Hulst, H. C.: 1970, *Astron. Astrophys.* **9**, 359.

van de Hulst, H. C. and Irvine, W. M.: 1962, *La Physique des planètes* (11th Liège International Astrophysical Symposium), p. 78.

Weickmann, H. K. and aufm Kampe, H. J.: 1953, *J. Meteor.* **10**, 204.

Weinman, J. A. and Guetter, P. J.: 1972, *J. Appl. Meteor.* **11**, 136.

Wick, G. C.: 1943, *Z. Phys.* **120**, 702.

Wing, G. M.: 1962, *An Introduction to Transport Theory*, John Wiley, New York, 169 pp.